Exploring the String Landscape:

The Dynamics, Statistics, and Cosmology of Parallel Worlds

Stein Pontus Ahlqvist

Submitted in partial fulfillment of the
requirements for the degree of
Doctor of Philosophy
in the Graduate School of Arts and Sciences

COLUMBIA UNIVERSITY

2013

ABSTRACT

Exploring the String Landscape:

The Dynamics, Statistics, and Cosmology of Parallel Worlds

Stein Pontus Ahlqvist

This dissertation explores various facets of the low-energy solutions in string theory known as the *string landscape*. Three separate questions are addressed – the tunneling dynamics between these vacua, the statistics of their location in moduli space, and the potential realization of slow-roll inflation in the flux potentials generated in string theory. We find that the tunneling transitions that occur between a certain class of supersymmetric vacua related to each other via monodromies around the conifold point are sensitive to the details of warping in the near-conifold regime. We also study the impact of warping on the distribution of vacua near the conifold and determine that while previous work has concluded that the conifold point acts as an accumulation point for vacua, warping highly dilutes the distribution in precisely this regime. Finally we investigate a novel form of inflation dubbed *spiral inflation* to see if it can be realized near the conifold point. We conclude that for our particular models, spiral inflation seems to rely on a de Sitter-like vacuum energy. As a result, whenever spiral inflation is realized, the inflation is actually driven by a vacuum energy.

Contents

List of Figures

ACKNOWLEDGMENTS

Over the last five years, I have had the pleasure to interact with many wonderful people and am grateful to many of them for their insights, support, and company. First and foremost, I would like to thank my wonderful wife Sheana who has been the most inspiring, thoughtful, and supportive friend I could have ever asked for. I also want to thank my adviser Brian Greene for helping me understand and, perhaps more importantly, appreciate physics. I also want to extend my appreciation to my defense committee for their patience and flexibility as well as their feedback and insights. I also want to thank David Kagan who has been incredibly generous with his time and help and with whom it has been a great pleasure working. I also want to thank Subir Sabharwal, Yonah Lemonik, Arthur Franke, Gary Cheng, Stefanos Marnerides, and Kurt Hinterbichler who besides being great friends have all made learning physics a pleasure.

Last, but certainly not least, I want to thank my parents Stein-Göran and Hélène Ahlqvist, as well as my sisters Gabriella Ahlqvist and Alexandra Schönning for their endless love and support.

DEDICATIONS

To Sheana, Mom, and Dad

Introduction

It has been a fundamental and largely unquestioned assumption in physics until the mid 20th century that the constituents of nature are point-like. While it may not seem like a radical idea, introducing extended objects such as strings into physics has given birth to an entire subfield of mathematical physics known as string theory. By simply requiring a quantum mechanical fundamental string to propagate in a Lorentz invariant way one can show that Einstein's equations of general relativity must be satisfied. What may be even more impressive is that one can also show that consistency can only be achieved in a specific space-time dimension. So, while other theories of physics can be consistently formulated in arbitrary dimensions, string theory *requires* there to be precisely ten dimensions.[1] Clearly, we only experience four such dimensions at low energy so it becomes crucial to understand what happens to the additional six. The most well-studied approach is to *compactify* the additional dimensions on an internal manifold leaving only four large dimensions.

Ideally, one would like to make predictions on how the dynamics of string theory affects low-energy physics in four dimensions. Here we currently reach a roadblock. As it turns out there are many consistent low-energy solutions of string theory, and currently it is not know which, if any, corresponds to our observable universe. This *landscape of string theory* is in many ways one of the major challenges of modern string theory mainly due to its vast size and computational complexity[2]. A heuristic argument based on counting the number of

[1] Interestingly, the fact that this calculation should even yield an integer is not clear at the outset.

[2] There is actually also a landscape in quantum field theory. See the concluding remarks for a brief discussion of this.

inequivalent flux compactifications for a generic Calabi-Yau manifold shows that there may be as many as 10^{500} distinct solutions, clearly too many to sort through one-by-one. Clearly it is of great importance to understand the structure of this landscape which is what we presently attempt.

We begin this dissertation with a review of the required background material. This includes Calabi-Yau manifolds and their associated moduli spaces, an in-depth discussion on warping in the deformed conifold geometry for type IIB supergravity, as well as a brief review of tunneling in quantum field theory and the numerical techniques that are useful in finding these tunneling solutions.

In chapter 2 we focus on understanding the tunneling dynamics in the string landscape. We find that tunneling solutions tend to be drawn incredibly close to the conifold point which corresponds to a degeneration of the compactification manifold. We conclude that the dynamics of the string landscape may be much more involved than previously thought.

In chapter 3 we discuss the statistical properties of the distribution of vacua in moduli space. In particular while past work has concluded that the conifold point acts as an accumulation point for vacua, we find that strong warping corrections highly dilute the distribution in precisely this regime.

Finally, in chapter 4 we investigate whether cosmological slow-roll inflation can be sustained in the landscape. In particular, we look to see if the recently proposed *spiral inflation* has any chance of being realized. Our results here are negative in that spiral inflation, when possible in our models, is actually driven by a vacuum energy rather than any novel form of inflation.

Chapter 1

Background

1.1 Extra Dimensions in String Theory

The work contained in chapters 2, 3, and 4 will focus on various aspects of the string landscape which more or less corresponds to the different compactifications of ten dimensional string theory to four dimensions. As a result, it is very important to understand precisely what these internal dimensions look like. We review the relevant concepts in this section beginning with a brief discussion on supersymmetry in four dimensions and then continuing to Calabi-Yau manifolds and their moduli spaces. The structure of Calabi-Yau manifolds and their space of smooth deformations is an incredibly rich subject. As a result we will here only be able to touch upon the particular concepts utilized in the remainder of this dissertation.

From the perspective of the string action, whether it be the bosonic or supersymmetric version, the dynamics of the string is encoded in a two dimensional field theory where the degrees of freedom can be interpreted as the embedding coordinates of the string, X^μ, $\mu = 0, 1, 2, \ldots, D-1$ and possibly their world-sheet superpartners. The space on which these fields propagate is the two dimensional string world-sheet which corresponds to the space-time surface that the string sweeps out over time. Even though the fields are part of a nontrivial representation of the Lorentz group, this appears in the field theory as a global internal symmetry and is therefore subject to anomalies. Requiring an anomaly free Lorentz symmetry constrains the number of space-time dimensions to be $D = 26$ in the case of a purely bosonic theory and $D = 10$ in supersymmetric string theories. Clearly this seems to be too many since we only observe four such dimensions and it becomes critical to explain what happens to the remaining six. A particularly useful approach to addressing this issue is provided by Kaluza-Klein compactification in which one assumes that the overall space-time takes on a product form between four dimensional Minkowski space M_4 and a six dimensional compact internal manifold M_6

$$M_{10} = M_4 \times M_6. \tag{1.1}$$

The question naturally arises what this internal manifold looks like. In particular, for the superstring one can show that $\mathcal{N} = 1$ supersymmetry in the four dimensional Minkowski space M_4 restricts the manifold to be of *Calabi-Yau* type.

1.1.1 Calabi-Yau Manifolds

The spectrums of the various superstring theories are supersymmetric. In the case of the type IIA and IIB string one obtains extended $\mathcal{N} = 2$ supersymmetry in ten dimensions while for the heterotic and type I strings, standard $\mathcal{N} = 1$ supersymmetry is realized. Based on the following phenomenological and computational reasons, it is reasonable to suspect that $\mathcal{N} = 1$ supersymmetry should emerge at high energies in four dimensions. In particular, the various coupling constants in the standard model seem to unify at high energies if one assumes that the standard model at some point becomes supersymmetric. Furthermore, the Higgs mass tends to receive large quantum corrections unless again supersymmetry emerges at high energies. Finally, supersymmetry also provides us with powerful computational tools. For all of these reasons, it is desirable to make sure that $\mathcal{N} = 1$ supersymmetry survives in $D = 4$ dimensions. Depending on the compactification manifold, various amounts of supersymmetry will survive in the effective four dimensional low-energy theory.

In fact, as we will shortly see, each supersymmetry in ten dimensions can give rise to as many as four supersymmetries in four dimensions. As a result, the $\mathcal{N} = 2$ supersymmetry of the type II string can result in as much as $\mathcal{N} = 8$ supersymmetry in four dimensions. This happens if one takes the internal six dimensional manifold to be a six torus, T^6. Clearly this is too much supersymmetry and as a result one has to look for manifolds that break more supersymmetry.

As has been shown in e.g. [1], the existence of a covariantly constant spinor implies that there are four-dimensional background field configurations that satisfy precisely $\mathcal{N} = 1$ supersymmetry. More precisely, the variations of the bosonic fields are proportional to fermionic fields which necessarily vanish classically. However, the variations of the fermionic fields could potentially break supersymmetry since they are proportional to bosonic fields which do not have to vanish classically. If we set some of these to zero (we will get back to the validity of this later when we discuss flux compactifications), one can show that the variation of the gravitino field is given by

$$\delta\psi_M = \nabla_M \epsilon, \tag{1.2}$$

where ϵ is the parameter for supersymmetry transformations (and is thus a spinor). In order for this to vanish it must be possible to find a covariantly constant spinor field. For the external space this, together with the assumption of maximal symmetry, leads us to the understanding that M_4 must indeed be four dimensional Minkowski space and that the spinors must themselves be constant. For the internal manifold however, the story is much more complex. One can of course always find a spinor field on the internal manifold that locally satisfies $\nabla_a \epsilon = 0$ by simply integrating this equation in some neighborhood. However, it is not always possible to do this globally due to topological obstructions. The statement that a covariantly constant spinor exists is equivalent to the fact that the manifold has special holonomy. The reason is that if one were to parallel transport this particular spinor around any closed loop, it would always return to itself. However, upon parallel transport around a closed loop, spinors on a six dimensional manifold generically transform according to the spinorial representation of $Spin(6) = SU(4)$. For a spinor of definite chirality this representation splits up and it would therefore transform either according to a fundamental or anti-fundamental representation. The only way that a covariantly constant spinor can exist is therefore if the true holonomy is not $SU(4)$ but rather a subgroup of it so that the fundamental of $SU(4)$ contains a singlet under this subgroup. This means that the holonomy must be at most $SU(3)$. If the holonomy is an even smaller subgroup, there will be multiple singlets which means that one obtains extended supersymmetry. In general one obtains one supersymmetry in four dimensions for each supersymmetry in ten dimensions up to a factor of the number of singlets in the fundamental under the holonomy group

$$\mathcal{N}_{4D} = \mathcal{N}_{10D} \times \text{Singlets}. \tag{1.3}$$

As a result, one finds for an $SU(3)$ holonomy manifold $\mathcal{N} = 1$ supersymmetry for the type I and heterotic string and $\mathcal{N} = 2$ supersymmetry for the type II string. Despite giving too much supersymmetry for the type II string we will still consider this compactification since one can add in so-called orientifold planes to the compactification which reduces this to $\mathcal{N} = 1$ supersymmetry. As a result, we are on the hunt for $SU(3)$ holonomy manifolds.

In fact, the existence of a covariantly constant spinor implies a few other properties of the compactification manifold [3, 8]. In particular, as we will discuss in the next section, it must be a complex Kähler manifold. Together with the special holonomy property mentioned above this implies that it must be a *Calabi-Yau* manifold. Just to reiterate, this analysis involved assuming that various bosonic fields vanish or take on constant values. As we will discuss later, turning these fields back on moves us away from the Calabi-Yau constraint and in fact stabilizes various aspects of the internal manifold that would otherwise be unconstrained and thereby (at least partially) solves the so-called *moduli problem.*

In summary, $\mathcal{N} = 1$ supersymmetry in the four extended dimensions dictate that the six internal dimensions must be compactified into a Calabi-Yau manifold. We now go on to discuss some of the properties of this class of manifolds.

Properties of Calabi-Yau Manifolds

A Calabi-Yau manifold is a particular type of a six dimensional manifold which can support complex coordinates in a consistent way (i.e. the transition functions are holomorphic). Moreover, a Calabi-Yau must be Kähler which implies that its metric can locally be written in terms of a Kähler potential,

$$g_{\mu\bar{\nu}} = \partial_\mu \bar{\partial}_{\bar{\nu}} K(z, \bar{z}). \tag{1.4}$$

Alternatively, a Kähler manifold is one whose Kähler form $J = i g_{\mu\bar{\nu}} dz^\mu \wedge d\bar{z}^{\bar{\nu}}$ is closed, that is $dJ = 0$. This can be shown to be equivalent to the statement above that the metric can be written in terms of the Kähler potential. Such a Kähler potential can generally not be continuously defined everywhere so one must work in patches $\{U_i\}$. In the intersection of two or more such patches, $U_i \cap U_j$, the different Kähler potentials must differ by Kähler transformations

$$\Delta K = f(z) + \bar{f}(\bar{z}). \tag{1.5}$$

These transformations leave the metric invariant

$$g_{\mu\bar{\nu}} = \partial_\mu \bar{\partial}_{\bar{\nu}} K \rightarrow \partial_\mu \bar{\partial}_{\bar{\nu}} (K + f(z) + \bar{f}(\bar{z})) = g_{\mu\bar{\nu}}. \tag{1.6}$$

The other components of the metric $g_{\mu\nu}$ and $g_{\bar{\mu}\bar{\nu}}$ vanish. A Calabi-Yau must also support a Ricci flat metric. More precisely $c_1(M_6)$, the first Chern class of M_6, must vanish. The first Chern class is, up to a factor of 2π, the cohomology class of the Ricci curvature 2-form

$$\mathcal{R} = R_{\mu\bar{\nu}} dz^\mu \wedge d\bar{z}^{\bar{\nu}}. \tag{1.7}$$

A highly nontrivial theorem conjectured by Calabi and later proved by Yau in the late 1970s states that any such manifold admits a Ricci flat metric whose corresponding Kähler form is in the same cohomology class as the original Kähler form. The opposite direction is trivially true since a vanishing Ricci form of course corresponds to the trivial cohomology class and therefore the first Chern class of the manifold must vanish. As a result these two definitions can be used interchangeably. Often one speaks of a Calabi-Yau threefold highlighting its complex dimension rather than its real dimension.

One very important consequence of being a Calabi-Yau manifold is that there exists a nowhere vanishing holomorphic 3-form [3, 8]

$$\Omega = \Omega_{\mu\nu\rho}(z) dz^\mu \wedge dz^\nu \wedge dz^\rho. \tag{1.8}$$

Since the components are holomorphic, this form is necessarily closed.

$$\begin{aligned} d\Omega &= (\partial + \bar{\partial})\Omega & (1.9) \\ &= \partial_\alpha \Omega_{\mu\nu\rho}(z) dz^\alpha \wedge dz^\mu \wedge dz^\nu \wedge dz^\rho + \bar{\partial}_{\bar{\alpha}} \Omega_{\mu\nu\rho}(z) d\bar{z}^{\bar{\alpha}} \wedge dz^\mu \wedge dz^\nu \wedge dz^\rho = 0 & (1.10) \end{aligned}$$

The first term vanishes since there are only three linearly independent one-forms (dz^1, dz^2, dz^3) while the wedge product involves four such forms. The second term vanishes because the components of Ω are holomorphic functions of the coordinates. Despite being closed, Ω cannot be exact since $\Omega \wedge \bar{\Omega}$ is proportional to the volume form and if the volume form were exact, the Calabi-Yau volume would vanish according to Stoke's theorem. As a result Ω defines a nontrivial cohomology class in $H^{3,0}$. Since the dimensionality of this class is given by the Hodge number $h^{3,0} = 1$ (see below), this is a representative of the (up to scalings) unique cohomology class in $H^{3,0}$. This fact will be very important to us when we later define integrals of this form over cycles of the Calabi-Yau since if Ω were exact, these would trivially vanish due to Stoke's theorem.

Before we move on, it will be advantageous for us to quickly mention the concept of Hodge numbers and the Hodge diamond. For real manifolds one can compute various topological numbers called Betti numbers which measures the dimensionality of the various de-Rahm cohomology groups. However, since these manifolds are complex, one can refine the notion of exact and closed forms to the holomorphic and anti-holomorphic sectors. In particular, one can consider (r, s) forms that are closed but not necessarily exact with respect to the exterior derivative $\bar{\partial}$. These forms organize into classes called $H^{r,s}_{\bar{\partial}}$ which were used above in discussing the holomorphic 3-form. The dimension of these various spaces are called the Hodge numbers, $h^{r,s}$ and can be arranged in the Hodge diamond. Using various relationships among them that arise from complex conjugation, Hodge duality, and Poincare duality one can compute most of these numbers. The only unspecified Hodge numbers for Calabi-Yau 3-folds are $h^{1,1}$ and $h^{1,2}$. The Hodge diamond therefore becomes

$$\begin{array}{ccccccc} & & & h^{3,3} & & & \\ & & h^{3,2} & & h^{2,3} & & \\ & h^{3,1} & & h^{2,2} & & h^{1,3} & \\ h^{3,0} & & h^{2,1} & & h^{1,2} & & h^{0,3} \\ & h^{2,0} & & h^{1,1} & & h^{0,2} & \\ & & h^{1,0} & & h^{0,1} & & \\ & & & h^{0,0} & & & \end{array} \longrightarrow \begin{array}{ccccccc} & & & 1 & & & \\ & & 0 & & 0 & & \\ & 0 & & h^{1,1} & & 0 & \\ 1 & & h^{1,2} & & h^{1,2} & & 1 \\ & 0 & & h^{1,1} & & 0 & \\ & & 0 & & 0 & & \\ & & & 1 & & & \end{array} \tag{1.11}$$

The two remaining Hodge numbers will provide us with the dimensionality of the space of smooth deformations of Calabi-Yau manifolds referred to as its moduli spaces.

1.1.2 Moduli Space of Calabi-Yau Manifolds

Given a certain Calabi-Yau, there exists a family of smooth deformations of the metric that one can perform that respects the Calabi-Yau structure. In other words, each Calabi-Yau really refers to an infinite set of smoothly connected manifolds. This space can be parametrized by a finite, albeit sometimes rather large, number of parameters.

Consider two nearby metrics g and $g+\delta g$. In order for these to both describe Calabi-Yau manifolds we must have

$$R_{mn}(g) = R_{mn}(g+\delta g) = 0. \tag{1.12}$$

One can then ask what sort of metric deformations δg are possible [3]. Many of these deformations will actually be equivalent to each other by simple coordinate transformations. After choosing a particular gauge, one can show that δg must satisfy the *Lichnerowicz equation*

$$\nabla^k \nabla_k \delta g_{mn} + 2R_{m\ n}^{\ p\ q} \delta g_{pq} = 0. \tag{1.13}$$

Consider then generic metric deformations δg_{mn}. Since this is a complex manifold, we may divide these up into two kinds of deformations: those of mixed indices, $\delta g_{\mu\bar{\nu}}$, and those of pure indices, $\delta g_{\mu\nu}$ and $\delta g_{\bar{\mu}\bar{\nu}}$. Out of these deformations one can define both $(1,1)$ and $(2,1)$ forms which can be shown to be harmonic (see the discussion below which parallels [3]). As a result, the number of linearly independent such deformations can be computed in terms of the Hodge numbers discussed above. In particular the deformations separate into two main classes: Kähler structure deformations and complex structure deformations.

Kähler Deformations

Recall that the Kähler form is given in terms of the metric as

$$J = i g_{\mu\bar{\nu}} dz^\mu \wedge d\bar{z}^{\bar{\nu}}. \tag{1.14}$$

As a result, the metric deformations of the mixed index type, $\delta g_{\mu\bar{\nu}}$ correspond to deformations of the Kähler form. These so-called Kähler structure deformations give rise to a $(1,1)$ form which, using the Lichnerowicz equation, can be shown to be harmonic [3]

$$\Delta\omega = 0 \qquad \text{with} \qquad \omega = \delta g_{\mu\bar{\nu}} dz^\mu \wedge d\bar{z}^{\bar{\nu}} \tag{1.15}$$

As a result, the number of independent Kähler parameters of our Calabi-Yau is given by the Hodge number $h^{1,1}$. Note however, that since $g^*_{\mu\bar{\nu}} = g_{\bar{\mu}\nu}$ the Kähler form is necessarily real. As a result the Kähler parameters parameterize an $h^{1,1}$ dimensional *real* space. Interestingly however there is also a 2-form potential B whose deformations can be combined with these to form a total of $h^{1,1}$ complex parameters. This is traditionally referred to as the *complexification of the Kähler cone* and we speak of the *complexified Kähler form*

$$\mathcal{J} = B + iJ. \tag{1.16}$$

The main point to take away however is simply that the number of complex parameters that preserve the Calabi-Yau structure while modifying the Kähler structure is $h^{1,1}$ which is a topological number specific to each Calabi-Yau family. Also note that since each Calabi-Yau comes equipped with a Kähler form, we must have at least one Kähler parameter, $h^{1,1} \geq 1$.

Complex Structure Deformations

One can also consider the metric deformations of pure type, that is $\delta g_{\mu\nu}$. Once these are implemented, it is clear the metric no longer takes on the Hermitian form of only mixed indices. Is it possible however that by a suitable change of coordinates, one can bring the metric back into such a form? The answer is yes, but that these coordinate transformations cannot be holomorphic since holomorphic transformations preserve the Hermitian metric structure. In other words, if such a holomorphic transformation $w(z), \bar{w}(\bar{z})$ did exist, the inverse transformation would have to take an Hermitian metric into one with nonzero pure components. However, this is not possible:

$$g^{(z)}_{\mu\nu} = \frac{\partial w^\alpha}{\partial z^\mu}\frac{\partial \bar{w}^{\bar{\beta}}}{\partial z^\nu} g^{(w)}_{\alpha\bar{\beta}} + \frac{\partial \bar{w}^{\bar{\alpha}}}{\partial z^\mu}\frac{\partial w^\beta}{\partial z^\nu} g^{(w)}_{\bar{\alpha}\beta} = 0 \quad \text{since} \quad \frac{\partial \bar{w}^{\bar{\alpha}}}{\partial z^\mu} = \frac{\partial \bar{w}^{\bar{\beta}}}{\partial z^\nu} = 0. \tag{1.17}$$

As a result, one must consider transformations that link inequivalent complex structures together. These are therefore referred to as *complex structure deformations*. In order to analyze these further, one can construct a $(2,1)$ form which again using the Lichnerowicz equation can be shown to be harmonic [3]

$$d\eta = 0 \qquad \text{with} \qquad \eta = \Omega_{abc} g^{c\bar{d}} \delta g_{\bar{d}\bar{e}} dz^a \wedge dz^b \wedge d\bar{z}^{\bar{e}} \tag{1.18}$$

There are therefore $h^{1,2}$ linearly independent metric deformations of this type. This time around, the components $\delta g_{\mu\nu}$ are allowed to be complex and the $h^{1,2}$ parameters are thus allowed to be complex as well.

To summarize, there are $h^{1,1} + h^{1,2}$ independent complex parameters that smoothly parameterize the space of metric deformations that are compatible with the Calabi-Yau structure. Since the various manifolds are smoothly deformable into each other it is possible to choose a different compactification manifold for each space-time point in four dimensions. This then implies that these $h^{1,1} + h^{1,2}$ complex parameters will appear in four dimensions as complex scalar fields. This field space is referred to as the *moduli space* of the string theory compactification. It is very important to recognize that these two sectors are independent and that the total moduli space factors into the Kähler side and complex structure side

$$\mathcal{M} = \mathcal{M}_{1,1} \times \mathcal{M}_{1,2}. \tag{1.19}$$

This implies that one can consistently focus on one of these sectors at a time.

An Example - the Quintic

As a canonical example of a Calabi-Yau manifold that will reappear later on, we here give a quick construction of the so-called quintic.

Consider four-dimensional complex projective space $\mathbb{CP}^4$ which is constructed from $\mathbb{C}^5 - \{0\}$ by identifying points $(z_1, \ldots, z_5) \sim \lambda(z_1, \ldots, z_5)$ for $\lambda \in \mathbb{C}$. This space is Kähler and compact although its first Chern class does not vanish. However, by restricting to a hyper surface defined by the vanishing of a quintic polynomial,

$$P(z_1, \ldots, z_5) = 0 \qquad \text{where} \qquad P(\lambda z_1, \ldots, \lambda z_5) = \lambda^5 P(z_1, \ldots, z_5), \tag{1.20}$$

one can retain the Kähler structure of the manifold while setting its first Chern class equal to zero. In other words, this hyper surface is a Calabi-Yau manifold. In principle, each quintic polynomial can give rise to its own distinct Calabi-Yau (although we will shortly see that there is some redundancy in this description). The various polynomials are of course smoothly related to each other by varying their coefficients. For a degree five polynomial in five variables there are

$$\begin{pmatrix} 9 \\ 4 \end{pmatrix} = 126 \tag{1.21}$$

monomials of the form $z_1^{a_1} \ldots z_5^{a_5}$ with $a_a + \ldots + a_5 = 5$. By a holomorphic change of coordinates in the five variables $z^1, \ldots, z^5$, some of these can be removed. In order for this transformation to be globally well defined, it must be of the form $w^i = \alpha^i + M^i_j z^j$. In order for it to also respect the projective identification in $\mathbb{CP}^4$, $(z^1, \ldots, z^5) \sim \lambda(z^1, \ldots, z^5)$, it must also be homogeneous in the coordinates so that the most general form is $w^i = M^i_j z^j$. The matrix M^i_j has 25 independent components, so that 25 of the original 126 parameters can be removed, leaving precisely 101 parameters that cannot be removed using holomorphic changes of coordinates. These therefore represent the complex structure deformations. The Kähler deformations are inherited from the complex projective space in which we are embedding this hyper-surface. As a result, the hodge numbers are $h^{1,1} = 1, h^{1,2} = 101$ for the quintic hyper-surface in $\mathbb{CP}^4$ which is traditionally called *the quintic*.

The Metric on Complex Structure Moduli Space

As mentioned above, the low-energy approximation to string theory will contain scalar fields that can be traced back to the various deformations of the compactification manifold consistent with the Calabi-Yau properties. It is of paramount interest to properly understand their low-energy dynamics. Most naturally one would like to obtain the form of the scalar potential that governs their dynamics. This can be a rather involved problem and so we will postpone a detailed discussion of this until later. Another important aspect of their dynamics is specified by their kinetic terms. Traditionally scalar fields are taken to have canonical kinetic terms

$$\mathcal{L}_{\text{kin}} = \sum_i \partial^\mu \phi_i \partial_\mu \bar{\phi}_i \tag{1.22}$$

However, as we will now discuss, the scalar fields that arise from deformations of the Calabi-Yau compactification manifold will have non-canonical kinetic terms

$$\mathcal{L}_{\text{kin}} = G_{ij}(\phi_a, \bar{\phi}_b)\partial^\mu \phi^i \partial_\mu \bar{\phi}^j. \tag{1.23}$$

This is tantamount to having a nontrivial metric on the moduli space [8]. We take this metric to be the Weil-Peterson metric

$$ds^2 = \frac{1}{2V}\int g^{a\bar{b}} g^{c\bar{d}} \left[\delta g_{ac}\delta g_{\bar{b}\bar{d}} + (\delta g_{a\bar{d}}\delta g_{c\bar{b}} + \delta B_{a\bar{d}}\delta B_{c\bar{b}})\right]\sqrt{g} d^6 x. \tag{1.24}$$

Here we are integrating over the entire Calabi-Yau and take V as its total volume.[1] We will for the remainder of this dissertation focus on the complex structure deformations and only in passing mention the Kähler structure part of the story. As a result, we can effectively work with the moduli space metric

$$ds^2 = \frac{1}{2V}\int g^{a\bar{b}} g^{c\bar{d}} \delta g_{ac}\delta g_{\bar{b}\bar{d}}\sqrt{g} d^6 x. \tag{1.25}$$

The variations δg_{ab} must be linear combinations of the $h^{1,2}$ allowed deformations. Let us decide on a basis for this space, $\delta g^{(\alpha)}_{ab}$ where the α labels the basis element. We can then

[1] It is important to realize that this metric on moduli space is physically distinct from the metric that exists on the Calabi-Yau itself. In fact, although we will soon determine the metric on moduli space, no nontrivial Calabi-Yau metrics are currently known.

write a generic deformation in terms of $h^{1,2}$ complex coordinates t^α as

$$\delta g_{ab} = t^\alpha \delta g_{ab}^{(\alpha)} \tag{1.26}$$

$$\delta g_{\bar{a}\bar{b}} = \bar{t}^{\bar{\alpha}} \delta g_{\bar{a}\bar{b}}^{(\bar{\alpha})}. \tag{1.27}$$

The moduli space metric can then be written as

$$ds^2 = 2G_{\alpha\bar{\beta}}\delta t^\alpha \delta \bar{t}^{\bar{\beta}} \qquad \text{with } G_{\alpha\bar{\beta}} = \frac{1}{4V}\int_{\mathcal{M}} g^{a\bar{b}} g^{c\bar{d}} \delta g_{ac}^{(\alpha)} \delta g_{\bar{b}\bar{d}}^{(\bar{\beta})} \sqrt{g} d^6 x \tag{1.28}$$

We will now run through a standard argument [3] that allows us to write $G_{\alpha\bar{\beta}}$ entirely in terms of the holomorphic 3-form Ω that is defined on the Calabi-Yau manifold. The main idea is as follows. When we decide to deform the metric by adding say $\delta g_{ab} = \delta t^\alpha \delta g_{ab}^{(\alpha)}$ and $\delta g_{\bar{a}\bar{b}} = \overline{\delta g_{ab}}$ we must, as mentioned above, also change coordinates in a way that changes the complex structure of the manifold. One should in principle be able to compute the necessary coordinate transformation (we take δt^α infinitesimal)

$$z^a \to z^a(z^1, z^2, \ldots, \bar{z}^1, \bar{z}^2, \ldots) \approx z^a + M_\alpha^a(z^1, z^2, \ldots, \bar{z}^1, \bar{z}^2, \ldots)\delta t^\alpha \tag{1.29}$$

for some function of the original coordinates M_α^a. Given this coordinate transformation, one can compute what happens to the holomorphic 3-form. In particular, it will no longer be of pure $(3,0)$ type since the basis 1-forms will pick up an anti-holomorphic part

$$dz^a \to dz^a + dM_\alpha^a \delta t^\alpha \tag{1.30}$$

$$= dz^a + \left(\frac{\partial M_\alpha^a}{\partial z^b} dz^b + \frac{\partial M_\alpha^a}{\partial \bar{z}^{\bar{b}}} d\bar{z}^{\bar{b}}\right)\delta t^\alpha \tag{1.31}$$

$$= (\delta_b^a + \frac{\partial M_\alpha^a}{\partial z^b}\delta t^\alpha) dz^b + \frac{\partial M_\alpha^a}{\partial \bar{z}^{\bar{b}}}\delta t^\alpha d\bar{z}^{\bar{b}}. \tag{1.32}$$

Furthermore since the 3-form components carry indices they also transform under the coordinate transformation. Putting all of this together, one finds that Ω becomes partly a $(3,0)$

form and partly a $(2,1)$ form. Since the exterior derivative is independent of the moduli space coordinates, these new forms must also be closed and therefore define cohomology classes in $H^{3,0}$ and $H^{2,1}$ as usual

$$\partial_\alpha \Omega \in H^{3,0} \oplus H^{2,1}. \tag{1.33}$$

Since Ω is a representative of the unique class (up to scalings) of the cohomology group $H^{3,0}$ (recall that the Hodge number $h^{3,0} = 1$), the $(3,0)$ part must be proportional to Ω itself and we therefore have

$$\partial_\alpha \Omega = K_\alpha \Omega + \chi_\alpha \tag{1.34}$$

for some closed $(2,1)$ form χ_α and function K_α. Note that K_α only depends on the moduli space coordinates and is completely independent of the coordinates on the Calabi-Yau itself. The reason for this is that if K_α depended on the Calabi-Yau coordinates, we would have defined another closed $(3,0)$ form $K_\alpha \Omega$ which is in a class of $H^{3,0}$ that is linearly independent of the class that Ω is in which contradicts the fact that $h^{3,0} = 1$.

One can of course run this argument backwards. Given a $(2,1)$ form χ_α and a value for K_α, one can compute the metric deformation δg_{ab}. If we define the components of χ_α as

$$\chi_\alpha = \frac{1}{2}(\chi_\alpha)_{ab\bar{c}} dz^a \wedge dz^b \wedge d\bar{z}^{\bar{c}}, \tag{1.35}$$

one obtains for the metric deformations

$$\delta g_{\bar{a}\bar{b}} = -\frac{1}{||\Omega||^2} \bar{\Omega}_{\bar{a}}{}^{cd} (\chi_\alpha)_{cd\bar{b}} \delta t^\alpha \tag{1.36}$$

where we have defined the scalar

$$||\Omega||^2 = \frac{1}{6} \Omega_{abc} \bar{\Omega}^{abc}. \tag{1.37}$$

In fact, $||\Omega||^2$ is constant over the Calabi-Yau manifold [3] (however it is not constant over the moduli space). One can then use this in the moduli space metric from (1.28) to obtain

$$G_{\alpha\bar{\beta}} = -\frac{\int \chi_\alpha \wedge \bar{\chi}_\beta}{\int \Omega \wedge \bar{\Omega}}. \tag{1.38}$$

Using the form for χ_α from (1.34), we can write this as

$$\begin{aligned} G_{\alpha\bar{\beta}} &= \frac{\int (\partial_\alpha\Omega - K_\alpha\Omega) \wedge (\bar{\partial}_{\bar{\beta}}\bar{\Omega} - K_{\bar{\beta}}\bar{\Omega})}{\int \Omega \wedge \bar{\Omega}} && (1.39) \\ &= -\left\{ \frac{\int \partial_\alpha\Omega \wedge \bar{\partial}_{\bar{\beta}}\bar{\Omega}}{\int \Omega \wedge \bar{\Omega}} - K_\alpha \frac{\int \Omega \wedge \bar{\partial}_{\bar{\beta}}\bar{\Omega}}{\int \Omega \wedge \bar{\Omega}} - K_{\bar{\beta}} \frac{\int \partial_\alpha\Omega \wedge \bar{\Omega}}{\int \Omega \wedge \bar{\Omega}} + K_\alpha K_{\bar{\beta}} \right\} && (1.40) \end{aligned}$$

At this point write $\partial_\alpha\Omega$ as $K_\alpha\Omega + \chi_\alpha$ again and similarly for $\bar{\partial}_{\beta}\bar{\Omega}$ in the middle two terms. Then recognize that the wedge product between a $(3,0)$ form such as $K_\alpha\Omega$ and a $(2,1)$ such as $\bar{\chi}_{\bar{\beta}}$ vanishes identically so that

$$G_{\alpha\bar{\beta}} = -\left\{ \frac{\int \partial_\alpha\Omega \wedge \bar{\partial}_{\bar{\beta}}\bar{\Omega}}{\int \Omega \wedge \bar{\Omega}} - K_\alpha K_{\bar{\beta}} \right\} \tag{1.41}$$

Of course Ω is holomorphic over the Calabi-Yau, but it can be shown that Ω varies holomorphically with respect to the moduli space coordinates as well [8]. As a result the following partial derivatives with respect to the moduli space coordinates vanish when applied to Ω and $\bar{\Omega}$

$$\begin{aligned} \partial_\alpha\bar{\Omega} &= 0 && (1.42) \\ \bar{\partial}_{\bar{\beta}}\Omega &= 0. && (1.43) \end{aligned}$$

The above expression for the metric can therefore be written as

$$G_{\alpha\bar{\beta}} = \partial_\alpha\partial_{\bar{\beta}} \left\{ -\log\left(i \int \Omega \wedge \bar{\Omega} \right) \right\}. \tag{1.44}$$

In other words, the moduli space of the given Calabi-Yau compactification is also Kähler, that is $G_{\alpha\bar{\beta}} = \partial_\alpha \partial_{\bar{\beta}} K$ with the Kähler potential

$$K = -\log\left(i \int \Omega \wedge \bar{\Omega}\right). \tag{1.45}$$

Note that K is real according to this definition

$$K^* = -\log\left(-i \int \bar{\Omega} \wedge \Omega\right) = -\log\left(i \int \Omega \wedge \bar{\Omega}\right) = K \tag{1.46}$$

since the two 3-forms Ω and $\bar{\Omega}$ anti-commute. In order to determine the form of the function K_α from (1.34) we take the wedge product of (1.34) with $\bar{\Omega}$ on both sides and integrate over the Calabi-Yau.

$$\int \partial_\alpha \Omega \wedge \bar{\Omega} = K_\alpha \int \Omega \wedge \bar{\Omega} + \int \chi_\alpha \wedge \bar{\Omega} \tag{1.47}$$

Since χ_α is a $(2,1)$ form and $\bar{\Omega}$ is a $(0,3)$ form, their wedge product vanishes identically and so the last term above is zero. One can then solve for K_α to find

$$K_\alpha = \frac{\int \partial_\alpha \Omega \wedge \bar{\Omega}}{\int \Omega \wedge \bar{\Omega}} \tag{1.48}$$

Once again, since Ω only depends on the moduli space coordinates t^α holomorphically and vice versa for $\bar{\Omega}$, the partial derivative can be moved out to give

$$K_\alpha = -\partial_\alpha K. \tag{1.49}$$

As a result, the $(2,1)$ form χ_α can actually be written as

$$\chi_\alpha = (\partial_\alpha + \partial_\alpha K)\Omega. \tag{1.50}$$

We will soon see that this particular combination can be interpreted as a covariant derivative with respect to Kähler transformations. Interestingly, although in principle one would imagine that $(\partial_\alpha + \partial_\alpha K)\Omega \in H^{3,0} \oplus H^{2,1}$, it is actually completely contained in $H^{2,1}$. We will get back to all of these expressions later on when we get to the bulk of the discussion.

Kähler Transformations

The holomorphic 3-form is only defined up to an overall scaling. With our understanding of the moduli space one can actually scale Ω differently at different points in moduli space. Consider then multiplying it by a moduli dependent function

$$\Omega \to e^{f(t)}\Omega. \tag{1.51}$$

Note that the scaling function is holomorphic in t^α which is consistent with our previous comments on how Ω must depend holomorphically on the moduli space coordinates. The Kähler potential then changes according to

$$e^{-K} \to i \int e^{f(t)}\Omega \wedge e^{\bar{f}(\bar{t})}\bar{\Omega} = e^{f(t)+\bar{f}(\bar{t})}e^{-K} \tag{1.52}$$

so that

$$K \to K - f(t) - \bar{f}(\bar{t}). \tag{1.53}$$

This is known as a *Kähler transformation*. As a result, the Kähler potential is only defined up to such transformations. Fortunately, as we mentioned above, the metric does not actually change under a Kähler transformation since it is obtained by applying both a holomorphic and an anti-holomorphic derivative to K. Furthermore, it is clear that the partial derivative does not transform covariantly under Kähler transformations when applied to Ω

$$\partial_\alpha\Omega \to \partial_\alpha \left(e^{f(t)}\Omega\right) = e^{f(t)}\partial_\alpha\Omega + e^{f(t)}\Omega\partial_\alpha f(t). \tag{1.54}$$

However, one can define the Kähler covariant derivative aluded to above

$$D_\alpha \Omega = \partial_\alpha \Omega + (\partial_\alpha K)\Omega. \tag{1.55}$$

This definition of the derivative does transform covariantly since the connection K_α transforms in such a way as to absorb the extra terms

$$D_\alpha \Omega = \partial_\alpha \Omega + (\partial_\alpha K)\Omega \to \partial_\alpha \left(e^{f(t)}\Omega\right) + (\partial_\alpha K - \partial_\alpha f(t)) \left(e^{f(t)}\Omega\right) = e^{f(t)} D_\alpha \Omega. \tag{1.56}$$

Similarly, it is clear that the form of the other Kähler covariant derivatives are

$$\begin{aligned} \bar{D}_{\bar{\alpha}} \Omega &= \bar{\partial}_{\bar{\alpha}} \Omega = 0 && (1.57) \\ D_\alpha \bar{\Omega} &= \partial_\alpha \bar{\Omega} = 0 && (1.58) \\ \bar{D}_{\bar{\alpha}} \bar{\Omega} &= \bar{\partial}_{\bar{\alpha}} \bar{\Omega} + (\bar{\partial}_{\bar{\alpha}} K)\bar{\Omega}. && (1.59) \end{aligned}$$

Period Functions and Special Geometry

It is clear from the above discussion that there is a tight link between the coordinates on the moduli space and the holomorphic 3-form. More precisely, given the holomorphic 3-form at two nearby points, one can compute the Kähler potential using (1.45) and then the $(2, 1)$ form $\chi_\alpha \delta t^\alpha$ using (1.50). The metric deformation δg_{ab} can then be found from (1.36). This can all be done without any explicit reference to the coordinate system t^α. As a result, Ω carries all the information in it pertaining to the coordinates on moduli space. One can therefore use the 3-form to create a set of coordinates for $\mathcal{M}_{1,2}$.

One way to do this is to consider integrals of Ω over various 3-cycles, the *periods* [3, 8]. Here it is important to recall that Ω is closed but not exact since the integral of an exact form over a 3-cycle must vanish. Although there are infinitely many 3-cycles, here we only care about 3-cycles in distinct homology classes. The reason is that according to Stoke's theorem the integral of a closed form such as Ω over 3-cycles in the same homology class (that is, they differ by the boundary of a 4-surface) are equal

$$\int_{M+\partial N} \Omega = \int_M \Omega + \int_{\partial N} \Omega = \int_M \Omega + \int_N d\Omega = \int_M \Omega. \tag{1.60}$$

We must thus find a basis of homology classes in H_3. We choose the *symplectic basis* where the cycles are split into two groups, the $\mathcal{A}$-*cycles* and the $\mathcal{B}$-*cycles* where none of the $\mathcal{A}$-cycles intersect each other and similarly for the $\mathcal{B}$-cycles. However, for each cycle in one group there is a cycle in the other group that does intersect it

$$A^I \cap A^J = 0 \quad B_I \cap B_J = 0 \quad A^I \cap B_J = -B_J \cap A^I = \delta^I_J. \tag{1.61}$$

This is analogous to how one can choose the cycles on a two dimensional surface. One can

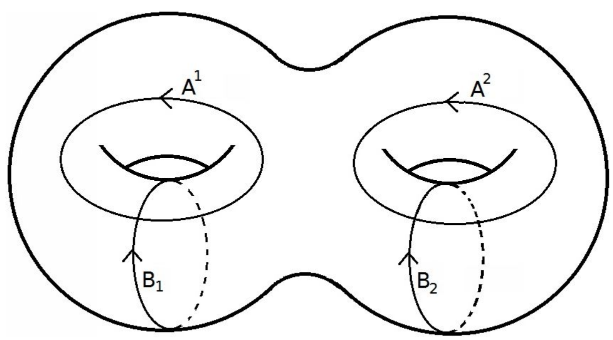

Figure 1.1: Here we illustrate the $\mathcal{A}$ and $\mathcal{B}$ cycles for a $g = 2$ surface in two dimensions. The 3-cycles on the Calabi-Yau would be higher dimensional generalizations of these.

then define the periods over these cycles as

$$X^I = \int_{A^I} \Omega \tag{1.62}$$

$$F_J = \int_{B_J} \Omega. \tag{1.63}$$

All of the information that Ω contains is also contained in the periods. This can easily be seen by writing Ω explicitly in terms of them as

$$\Omega = X^I \alpha_I - F_J \beta^J. \tag{1.64}$$

Here we have introduced the 3-forms α_I and β^J dual to these cycles A^I and B_J so that

$$\int_{A^J} \alpha_I = \delta_I^J \quad \text{and} \quad \int_{B_J} \alpha_I = 0 \tag{1.65}$$

$$\int_{B_J} \beta^I = -\delta_J^I \quad \text{and} \quad \int_{A^J} \beta^I = 0. \tag{1.66}$$

The periods X^I, F_J must therefore contain enough information to construct a coordinate system for the moduli space. In fact, there is a large redundancy among them since there are more periods than there should be coordinates. In particular there are $\dim(H_3) = b_3$ distinct classes of 3-cycles. Using the fact that H_3 and H^3 are isomorphic to each other, this equals b^3. Furthermore, this Betti number can be written in terms of the Hodge numbers as $b^3 = h^{3,0} + h^{2,1} + h^{1,2} + h^{0,3} = 2(1 + h^{1,2})$. There are therefore more than twice as many classes of 3-cycles as there are moduli space coordinates. As a result, the F_J periods can be taken to depend on the X^I periods

$$F_J = F_J(X^I). \tag{1.67}$$

However, the various X^Is still overparametrize the space since there are $h^{1,2}+1$ such periods. This is accounted for by noting that Ω is itself only defined up to an overall scaling. The X^I are therefore projective coordinates. In a patch where $X^0 \neq 0$ one can then define the $h^{1,2}$ coordinates

$$t^\alpha = \frac{X^\alpha}{X^0} \qquad \text{for } \alpha = 1, 2, \ldots, h^{1,2}. \tag{1.68}$$

The fact that the periods F_J depend on the periods X^I leads to the idea of *special geometry*

[8]. To see how this works, consider differentiating Ω with respect to X^I

$$\partial_I \Omega = \alpha_I - \frac{\partial F_J}{\partial X^I} \beta_J. \tag{1.69}$$

Since $\partial_I \Omega$ must be the sum of a $(2,1)$ form and a $(3,0)$ form as we showed above, the wedge product $\Omega \wedge \partial_I \Omega$ vanishes so that

$$\int \Omega \wedge \partial_I \Omega = 0. \tag{1.70}$$

In terms of the periods, this implies that

$$F_I = X^J \partial_I F_J. \tag{1.71}$$

This can trivially be rewritten as

$$F_I = \partial_I \mathcal{F} \tag{1.72}$$

where we have defined the *pre-potential*,

$$\mathcal{F} = \frac{1}{2} X^I F_I \tag{1.73}$$

The fact that the periods F_I can be derived from a single function, $\mathcal{F}$ is referred to as *special geometry* [8].

1.2 The Type II Superstring

There are five consistent string theories in ten dimensions. Throughout this dissertations, we will focus exclusively on one of these called type IIB string theory, or more precisely its low-energy limit, type IIB supergravity. In this section we briefly review the idea of the superstring and provide a heuristic derivation of the field content of type IIB supergravity. We then write down the action for this theory and discuss its $SL(2,\mathbb{Z})$ symmetry.

The first approach toward writing down a string action is the Polyakov action for the bosonic string. However, this action only leads to states which are space-time bosons and as such is not phenomenologically viable. There are two main approaches for incorporating fermions into the theory. The most natural approach would be to formulate the theory not in D dimensional space-time, but rather in superspace. There is however another equivalent formulation known as the Ramond-Neveu-Schwarz (RNS) formalism that we employ here. It is not immediately clear that these two formulations are equivalent or even that the RNS formalism results in space-time fermions although the latter of these claims will be confirmed below. The main idea of the RNS formalism is to add fermonic fields to the *world-sheet* theory in such a way as to respect world-sheet supersymmetry. As a result, the spinors must themselves transform as vectors under the global Lorentz group and thus carry a vector index. Furthermore, in $D=2$, it is possible to define Majorana-Weyl spinors. We take the spinors ψ_+^μ and ψ_-^μ below to be of precisely this form for positive and negative chirality respectively. The superstring action is then

$$S=-\frac{1}{4\pi\alpha'}\int d^2\sigma\left(\partial_\alpha X_\mu\partial^\alpha X^\mu-2i\psi_+^\mu\partial_-\psi_{\mu+}-2i\psi_-^\mu\partial_+\psi_{\mu-}\right). \tag{1.74}$$

We will now continue by discussing the open and closed superstrings.

1.2.1 The Open String

Boundary Conditions

Varying the action in (1.74) with respect to the fermionic fields yields the usual equations of motion that one would expect

$$\partial_\pm \psi^\mu_\mp = 0. \tag{1.75}$$

These yield left moving and right moving sectors. Just like for the bosonic string we must also specify our boundary conditions. In the case of the bosonic string, the action contains two derivatives. As a result, the boundary term can be sent to zero by either choosing fixed endpoints (Dirichlet boundary conditions) or vanishing σ derivative (Neumann boundary conditions). In our case, the action is only first order in derivatives, so we won't be able to send the boundary terms to zero by simply setting the σ derivatives to zero. However, at the same time we now have two independent fields ψ_+ and ψ_-. As a result, it may not be necessary to have both of these fields fixed at $\sigma = 0, \pi$. Instead, one may be able to play the fields off each other. In particular, the boundary term is

$$\delta S \supset \int d\tau \left[\left(\psi_+ \delta\psi_+ - \psi_- \delta\psi_-\right)_{\sigma=\pi} - \left(\psi_+ \delta\psi_+ - \psi_- \delta\psi_-\right)_{\sigma=0} \right]. \tag{1.76}$$

We can make this vanish by taking

$$\psi_+ = \pm\psi_- \qquad \text{at the endpoints of the string.} \tag{1.77}$$

These two choices are both consistent. The choice $\psi_+ = \psi_-$ is called *Ramond* boundary conditions (denoted R for short) while the other choice, $\psi_+ = -\psi_-$ is called Neveu-Schwarz boundary conditions (denoted NS for short). One can show that the states that arise from the Ramond sector are space-time fermions while those from the Neveu-Schwarz sector are space-time bosons.

Massless Field Content

The next step in the analysis involves writing the fermionic fields in terms of a Fourier expansion. The coefficients of these modes become raising and lowering operators in the quantum theory, something that is familiar from standard quantum field theory as well as from the bosonic string. Just like for the bosonic string, the ground state for the superstring is tachyonic. However, there is a consistent truncation of the theory which keeps only those states with an odd number of (world-sheet) fermionic raising operators. As a result, the tachyonic state is eliminated and the new set of states after this *GSO projection* have non-negative mass-squared. The massless states (which are the ones that are kept in a low-energy effective supergravity limit) consists of a massless vector field in the NS sector, $\mathbf{8}_v$ and a massless spinor in the R sector. Since the spinor is massless it transforms under the little group $SO(8)$. The spinorial representation of this group has dimension $2^{8/2} = 16$ but is reducible into two inequivalent Weyl spinors each of dimension 8, $\mathbf{16} = \mathbf{8}_L \oplus \mathbf{8}_R$. Whether one chooses the left-handed or right-handed spinor is a matter of convention for the open string, so we will for convenience simply choose the left-handed one. As a result, the open string gives us a low-energy field content of

$$\mathbf{8}_v \oplus \mathbf{8}_L. \tag{1.78}$$

A point that is far from obvious is that the supergravity theory is supersymmetric.

1.2.2 The Closed String

As is familiar from the bosonic string, the closed string sector can be thought of as two copies of the open string tensored together. As a result, the low-energy field content of the closed string will be that of $(\mathbf{8}_v \oplus \mathbf{8}_{Spinor}) \otimes (\mathbf{8}_v \oplus \mathbf{8}_{Spinor})$. Now, in the open string the chirality of the spinorial sector was a matter of convention. However, here we obtain two distinct possibilities: do the two sectors have the same or opposite chirality? These turn out to be physically distinct theories with different field content. In particular, one obtains type IIA string theory/supergravity if the two spinors have opposite chirality while one obtains type IIB string theory/supergravity if the two spinors have the same chirality. Since we will focus on the type IIB theory for the remainder of this dissertation, we just work out the field content of type IIB. The two spinors have the same chirality for type IIB, but which chirality is still a matter of convention. Let us pick the $\mathbf{8}_L$ for definiteness. The massless sector then becomes

$$(\mathbf{8}_v \oplus \mathbf{8}_L) \otimes (\mathbf{8}_v \oplus \mathbf{8}_L) = (\mathbf{8}_v \otimes \mathbf{8}_v) \oplus (\mathbf{8}_v \otimes \mathbf{8}_L) \oplus (\mathbf{8}_L \otimes \mathbf{8}_v) \oplus (\mathbf{8}_L \otimes \mathbf{8}_L) \tag{1.79}$$

The first term represents the NS-NS sector since it is obtained by tensoring two copies of the field content that originates in the NS sector. The middle two terms similarly represents the NS-R and R-NS sectors respectively while the final term represents the R-R sector. Out of these terms, only the NS-NS and R-R sectors lead to space-time bosons (the remaining ones result in their fermionic superpartners). The NS-NS sector follows the standard anti-symmetric tensor/symmetric traceless tensor/trace decomposition

$$\mathbf{8}_v \otimes \mathbf{8}_v = \mathbf{1} \oplus \mathbf{28} \oplus \mathbf{35}. \tag{1.80}$$

The last of these fields is the graviton in 10 dimensions while the first one is the scalar known as the *dilaton*. The middle field is the antisymmetric tensor (or more precisely, 2-form). The NS-NS sector thus gives rise to the fields

$$\text{NS-NS} \quad \rightarrow \quad g_{MN} \ , \ B^{(2)}_{MN} \ , \ \phi. \tag{1.81}$$

As for the R-R sector, the reduction into irreducible representations of $SO(8)$ gives us p-form fields of three different orders with dimensions 1, 28, and 35[2]

$$\mathbf{8}_L \otimes \mathbf{8}_L = \mathbf{1} \oplus \mathbf{28} \oplus \mathbf{35}. \tag{1.82}$$

These R-R p-form fields are traditionally labeled as follows

$$\text{R-R} \quad \rightarrow \quad C^{(0)} \ , \ C^{(2)}_{MN} \ , \ C^{(4)}_{MNPQ}. \tag{1.83}$$

They of course have corresponding field strengths,

$$F_1 = dC^{(0)} \tag{1.84}$$

$$F_3 = dC^{(2)} \tag{1.85}$$

$$F_5 = dC^{(4)}. \tag{1.86}$$

We now move on to the low-energy supergravity limit that this field content gives us.

1.2.3 Type IIB Supergravity

The fields above interact at low energies according to the following type IIB supergravity action

$$S_{IIB} = \frac{1}{2\kappa_{10}^2}\int d^{10}x\sqrt{-g}\left(R - \frac{|\partial\tau|^2}{2\tau_I^2} - \frac{|G_3|^2}{12\tau_I} - \frac{|\tilde{F}_5|^2}{4\cdot 5!}\right) + \frac{1}{8i\kappa_{10}^2}\int \frac{C^{(2)}\wedge G_3 \wedge \bar{G}_3}{\tau_I} \tag{1.87}$$

Here we have combined the field content from the previous section in various convenient forms. In particular we have defined the axio-dilaton by combining the zero form R-R field with the NS-NS dilaton

$$\tau = C^{(0)} + ie^{-\phi}. \tag{1.88}$$

[2]Note that the dimensionality of this 4-form reflects the constraint that we discuss later that its field strength must be self dual

We have also combined the NS-NS 3-form field strength $H_3 = dB^{(2)}$ and the R-R 3-form field strength $F_3 = dC^{(2)}$ into

$$G_3 = F_3 - \tau H_3. \tag{1.89}$$

Finally, we have defined

$$\tilde{F}_5 = F_5 - \frac{1}{2}C^{(2)} \wedge H_3 + \frac{1}{2}F_3 \wedge B^{(2)} \tag{1.90}$$

This 5-form is self dual, something that must be imposed separately from the equations of motion

$$*\tilde{F}_5 = \tilde{F}_5. \tag{1.91}$$

An interesting aspect of this action is that it exhibits an explicit $SL(2,\mathbb{R})$ symmetry under which τ and G_3 transform as

$$\tau \rightarrow \frac{a\tau + b}{c\tau + d} \tag{1.92}$$

$$G_3 \rightarrow \frac{G_3}{c\tau + d}. \tag{1.93}$$

In the quantum theory, this is broken to an $SL(2,\mathbb{Z})$ symmetry.

1.3 Flux Compactification

In chapters 2, 3, and 4 we will investigate various aspects of the potentials that govern the dynamics of the moduli of Calabi-Yau compactifications. In this section we review how these potentials arise via so-called *flux compactification* following the argument due to [12]. In particular we begin by discussing the notion of warped compactifications which are necessary modifications to the compactification of supergravity once fluxes are introduced. We then go on to to discuss the back-reaction of these fluxes on the geometry near a singular configuration of the Calabi-Yau called the *conifold* [4, 5]. This back-reaction due to warping will be essential in all of the following chapters.

As we have eluded to a few times already, each Calabi-Yau manifold actually represents an infinite number of distinct manifolds that are connected in a multi-dimensional moduli space. The parameters of this space become massless scalar fields upon compactification. Since no massless scalar fields have ever been observed, this presents us with a problem – *the moduli problem*. The moduli come in two distinct sectors, the Kähler moduli and the complex structure moduli. Out of these two sectors, the latter can be stabilized via *flux compactifications*. The idea is to turn on background configurations for the 3-form fluxes F_3 and H_3 from type IIB supergravity to achieve the stabilization. Interestingly these background configurations can exist without sources much in the same way that a nonzero vector field can exist on a torus. There are however some subtleties about this approach. As a result, one must be slightly more general. In particular one considers *warped compactifications* where the space-time manifold does not quite factor into and external and internal piece but rather as

$$ds^2 = e^{2A(y)}\eta_{\mu\nu}dx^\mu dx^\nu + e^{-2A(y)}g_{mn}dy^m dy^n. \tag{1.94}$$

Here $\mu, \nu = 0, 1, 2, 3$ denote four dimensional space-time while $m, n = 5, 6, \ldots, 9$ represent the internal space. Notice the nontrivial *warp factor* in front of the Minkowski metric and the Calabi-Yau[3] metric, g_{mn}, in (1.94). This implies that as one moves in the internal space, the effective scale of the external space varies. Furthermore, note that in order to maintain four dimensional Poincaré invariance, the warp factor can only depend on the internal coordinates $A = A(y)$. For a long time, it was believed that such warped compactifications were impossible due to a no-go theorem [10] that we now turn to.

1.3.1 No-Go Theorem

Here we review the results from [10]. We will consider the most general background configuration of type IIB supergravity that is consistent with four dimensional Poincaré invariance. The axio-dilaton can only depend on the internal coordinates,

$$\tau = \tau(y). \tag{1.95}$$

The 5-form field strength $\tilde{F}_5$ can furthermore only have either four components in the external four dimensional space or none at all. These are of course related via Hodge duality, and since this 5-form is already self dual, we can write the most general background configuration for it as

$$\tilde{F}_5 = (1 + *)[d\alpha(y) \wedge dx^0 \wedge dx^1 \wedge dx^2 \wedge dx^3]. \tag{1.96}$$

Finally, there is no way for the 3-form fluxes F_3, H_3 to take on any external components without breaking Poincaré invariance. As a result, we must take

$$F_3, H_3 \in H^3(M_6, \mathbb{Z}). \tag{1.97}$$

The fact that we are here restricting to the integer cohomology is simply because the fluxes must be quantized according to a generalized Dirac quantization condition.

[3]Technically once we allow for non-vanishing background configurations for the various form fields, our analysis that showed that the internal space must be a Calabi-Yau is invalidated. However, one can run through a similar argument to show that the internal manifold must still be conformally Calabi-Yau which precisely means that the metric must take the form of (1.94) with g_{mn} a Calabi-Yau metric.

One can then use these background configurations in the trace reversed Einstein field equations [10] obtained by varying the type IIB action with respect to the metric,

$$R_{MN} = \kappa_{10}^2 \left(T_{MN} - \frac{1}{8} g_{MN} T \right), \tag{1.98}$$

where T_{MN} is the stress energy tensor of the type IIB field content and T its trace. By looking at the external components of this equation $M, N = 0, 1, 2, 3$ and tracing over them, one then obtains an equation for the warp factor

$$\nabla^2 e^{4A} = e^{2A} \frac{G_{mnp} \bar{G}^{mnp}}{12 \tau_I} + e^{-6A} [\partial_m \alpha \partial^m \alpha + \partial_m e^{4A} \partial^m e^{4A}]. \tag{1.99}$$

Here, the Laplacian as well as all the implied metric contractions in e.g. $\partial_m \alpha \partial^m \alpha$ are obtained using the Calabi-Yau metric g_{mn}. Now, integrate this expression over the entire Calabi-Yau. The left-hand side must vanish since it is a total derivative. The right-hand side must therefore also vanish upon integration. However, the right-hand side is positive semi-definite. The only way that the integral of the right-hand side can vanish is therefore if each term vanishes identically. One then obtains the no-go theorem that states that the only possible background configurations are

$$G_3 = 0 \tag{1.100}$$

$$e^{4A} = \text{constant} \tag{1.101}$$

$$\tilde{F}_5 = 0 \tag{1.102}$$

The last condition follows from the fact that α is constant. As a result, one finds that the contribution of the various form fields vanishes and therefore that they cannot be used to stabilize the internal manifold. There is however a nice way to evade this no-go theorem. This involves adding various sources to the story.

1.3.2 Adding Local Sources

So far we have only written down the part of the low-energy theory pertaining to the gauge fields. In particular, we have not yet discussed what objects source the various fields. A generalized version of Gauss' law states that once we have found an object that sources the field strength F_p one can find its charge by surrounding it by a higher dimensional sphere and then integrating the field strength over it. For a field strength F_p, this must be a p dimensional sphere, S^p. As a result, the object must have precisely $p+1$ transverse spatial dimensions. Given a total of $D-1$ spatial dimensions, the object must itself be $D-p-2$ dimensional. These higher dimensional objects are well known from a discussion of open strings, they are D-branes. As a result, the field strengths of type IIB supergravity couple magnetically[4] to the following D-branes

$$F_1 \qquad \text{couples magnetically to} \qquad D7 \text{ branes} \tag{1.103}$$

$$F_3 \qquad \text{couples magnetically to} \qquad D5 \text{ branes} \tag{1.104}$$

$$F_5 \qquad \text{couples magnetically to} \qquad D3 \text{ branes} \tag{1.105}$$

Similarly, one can couple electrically to various branes. The same counting works as above expect that one finds the charge by integrating $*F_p$ over a sphere rather than F_p. As a result, F_p couples electrically to a brane with dimension $p-2$.

$$F_1 \qquad \text{couples electrically to} \qquad D(-1) \text{ branes} \tag{1.106}$$

$$F_3 \qquad \text{couples electrically to} \qquad D1 \text{ branes} \tag{1.107}$$

$$F_5 \qquad \text{couples electrically to} \qquad D3 \text{ branes} \tag{1.108}$$

The D(-1) brane is a D-instanton while the D1 brane is a D-string.

By considering these sources in addition to the field strengths, one finds that warped

[4]Which one is called electric and which one is called magnetic is a matter of convention.

compactifications become possible [12]. In particular the sources will contribute to the right-hand side of Einstein's equations

$$\nabla^2 e^{4A} = e^{2A}\frac{G_{mnp}\bar{G}^{mnp}}{12\tau_I} + e^{-6A}[\partial_m\alpha\partial^m\alpha + \partial_m e^{4A}\partial^m e^{4A}] + \kappa_{10}^2 e^{2A}(T^m_m - T^\mu_\mu)_{loc}. \qquad (1.109)$$

Note that the relative minus sign in the contribution of these sources to the right-hand side is a direct consequence of the trace reversed Einstein equations. Now, as long as the contribution of the sources is positive semi-definite, one again finds, by integrating the two sides over the internal space, that the flux G_3 must vanish, that the warp factor is constant and that $\tilde{F}_5 = 0$. However, if the contribution is instead *negative*, is is possible to satisfy Einstein's equations while having a nontrivial flux background and warp factor. Thus, nontrivial warped/flux compactifications are possible when

$$(T^m_m - T^\mu_\mu)_{loc} < 0. \qquad (1.110)$$

In order to proceed from here, we introduce another constraint on the fluxes since the above expression does not determine the form of the background fields by itself. This leads us to introduce the *tadpole condition*

1.3.3 Tadpole Condition

Consider the definition of the 5-form field strength, $\tilde{F}_5$ in (1.90). Taking the exterior derivative of both sides and using the definitions for F_3 and H_3 gives us

$$d\tilde{F}_5 = F_3 \wedge H_3. \qquad (1.111)$$

Integrating this over the internal manifold gives us (since the left-hand side is exact)

$$\int F_3 \wedge H_3 = 0. \qquad (1.112)$$

However, as mentioned above, we must now also include localized sources. Some of these sources generate a D3 brane charge that sources this 5-form flux. Clearly D3 branes accomplish this, but it turns out that even D7 branes carry an induced D3 brane charge as do O3 planes [12]. In fact, O3 planes carry a negative D3 charge. We must therefore also include a source term on the right-hand side of the expression above for $d\tilde{F}_5$

$$d\tilde{F}_5 = F_3 \wedge H_3 + 2\kappa_{10}^2 T_3 \rho_3, \tag{1.113}$$

where ρ_3 is the D3 charge density. The tadpole condition is then obtained by integrating this over the manifold just as before

$$\frac{1}{2\kappa_{10}^2 T_3} \int F_3 \wedge H_3 + Q_3 = 0. \tag{1.114}$$

Now, as mentioned above this charge Q_3 can arise from two sources. Either it is directly due to D3 branes that fill the external 3 spatial dimensions, or it could be due to D7 branes that are wrapping various 4-cycles in the Calabi-Yau and filling the external 3 spatial dimensions or O3 planes that are space filling [12]. One can then rewrite the tadpole condition as

$$\frac{1}{2\kappa_{10}^2 T_3} \int F_3 \wedge H_3 + N_{D3} = L. \tag{1.115}$$

Here L is the D3 charge due to all other sources besides D3 branes while N_{D3} is simply the number of D3 branes. If one views the type IIB theory as arising as a limit of a certain F-theory compactification (more on this later), one can compute L in terms of the Euler character of the corresponding 4-fold CY_4

$$L = \frac{\chi(CY_4)}{24}. \tag{1.116}$$

Returning to (1.113), we can write it in terms of α, G_3 and e^{2A} from before as

$$\nabla^2\alpha = ie^{2A}\frac{G_{mnp} *_6 \bar{G}^{mnp}}{12\tau_I} + 2e^{-6A}\partial_m\alpha\partial^m\alpha + 2\kappa_{10}^2 e^{2A}T_3\rho_3. \tag{1.117}$$

Here $*_6$ refers to the Hodge dual in the internal space. Combining this expression with that of the Einstein equations from before, (1.109), we find

$$\nabla^2(e^{4A}-\alpha) = \frac{e^{2A}}{24\tau_I}|iG_3 - *_6G_3|^2 + e^{-6A}|\partial(e^{4A}-\alpha)|^2 + \frac{1}{2}\kappa_{10}^2 e^{2A}(T_m^m - T_\mu^\mu - 4T_3\rho_3). \tag{1.118}$$

Let us suppose that the sources satisfy the BPS-like condition

$$T_m^m - T_\mu^\mu = 4T_3\rho_3. \tag{1.119}$$

It then becomes clear (again by integrating both sides) that warped compactifications only become possible if

$$*_6G_3 = iG_3 \tag{1.120}$$

$$e^{4A} = \alpha. \tag{1.121}$$

Notice, that unlike the previous case without sources, including sources does not imply a vanish flux nor a trivial warping. As a result, flux compactifications *are* possible as long as the appropriate sources are included and the complex structure moduli can, as we will see below, therefore be stabilized.

1.3.4 Four Dimensional Physics

Now that we have illustrated that flux compactifications are in fact possible, we continue to discuss the four dimensional effects of such a setup. In four dimensions, the moduli will appear as scalar fields. However, unlike the zero flux unwarped case, their dynamics is now governed by a nontrivial potential. Such a potential can be derived from the Gukov-Vafa-Witten superpotential [62]

$$W = \int G_3 \wedge \Omega. \tag{1.122}$$

Here Ω is the holomorphic 3-form on the Calabi-Yau and the integral is taken over the entire Calabi-Yau space. Just as before we also have the Kähler potential obtained by integrating $\Omega \wedge \bar{\Omega}$ over the Calabi-Yau [3]

$$K_{cs} = -\log\left(i \int \Omega \wedge \bar{\Omega}\right). \tag{1.123}$$

This will only depend on the complex structure moduli. The Kähler potential for the axio-dilaton is given by a similar formula except that one uses the holomorphic 1-form on a torus rather than Ω_3. The result is

$$K_{ad} = -\log(-i(\tau - \bar{\tau})). \tag{1.124}$$

The entire Kähler potential is then given by considering both of these sectors

$$K = K_{cs} + K_{ad}. \tag{1.125}$$

From the Kähler potential, we can derive the Kähler connection K_a and the Kähler metric $K_{a\bar{b}}$ just as before[5,6]

$$K_a = \partial_a K \tag{1.126}$$

$$K_{a\bar{b}} = \partial_a \partial_{\bar{b}} K \tag{1.127}$$

[5] There are actually nontrivial corrections to the Kähler metric and connection when warping is introduced. These will be very important in the remainder of this dissertation so we will spend a considerable amount of effort understanding these below.

[6] Note that before we defined $K_a = -\partial_a K$. From this point on we will drop the minus sign and simply let $K_a = \partial_a K$ for simplicity.

Using the connection we can, as before, define the Kähler covariant derivative acting on the superpotential

$$D_a W = (\partial_a + K_a) W \tag{1.128}$$

$$D_{\bar{b}} W = \partial_{\bar{b}} W \tag{1.129}$$

We can now write down the scalar potential that the moduli see. It follows the standard supergravity form

$$V = e^K \left(K^{a\bar{b}} D_a W \bar{D}_{\bar{b}} \bar{W} - 3|W|^2 \right). \tag{1.130}$$

One can also consider the overall volume modulus, ρ with its corresponding Kähler potential

$$K_{vm} = -3 \log(-i(\rho - \bar{\rho})). \tag{1.131}$$

Notice that the covariant derivative of W with respect to the volume modulus is given by

$$D_\rho W = K_\rho W = \frac{-3}{\rho - \bar{\rho}} W. \tag{1.132}$$

This, together with the fact that

$$K^{\rho\bar{\rho}} = \frac{3}{|\rho - \bar{\rho}|^2}, \tag{1.133}$$

implies that the final term $-3|W|^2$ is cancelled against the contribution from the volume modulus

$$K^{\rho\bar{\rho}} D_\rho W \bar{D}_{\bar{\rho}} \bar{W} - 3|W|^2 = \frac{|\rho - \bar{\rho}|^2}{3} \frac{9}{|\rho - \bar{\rho}|^2} |W|^2 - 3|W|^2 = 0. \tag{1.134}$$

These models are referred to as *no-scale* models. We will work with these for the remainder of this dissertation. The scalar potential therefore takes the form

$$V = \frac{e^{K_{cs}}}{16 \tau_I \rho_I^3} \left(K^{a\bar{b}} D_a W \bar{D}_{\bar{b}} \bar{W} \right). \tag{1.135}$$

Here the sum runs over both the complex structure moduli as well as the axio-dilaton. We have explicitly used the form for the Kähler potential for the axio-dilaton and the volume modulus in the pre-factor. Note that we assume that ρ_I is fixed elsewhere and as a result is just a constant factor that does not affect the dynamics.

1.3.5 Warping Correction to The Kähler Metric

As mentioned above, there will be corrections to the Kähler metric and connection (and therefore also to the kinetic terms and the potential in the Lagrangian) once warping and fluxes are included. Roughly this can be thought of as the back-reaction of the fluxes on the geometry. This correction will be one of the more important aspects throughout the remainder of this analysis, so we spend a considerable amount of effort understanding it here.

The original formula for the Kähler metric in the absence of any warping was derived in the section on geometry above, and is

$$K = -\log\left(i\int \Omega\wedge\bar{\Omega}\right). \tag{1.136}$$

This was all derived using the fact that the compactification manifold is a Calabi-Yau space. Since we are now considering warped compactifications, such an analysis is not quite accurate anymore. A full treatment of the geometry of the moduli space now requires generalized complex geometry. However, in [42, 43] it was argued that an effective Kähler metric can be derived using the following correction

$$K = -\log\left(i\int e^{-4A}\Omega\wedge\bar{\Omega}\right) \tag{1.137}$$

where e^{-4A} is the warp factor from above. The idea behind this correction can be understood roughly as follows. In the unwarped case, $\Omega\wedge\bar{\Omega}$ is proportional to the volume form on the Calabi-Yau. This is most clearly seen by recognizing that the Hodge number $h^{3,3} = 1$ and thus that any $(3,3)$ form with non-vanishing integral over the Calabi-Yau must lie in the same cohomolgy class as the volume form. Therefore, $\Omega \wedge \bar{\Omega}$ can differ from the volume form by at most a total derivative. Now, when warping is included it is reasonable to suspect (at least to first order) that the correct formula for the Kähler potential would be modified in the same way that the volume form would be modified. This is captured by how the 10D and 4D Planck scales are related. To see how this works, consider the gravitational action in 10D,

$$S \sim M_{10}^8 \int R_{10} \sqrt{G} d^{10}x \tag{1.138}$$

where M_{10} is the 10D Planck scale, R_{10} is the 10D Ricci scalar, and G is the warped metric. Integrating out the six internal dimensions, we should end up with

$$S \sim M_4^2 \int R_4 \sqrt{g} d^4x. \tag{1.139}$$

Where M_4 is the 4D Planck scale, R_4 is the 4D effective Ricci scalar, and g is the effective 4D metric. In particular, we see that the 4D and 10D Planck scales are related by integrating out all of the internal y-dependence. Counting everything up, we see that we get a factor of e^{-6A} from the warping correction on the internal space, another factor of e^{4A} from the warping correction on the external space, and finally a factor of e^{-2A} from how the Ricci scalar depends on the warp factor (this is easily seen by considering a Weyl scaling). Multiplying these together, we see that the two Planck scales are related by an an exponential factor[7] equal to e^{-4A}. This is then the warp factor that should be included in the correction to the Kähler potential.

It is therefore evident that in order to find the warp correction to the Kähler metric, one must first find the warp factor e^{-4A}. For general compactifications with small fluxes, one does not expect a very large warp correction. However, there are certain singular configurations

[7]This is another nice aspect of warped compactifications. The fact that the two scales can be related exponentially allows one to address the hierarchy problem effectively. In fact, warped metrics have been studied for this reason alone.

of the Calabi-Yau geometry where certain cycles of the manifold that can support fluxes collapse. In these circumstances, it is expected that the corrections due to warping become important. We will now briefly study these singular Calabi-Yau limits which are called conifolds and then continue by analyzing the warp factor near the tip of the conifold.

1.3.6 The Conifold Geometry

Many Calabi-Yau manifolds can be constructed as intersections of hypersurfaces in products of complex projective space. The simplest example was discussed above and is given by the vanishing of a quintic polynomial in $\mathbb{CP}^4$

$$P(z_1, \ldots, z_5) = 0 \tag{1.140}$$

where $z_1, \ldots, z_5$ are projective coordinates in $\mathbb{CP}^4$. In general, the direction orthogonal to the hyper surface is given by the gradient $\partial_i P$. However, in the particular case where this vanishes together with the polynomial itself, one finds that the manifold develops a singularity [4]. As an example we can consider the mirror manifold [7, 2] [8] to the quintic which is given by the vanishing of the quintic polynomial in $\mathbb{CP}^4$

$$P(z_1, \ldots, z_5) = z_1^5 + z_2^5 + z_3^5 + z_4^5 + z_5^5 - 5\psi z_1 z_2 z_3 z_4 z_5 = 0. \tag{1.141}$$

The gradient of this polynomial is given by

$$\partial_i P = 5z_i^4 - 5\psi z_1 z_2 z_3 z_4 z_5 / z_i. \tag{1.142}$$

[8] We won't discuss mirror symmetry at all in this dissertation, but it is worthwhile quickly mentioning that most known Calabi-Yau manifolds come in mirror pairs whose hodge numbers $(h^{1,1}, h^{1,2})$ are interchanged. As a result, the mirror of the quintic, called the *mirror quintic* has only one complex structure parameter since the quintic itself has one Käbler parameter.

The vanishing of the gradient then gives us (after multiplying through by z_i) the set of equations

$$\begin{aligned} 5z_1^5 - 5\psi z_1 z_2 z_3 z_4 z_5 &= 0 \\ 5z_2^5 - 5\psi z_1 z_2 z_3 z_4 z_5 &= 0 \\ 5z_3^5 - 5\psi z_1 z_2 z_3 z_4 z_5 &= 0 \\ 5z_4^5 - 5\psi z_1 z_2 z_3 z_4 z_5 &= 0 \\ 5z_5^5 - 5\psi z_1 z_2 z_3 z_4 z_5 &= 0. \end{aligned}$$

Multiplying these five equations together gives us a constraint on ψ

$$\psi^5 = 1. \tag{1.143}$$

For the particular manifold where $\psi = 1$, there is a singular point on the manifold. If one sits at the singularity and defines a local coordinate system (w_1, w_2, w_3, w_4) in the embedding space of $\mathbb{CP}^4$ such that the origin $w_i = 0$ correspond to the singular point, the manifold can locally be described by the vanishing of some function of the four local coordinates w_i

$$f(w_1, w_2, w_3, w_4) = 0. \tag{1.144}$$

A hallmark of a singularity is that there is no first order approximation to the surface at that point. As a result, if one attempts to Taylor expand the function f near the singularity, one sees that there is no first order term

$$f(w_1, w_2, w_3, w_4) = f(0,0,0,0) + w_i \partial_i f(0,0,0,0) + \frac{1}{2} w_i w_j \partial_i \partial_j f(0,0,0,0) = \frac{1}{2} w_i w_j \partial_i \partial_j f(0,0,0,0). \tag{1.145}$$

Thus, it is locally given by the vanishing of a quadratic polynomial. Any such polynomial can be brought to the standard form below via a linear coordinate transformation. Let us suppose that the original coordinates w_i were chosen precisely this way so that near the singular point we have

$$w_1^2 + w_2^2 + w_3^2 + w_4^2 = 0. \tag{1.146}$$

Now, notice that if w_i represents a point that satisfies the above quadratic equation, then so does the point with coordinates λw_i where λ is some arbitrary complex constant. As a result, the surface near the singularity is in fact a cone. The manifold is therefore called the *conifold*. The singular point itself corresponds to the tip of the cone. Notice as a passing remark that in the case where there are multiple complex structure parameters, one can imagine fixing all but one of these and tuning the remaining one until the space develops a conical singularity. As a result, the points in moduli space that correspond to a conifold geometry is a complex co-dimension one subspace. In the case of the mirror quintic which only has one complex structure modulus, this is therefore a point.

In general, a cone can be described by a base manifold whose size shrinks to zero as one approaches the tip of the cone. In the traditional two dimensional cone, this would just be a circle. However, here the base must be a five dimensional manifold. To find its topology, we imagine centering a seven sphere S^7 at the tip of the conifold with radius R [4, 5]. The intersection between this sphere and the conifold itself then represents the base space. We thus have the two constraints

$$\sum_{A=1}^{4} (w_A)^2 = 0 \tag{1.147}$$

$$\sum_{A=1}^{4} |w_A|^2 = R^2. \tag{1.148}$$

In order to solve these equations, we introduce the vector

$$w = \begin{pmatrix} w_1 \\ w_2 \\ w_3 \\ w_4 \end{pmatrix}. \tag{1.149}$$

The two equations can then be written as

$$w^T w = 0 \tag{1.150}$$

$$w^\dagger w = R^2. \tag{1.151}$$

Splitting the vector w into real and imaginary parts $w = x + iy$, we find the three equations

$$x \cdot x = R^2/2 \tag{1.152}$$

$$y \cdot y = R^2/2 \tag{1.153}$$

$$x \cdot y = 0. \tag{1.154}$$

The first two equations describe 3-spheres. However, the last equation forces x, y to be orthogonal to each other. As a result, the x may parameterize a three-sphere while the y may parametrize a two-sphere. The base, which we will denote $T^{1,1}$, is topologically the product

$$T^{1,1} \sim S^3 \times S^2. \tag{1.155}$$

Although no Calabi-Yau metric is known, one can deduce the metric near the tip of the conifold. In particular, it must take the standard cone-form

$$ds^2 = d\rho^2 + \rho^2 d\Sigma^2 \tag{1.156}$$

where $d\Sigma^2$ is the metric on $T^{1,1}$. One can show that there is a unique metric $d\Sigma^2$ that gives a Ricci flat metric ds^2 [4, 5]. This metric is given by

$$d\Sigma^2 = \frac{1}{9}(2d\beta + \cos\theta_1 d\phi_1 + \cos\theta_2 d\phi_2)^2 + \frac{1}{6}(d\theta_1^2 + \sin^2\theta_1 d\phi_1^2 + d\theta_2^2 + \sin^2\theta_2 d\phi_2^2). \quad (1.157)$$

Here $\theta_1, \theta_2 \in [0, \pi]$ while $\phi_1, \phi_2, \beta \in [0, 2\pi]$ are the coordinates on $T^{1,1}$. One can restrict to the S^3 base or the S^2 fiber by choosing [52]

- S^3 base – set $\theta_2 = \phi_2 = 0$
- S^2 fiber – set $\beta = 0$ (or some other constant), $\theta_1 = \theta_2$, and $\phi_1 = -\phi_2$.

We now define the following 1-forms [11]

$$\begin{aligned}
e^1 &= -\sin\theta_1 d\phi_1 \\
e^2 &= d\theta_1 \\
e^3 &= \cos 2\beta \sin\theta_2 d\phi_2 - \sin 2\beta d\theta_2 \\
e^4 &= \cos 2\beta d\theta_2 + \sin 2\beta \sin\theta_2 d\phi_2 \\
e^5 &= 2d\beta + \cos\theta_1 d\phi_1 + \cos\theta_2 d\phi_2.
\end{aligned}$$

Then using these, we define

$$\begin{aligned}
g^1 &= \frac{1}{\sqrt{2}}\left(e^1 - e^3\right) \\
g^2 &= \frac{1}{\sqrt{2}}\left(e^2 - e^4\right) \\
g^3 &= \frac{1}{\sqrt{2}}\left(e^1 + e^3\right) \\
g^4 &= \frac{1}{\sqrt{2}}\left(e^2 + e^4\right) \\
g^5 &= e^5.
\end{aligned}$$

In terms of this last basis, we see that the metric on the base becomes

$$d\Sigma^2 = \frac{1}{9}(g^5)^2 + \frac{1}{6}\sum_{i=1}^{4}(g^i)^2. \tag{1.158}$$

The volume form on the base $T^{1,1}$ is therefore $\frac{1}{6^2\cdot 3}g^1 \wedge g^2 \wedge g^3 \wedge g^4 \wedge g^5$ so that the volume of the base is

$$\mathrm{Vol}(T^{1,1}) = \int_{T^{1,1}} \frac{1}{6^2\cdot 3} g^1 \wedge g^2 \wedge g^3 \wedge g^4 \wedge g^5 = \frac{1}{2^2 3^3}\int_{T^{1,1}} e^1 \wedge e^2 \wedge e^3 \wedge e^4 \wedge e^5 \tag{1.159}$$

Using the expressions above for the basis e^i we find that the volume is

$$\mathrm{Vol}(T^{1,1}) = \frac{1}{2\cdot 3^3}\left(\int_0^{2\pi} d\phi\right)\left(\int_{-1}^{1} d\cos\theta\right) = \frac{16}{27}\pi^3. \tag{1.160}$$

It will be helpful to define the forms [52]

$$\begin{aligned}
\omega_{1i} &= 2d\beta + \cos\theta_i d\phi_i \qquad \text{for } i = 1,2 \\
\omega_2 &= \frac{1}{2}(g^1\wedge g^2 + g^3 \wedge g^4) = \frac{1}{2}(e^1 \wedge e^2 + e^3 \wedge e^4) = \frac{1}{2}(\sin\theta_1 d\theta_1 \wedge d\phi_1 - \sin\theta_2 d\theta_2 \wedge d\phi_2) \\
\omega_3 &= \omega_2 \wedge g^5 = d(\omega_{12}\wedge\omega_{11}).
\end{aligned} \tag{1.161}$$

The forms ω_2 and ω_3 can be integrated over the 2-sphere fiber and 3-sphere base respectively. The result for the fiber is (recall that the fiber is obtained by setting $\beta = 0$, $\theta_1 = \theta_2$, and $\phi_1 = -\phi_2$)

$$\int_{S^2}\omega_2 = \int_{S^2}\sin\theta d\theta\wedge d\phi = 4\pi. \tag{1.162}$$

The result for the S^3 base is given by (again, setting $\theta_2 = \phi_2 = 0$ to restrict to the base)

$$\int_{S^3}\omega_3 = \int_{S^3}\frac{1}{2}(\sin\theta d\theta\wedge d\phi)\wedge(2d\beta + \cos\theta d\phi) = \int_{S^3}\sin\theta d\theta \wedge d\phi\wedge d\beta = 8\pi^2. \tag{1.163}$$

Later on we will need to consider the Hodge dual of various forms on the six dimensional conifold. As a result, it will be beneficial to work out the Hodge dual of the form ω_3 above. Note that this is the six dimensional dual, so we denote it as $*_6$. We therefore wish to compute

$$*_6\omega_3 = \frac{1}{2}(*_6(g^1 \wedge g^2 \wedge g^5) + *_6(g^3 \wedge g^4 \wedge g^5)). \tag{1.164}$$

This is very easy to compute if one introduces the basis of forms

$$\lambda_i = \rho g^i/\sqrt{6} \qquad \text{for } i = 1,2,3,4 \tag{1.165}$$

$$\lambda_5 = \rho g^5/3 \tag{1.166}$$

$$\lambda_6 = d\rho. \tag{1.167}$$

In terms of this basis, the metric becomes the Kronecker delta. In this case it is simple to compute the Hodge dual of ω_3 to be

$$\begin{aligned}
*_6\omega_3 &= \frac{1}{2}\frac{6\cdot 3}{\rho^3}(*_6(\lambda_1 \wedge \lambda_2 \wedge \lambda_5) + *_6(\lambda_3 \wedge \lambda_4 \wedge \lambda_5)) \\
&= \frac{1}{2}\frac{6\cdot 3}{\rho^3}(\lambda_3 \wedge \lambda_4 \wedge \lambda_6 + \lambda_1 \wedge \lambda_2 \wedge \lambda_6) \\
&= \frac{1}{2}\frac{3}{\rho}(g^3 \wedge g^4 \wedge d\rho + g^1 \wedge g^2 \wedge d\rho) \\
&= \frac{3}{\rho} d\rho \wedge \omega_2
\end{aligned} \tag{1.168}$$

This is in fact exact since ω_2 is closed:

$$*_6\omega_3 = d(3\log\rho\,\omega_2). \tag{1.169}$$

Now, given a 3-form

$$\mathcal{A}\omega_3 + \mathcal{B} *_6 \omega_3 \tag{1.170}$$

we see (using $*_6^2 = -1$) that it is imaginary self dual if $\mathcal{B} = -i\mathcal{A}$ and can therefore be written as

$$\mathcal{A}(\omega_3 - i *_6 \omega_3). \tag{1.171}$$

Note also that this form is exact with a potential

$$\mathcal{A}\left(\frac{1}{2}\omega_{12} \wedge \omega_{11} - 3i \log \rho\, \omega_2\right). \tag{1.172}$$

1.3.7 Branes and Fluxes on the Conifold

We have now developed the necessary machinery to understand how fluxes impact four dimensional physics when the compactification manifold approaches a conifold singularity. Our goal is now to compute the warp factor e^{-4A} [11]. As per our discussion above, we know that for the case of sources that saturate the BPS-like bound in equation (1.119), the warp factor can be read off from the 5-form $\tilde{F}_5$

$$e^{-4A} = \alpha \qquad \text{where} \qquad \tilde{F}_5 = (1+*)d\alpha \wedge dx^0 \wedge dx^1 \wedge dx^2 \wedge dx^3. \tag{1.173}$$

The goal is therefore to find the expression for this five-form. We will accomplish this by analyzing the tadpole condition. In particular we know that

$$d\tilde{F}_5 = 2\kappa_{10}^2 T_3 \rho_3 + H_3 \wedge F_3. \tag{1.174}$$

As a result, both $H_3 \wedge F_3$ and ρ_3 can be thought of as sourcing the 5-form. We will analyze both of these below. Let us begin with ρ_3. Suppose that we stack N_{D3} D3 branes at the tip of the conifold that are point-like in the internal space and fill the external space. The five-form $\tilde{F}_5$ must therefore have a part to it, let us call it F_5 since it can be identified with the R-R 5-form $F_5 = dC_4$, that satisfies

$$\frac{1}{(4\pi^2\alpha')^2}\int_{T^{1,1}} F_5 = N_{D3}. \tag{1.175}$$

As a result, we can write F_5 as

$$F_5 = \frac{1}{2}\pi\alpha'^2 N_{D3}\,\omega_2 \wedge \omega_3 = 27\pi\alpha'^2 N_{D3}\mathbf{Vol}(T^{1,1}) \tag{1.176}$$

where $\mathbf{Vol}(T^{1,1})$ is the volume form on the conifold base. We will get back to this expression for F_5 later, but for now let us move on the the other contribution to $\tilde{F}_5$, $H_3 \wedge F_3$. In particular, suppose that we also place a stack of N D5 branes that wrap one of the S^2 fibers and otherwise is localized at the tip of the conifold. The 3-form F_3 must then satisfy

$$\frac{1}{4\pi^2\alpha'}\int_{S^3} F_3 = N. \tag{1.177}$$

This suggests that the 3-form can be written as

$$F_3 = \frac{\alpha'}{2}N\omega_3 + f *_6 \omega_3. \tag{1.178}$$

Note here the second term $f *_6 \omega_3$. This is needed later when we impose the self duality constraint on G_3. Here it does not contribute to the integral, so we are free to add it in. We also allow an NS-NS flux to source H_3 so that

$$\frac{1}{4\pi^2\alpha'}\int_{S^3} H_3 = M. \tag{1.179}$$

This similarly implies that H_3 can be written as

$$H_3 = \frac{\alpha'}{2}M\omega_3 + h *_6 \omega_3. \tag{1.180}$$

Let us now determine f and h. This is done by requiring the 3-form flux $G_3 = F_3 - \tau H_3$ to be imaginary self dual. Using the expressions for F_3 and H_3 above we find that

$$\begin{aligned} G_3 &= \frac{\alpha'}{2} N\omega_3 + f *_6 \omega_3 - \tau\frac{\alpha'}{2} M\omega_3 - \tau h *_6 \omega_3 && (1.181)\\ &= \left(\frac{\alpha'}{2}N - \tau\frac{\alpha'}{2}M\right)\omega_3 + (f - \tau h) *_6 \omega. && (1.182)\end{aligned}$$

In order for G_3 to be imaginary self dual we therefore need (according to (1.171)) that

$$f - \tau h = -i\left(\frac{\alpha'}{2}N - \tau\frac{\alpha'}{2}M\right). \quad (1.183)$$

Collecting up real and imaginary parts, we find

$$\begin{aligned} f &= \frac{\alpha'}{2\tau_I}(N\tau_R - |\tau|^2 M) && (1.184)\\ h &= \frac{\alpha'}{2\tau_I}(N - \tau_R M). && (1.185)\end{aligned}$$

We will use the $SL(2,\mathbb{Z})$ symmetry of type IIB supergravity to set the NS-NS flux to zero, $M = 0$. The 3-form fluxes are then

$$\begin{aligned} F_3 &= \frac{\alpha'}{2}N\omega_3 + \frac{\alpha' N\tau_R}{2\tau_I} *_6 \omega_3 && (1.186)\\ H_3 &= \frac{\alpha'}{2\tau_I}N *_6 \omega_3 && (1.187)\end{aligned}$$

We can then compute the wedge product $H_3 \wedge F_3$ to be

$$H_3 \wedge F_3 = \frac{\alpha'^2 N^2}{4\tau_I} *_6 \omega_3 \wedge \omega_3 = 27 \cdot \frac{3N^2}{2\tau_I}\frac{d\rho}{\rho} \wedge \mathbf{Vol}(T^{1,1}). \quad (1.188)$$

Notice that this can be written as a total derivative

$$H_3 \wedge F_3 = d\left(27 \cdot \frac{3N^2}{2\tau_I}\log\frac{\rho}{\rho_0}\mathbf{Vol}(T^{1,1})\right). \quad (1.189)$$

As a result, the contribution to $\tilde{F}_5$ itself from this must roughly be

$$\tilde{F}_5 \sim 27 \cdot \frac{3N^2}{2\tau_I} \log \frac{\rho}{\rho_0} \mathbf{Vol}(T^{1,1}) \tag{1.190}$$

with the caveat that it must of course be self dual. Let us define

$$N_{eff}(\rho) = N_{D3} + \frac{3N^2}{2\pi\tau_I} \log \frac{\rho}{\rho_0}. \tag{1.191}$$

We can then write the 5-form as

$$\tilde{F}_5 = (1 + *)\mathcal{F}_5 \tag{1.192}$$

where we have defined

$$\mathcal{F}_5 = 27\pi\alpha'^2 N_{eff}(\rho)\mathbf{Vol}(T^{1,1}). \tag{1.193}$$

We are now almost done. Recall that the ultimate goal is to find the warp factor which can be read off from the expression for $\tilde{F}_5$. In particular, we would have to write $\tilde{F}_5$ as in (1.173). However, here it is written in terms of the internal components. As a result, we must then compute the Hodge dual of $\mathcal{F}_5$ above

$$\tilde{F}_5 = (1 + *)\mathcal{F}_5 = (1 + *) * \mathcal{F}_5. \tag{1.194}$$

We turn to this computation now.

1.3.8 Warping on the Conifold

In order to finally compute the warp factor, we must compute the Hodge dual of $\mathcal{F}_5$ above which is equivalent to computing $*\mathbf{Vol}(T^{1,1})$ [11]. In order to do this, we recall that the $T^{1,1}$ metric becomes δ_{ij}/ρ^5 in the basis λ^i. However, in this case we must compute the dual in the full 10D theory. As a result, it would be beneficial to consider a basis in which the full

10D metric becomes δ_{MN}. The is accomplished by introducing the forms

$$
\begin{aligned}
E^\mu &= e^A dx^\mu && (1.195)\\
F^i &= e^{-A}\lambda_i. && (1.196)
\end{aligned}
$$

In terms of this basis, the volume form on $T^{1,1}$ becomes

$$
\mathbf{Vol}(T^{1,1}) = \frac{1}{\rho^5}\lambda_1\wedge\lambda_2\wedge\lambda_3\wedge\lambda_4\wedge\lambda_5 = \frac{e^{5A}}{\rho^5}F^1\wedge F^2\wedge F^3\wedge F^4\wedge F^5 \tag{1.197}
$$

We therefore have

$$
\begin{aligned}
*\mathbf{Vol}(T^{1,1}) &= \frac{e^{5A}}{\rho^5} * (F^1\wedge F^2\wedge F^3\wedge F^4\wedge F^5) && (1.198)\\
&= \frac{e^{5A}}{\rho^5}E^0\wedge E^1\wedge E^2\wedge E^3\wedge F^6 && (1.199)\\
&= \frac{e^{8A}}{\rho^5}d\rho\wedge dx^0\wedge dx^1\wedge dx^2\wedge dx^3. && (1.200)
\end{aligned}
$$

Using this in the expression for $\mathcal{F}_5$ we can now finally read off for the warp factor that

$$
\frac{d\alpha}{\alpha^2} = 27\pi\alpha'^2\frac{N_{eff}(\rho)d\rho}{\rho^5}. \tag{1.201}
$$

Integrating this we find

$$
e^{-4A} = c + \frac{27\pi\alpha'^2}{4\rho^4}\left(\frac{N_{D3}}{\tau_I} + \frac{3N^2\log(\rho/\rho_0)}{2\pi\tau_I^2} + \frac{3N^2}{8\pi\tau_I^2}\right). \tag{1.202}
$$

We have included a constant of integration c above that reflects an overall scaling of the Calabi-Yau. This is therefore related to the Kähler side of the story.

We now have a good understanding of how warping and fluxes affect the 10D physics. The question still remains how this translates to four dimensions. In other words, we still have to compute the warped Kähler metric that is derived from the potential in (1.137). We turn to this now.

1.3.9 Warped Kähler Metric on the Deformed Conifold

We expect the back-reaction due to warping/fluxes to become important as one approaches the tip of the conifold. In other words, as long as one stays away from the singularity, the warp factor shouldn't really impact the physics much. As a result, it seem reasonable to split the integral over the Calabi-Yau into two pieces, one that reflects the contribution near the tip of the cone and another one that reflects the contribution due to the remaining bulk of the Calabi-Yau where the warp factor is simply given by c [42, 47].

$$K = -\log\left(ic\int_{Bulk}\Omega\wedge\bar{\Omega} + i\int_{Conifold}e^{-4A}\Omega\wedge\bar{\Omega}\right) \tag{1.203}$$

If we define

$$K_{Bulk} = -\log\left(ic\int_{Bulk}\Omega\wedge\bar{\Omega}\right), \tag{1.204}$$

we can (to first order) write the full Kähler potential as

$$K = K_{Bulk} - ie^{K_{Bulk}}\int_{Conifold}e^{-4A}\Omega\wedge\bar{\Omega}. \tag{1.205}$$

The warping correction to the Kähler metric[9], $\hat{K}_{\xi\bar{\xi}}$ then becomes [42, 47]

$$\hat{K}_{\xi\bar{\xi}} = -ie^{K_{Bulk}}\int_{Conifold}e^{-4A}\chi\wedge\bar{\chi}. \tag{1.206}$$

where χ is the $(2,1)$ form that corresponds to complex structure deformations

$$\chi = \frac{1}{8\pi^2}(\omega_3 - i *_6 \omega_3) = \frac{1}{8\pi^2}\left(\omega_3 - 3i\frac{d\rho}{\rho}\wedge\omega_2\right). \tag{1.207}$$

[9]Here ξ is defined as complex structure parameter that vanishes at the conifold point and is normalized according to $\xi = \int_{S^3}\Omega$.

We thus have

$$\chi \wedge \bar{\chi} = \frac{i}{32\pi^4}\omega_3 \wedge *_6\omega_3 = -\frac{81i}{16\pi^4}\frac{d\rho}{\rho} \wedge \mathbf{Vol}(T^{1,1}). \tag{1.208}$$

Near the tip of the conifold, the warp factor is only a function of ρ. As a result, the integral for the warp correction to the metric becomes a single integral

$$\hat{K}_{\xi\bar{\xi}} = \frac{3}{\pi}e^{K_{Bulk}} \int_{\rho_0}^{\Lambda_0} \frac{d\rho}{\rho} e^{-4A(\rho)}. \tag{1.209}$$

Here we have introduced two limits on the integral over ρ that must be discussed. The upper limit is straight-forward, since the conifold geometry at some point must be glued into the bulk of the Calabi-Yau geometry. As a result, we cut off the integral at some point Λ_0. However, the lower limit is slightly more subtle and has to do with the deformed conifold geometry. For the singular conifold, ρ may be taken arbitrarily small. However, from the moduli space perspective, there exists deformations that takes one away from the strictly singular conifold. In particular, while for the singular conifold the entire space $T^{1,1} \sim S^3 \times S^2$ collapses, a finite size of the S^3 is retained for the deformed conifold. As a result, there is actually a lower limit to how small ρ can become. If we take the complex structure parameter ξ to gauge the size of this sphere according to

$$\xi = \int_{S^3} \Omega, \tag{1.210}$$

We see that ρ_0 must be related to $|\xi|$ according to

$$\rho_0 \sim |\xi|^{1/3}. \tag{1.211}$$

Using this in the expression for the warp correction to the metric above, we find that

$$\hat{K}_{\xi\bar{\xi}} \sim c_1 \log \frac{\Lambda_0^3}{|\xi|} + \frac{c_2}{|\xi|^{4/3}}. \tag{1.212}$$

This result will have to be combined with the result for the Bulk (which we compute later).

The main message to take away from this analysis is that there is a significant contribution to the Kähler metric for small $|\xi|$ that goes like $|\xi|^{-4/3}$. This will be diluted by the overall volume of the Calabi-Yau, and so will generally be multiplied by some small constant C_w

$$K_{\xi\bar{\xi}} \sim C_w|\xi|^{-4/3} \qquad \text{for sufficiently small } |\xi|. \tag{1.213}$$

This warp correction will be incredibly important through the remainder of the discussion.

1.4 Tunneling in Quantum Field Theory

In chapter 2 we will undertake a detailed investigation of the tunneling dynamics in the landscape. In particular we investigate the instanton trajectories (or more precisely the domain walls) connecting vacua related to each other by monodromies (closed loops) around the conifold. In order to fully appreciate the arguments presented in that section it is very important to have a firm grasp of tunneling in quantum field theory. An excellent exposition of such processes has been given by Coleman, Callan, and de Luccia in the seminal papers *Fate of the false vacuum: Semiclassical theory*, *Fate of the false vacuum II: First quantum corrections*, and *Gravitational effects on and of vacuum decay* [13, 14, 15]. Here we briefly review their original arguments in a form relevant to the rest of our discussion.

Consider a scalar field theory with a potential $V(\phi)$ that has multiple non-degenerate local minima. For simplicity, suppose that there are two minima located at points ϕ_F and ϕ_T with ϕ_T being the global minimum and that we shift the potential by a constant so that $V(\phi_F) = 0$. An example of such a potential can be seen in figure 1.2. Classically, a field that takes on the homogeneous value $\phi(x) = \phi_F$ can exist in that state indefinitely. However, quantum mechanics renders such a state unstable to quantum tunneling. Keeping with this idea, we will refer to the field configuration where ϕ takes on the homogeneous value $\phi(x) = \phi_F$ as the *false vacuum* while the corresponding homogeneous state with $\phi(x) = \phi_T$ will be referred to as the *true vacuum*. One would of course like to understand the dynamics that underlies such a tunneling event and furthermore be able to compute the rate at which such events take place. The relevant quantity is of course the tunneling rate per unit volume, Γ/V. As Coleman showed us [13, 14, 15], this rate is computed by considering the Euclideanized theory with potential $-V(\phi)$:

$$\mathcal{L} = \frac{1}{2}(\dot{\phi}^2 + (\nabla\phi)^2) + V(\phi). \tag{1.214}$$

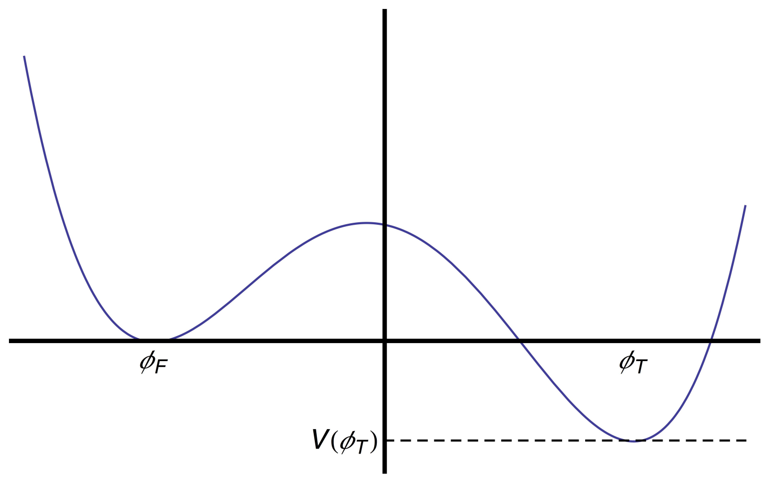

Figure 1.2: An example of a potential with two non-degenerate minima.

Up to a prefactor, the tunneling rate is then given by

$$\Gamma/V = e^{-S_E}, \tag{1.215}$$

where S_E is the action of a trajectory in field space, traditionally called the *bounce*, that begins at the false vacuum at Euclidean time $\tau = -\infty$ and continues to a field configuration where a part of space-time has transitioned into the true vacuum which we will take to occur at time $\tau = 0$ where it momentarily stops. The trajectory then continues to move back to the false vacuum at Euclidean time $\tau = +\infty$ (which is why it is called the bounce). Although, a priori any kind of trajectory seems admissible, Coleman proved that the dominant decay channel is given by the one that is $O(4)$ symmetric. In such a case, the field only really depends on the various coordinates and time through the quantity ρ where $\rho^2 = \tau^2 + \vec{r}^2$ so that $\phi(\tau, x_1, \ldots, x_{D-1}) \to \phi(\rho)$.

Using this ansatz in the action, the D dimensional field theory becomes a 0+1 dimensional action of a point particle rolling in the inverted potential where we would identify ρ as the time variable. The equations of motion combine into the single ordinary differential equation

$$\frac{d^2\phi(\rho)}{d\rho^2} + (D-1)\frac{d\phi(\rho)}{d\rho} - V'(\phi) = 0. \tag{1.216}$$

This equation is supplemented by two boundary conditions. The fact that the field must approach the false vacuum at infinity gives us the first boundary condition below. The second boundary condition simply arises because we have chosen $\tau = 0$ to be the time at which the field configuration reverses direction, i.e. *bounces*. An example trajectory in the $O(4)$ symmetric case can be seen in figure (1.3). The goal is therefore to find the bounce trajectory and to compute its action.

$$\phi(\rho = \infty) = \phi_F \tag{1.217}$$

$$\frac{d\phi}{d\rho}(\rho = 0) = 0 \tag{1.218}$$

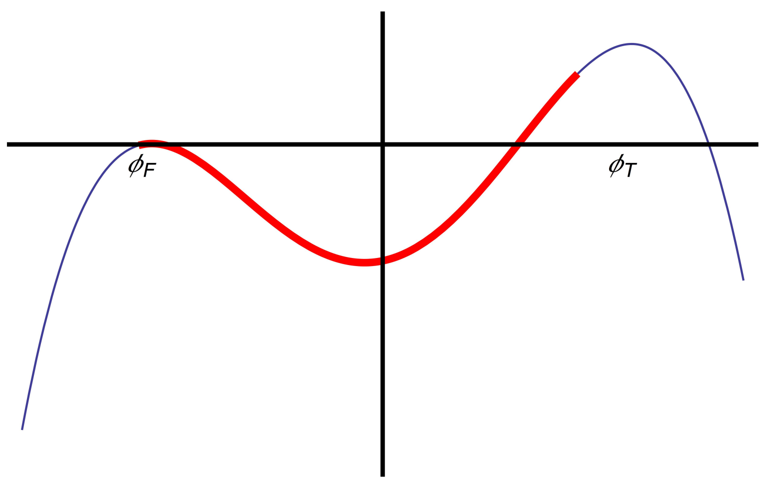

Figure 1.3: The bounce for the Euclidean (inverted) potential

1.4.1 Thin Wall Approximation

Solving this problem is in general quite difficult. This can be traced back to the fact that the boundary condition in (1.218) are of Neumann type and therefore don't tell us *where* to begin at $\tau = 0$. Given a generic potential with nontrivial vacuum structure one must generally resort to numerics in order to find the bounce. However, there is an interesting class of potentials for which an approximate analytical solution exists. To see how this goes, please notice that (1.216) is precisely the equation of motion for a point particle in the potential $-V$ with a time dependent friction term and that this friction term vanishes at sufficiently large ρ. Now, suppose that the two vacua of $V(\phi)$ are almost degenerate. Then if one wishes to end at ϕ_F at $\rho = +\infty$, one cannot afford to lose too much energy. The trajectory must therefore begin very close to ϕ_T and stay there for very long until the friction term has died off and only then begin moving to the false vacuum. In other words, the bounce very closely solves the equation of motion without a friction term and with Dirichlet boundary conditions on both ends

$$\frac{d^2\phi(\rho)}{d\rho^2} - V'(\phi) = 0. \tag{1.219}$$

$$\phi(\rho = \infty) = \phi_F \tag{1.220}$$

$$\phi(\rho = 0) = \phi_T. \tag{1.221}$$

This of course is nothing but a soliton (stationary solution with fixed boundary conditions) interpolating between the two minima. The field therefore spends a long time at the true minimum, ϕ_T and then quickly transitions to values near the false vacuum where it stays until $\rho \to \infty$. As a result, the transition between the two minima is effectively localized in a very narrow region in ρ. These solutions are therefore called *thin wall* solutions and the method of approximating the tunneling solutions by a soliton is called the *thin wall approximation*. An example of such a configuration in one dimension can be seen in figure (1.4). There we shifted the coordinate so that the wall occurs at $\rho = 0$. Once the tunneling event has occurred, the field begins its classical evolution in the state where $\tau = 0$. From that point on it evolves according to the Minkowski space equations of motion which are analytic continuations of the Euclideanized equations. As a result, the dynamics is given by the same functional form $\phi(\rho)$ but with $\rho^2 = -t^2 + \vec{r}^2$. The initial field configuration is then that of a *bubble* the interior of which is in the true vacuum and the exterior of which is in

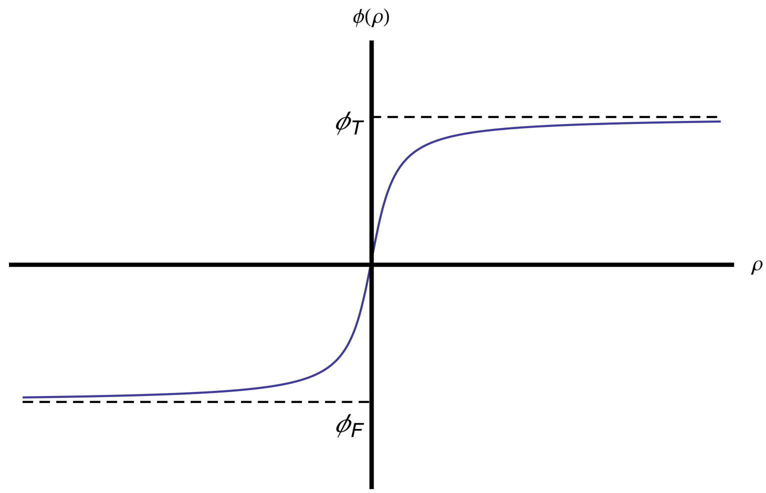

Figure 1.4: An example soliton that interpolates between the two vacua where we have shifted the coordinate so that the wall occurs at $\rho = 0$.

the false vacuum. The overall action of the bounce has two main contributions: that due to the interior of the bubble and that due to the bubble wall itself. If we suppose that the bubble takes on a radius R, we have

$$S_E = \int d\rho\, \rho^{D-1}\, \Omega_D\, \mathcal{L}_E = \frac{\Omega_D}{D} R^D(-V(\phi_T)) + \Omega_D R^{D-1} S_W. \tag{1.222}$$

Here, S_W is the action of the wall (i.e. soliton) and Ω_D is the solid angle in D dimensions. In order to obtain a true tunneling solution, we must now find the saddle point of the action by maximizing the action above over its only negative mode [14]. Inserting the appropriate value for R back into the expression for S_E gives us

$$R = \frac{(D-1)S_W}{\epsilon} \tag{1.223}$$

$$S_E = \frac{\Omega_D S_W^D}{D}\left(\frac{D-1}{\epsilon}\right)^{D-1}, \tag{1.224}$$

where we for defined $\epsilon = V(\phi_F) - V(\phi_T)$ for notational clarity. Note that the Euclidean action goes to infinity for degenerate vacua ($\epsilon \to 0$) and thus the tunneling rate vanishes as one would expect.

1.5 Numerical Techniques

In chapter 2 we will need to find instanton trajectories in a multi-dimensional landscape. As argued above, this entails solving a set of nonlinear coupled differential equations with non-trivial boundary conditions. Very often one must resort to numerical methods in these cases. Here we review two of the main numerical techniques that are used in finding such solutions [16, 52]. In chapter 2 we will employ the relaxation technique as well as its generalization near singular points in field space both of which are described in detail below.

Given a generic potential with multiple non-degenerate minima, one can ask what the tunneling rate is from a given false vacuum into either the true vacuum or another false vacuum of lower energy via Coleman de Luccia instantons. Only in particular cases can these rates be computed analytically. In particular, for an N dimensional field space with coordinates ϕ_i with $i = 1, 2, \ldots, N$ one must solve the set of differential equations

$$\frac{d^2\phi_i}{d\rho^2} + (D-1)\frac{d\phi_i}{d\rho} + \frac{\partial V}{\partial \phi_i} = 0, \tag{1.225}$$

subject to the boundary conditions

$$\phi(\rho = \infty) = \phi_F \tag{1.226}$$

$$\frac{d\phi}{d\rho}(\rho = 0) = 0, \tag{1.227}$$

where ϕ_F is taken as the initial false vacuum and ϕ_T is the vacuum to which we are tunneling which may or may not be the true vacuum. In general these differential equations are nonlinear and coupled and are therefore incredibly difficult to solve analytically and one must rather generically resort to numerics. Here we discuss two main numerical approaches to solving these sets of differential equations: the *shooting method* and the *relaxation method* [16].

1.5.1 The Shooting Method

Let us for now focus on a single scalar field, that is set $N = 1$, so that our field space becomes one-dimensional. Then the system of equations becomes a single nonlinear differential equation. Note that the equations (1.225) are equivalent to the equations describing a point particle moving in the inverted potential $-V$ with a time dependent frictional term that dies off as $\rho \to \infty$. Coleman originally showed us that this equation always has a solution using his famous overshot/undershoot argument which utilizes the fact that the motion of a particle varies continuously with the initial conditions [13]. In particular he considered dropping the particle with zero initial velocity from various points on the potential near the vacuum ϕ_T and watching it move along the potential. If we place the particle too far down the potential the particle will not have enough energy to reach ϕ_F at future infinity, see figure 1.5. However, if we instead place the particle very near the vacuum ϕ_T it will linger there for a very long time at which point the frictional term will have disappeared. At that point the particle will have so much energy that it will not just reach the vacuum ϕ_F, but it will overshoot it, see figure 1.5. Coleman then deduced using continuity that a solution must exist for some intermediate point. Although originally used for an existence

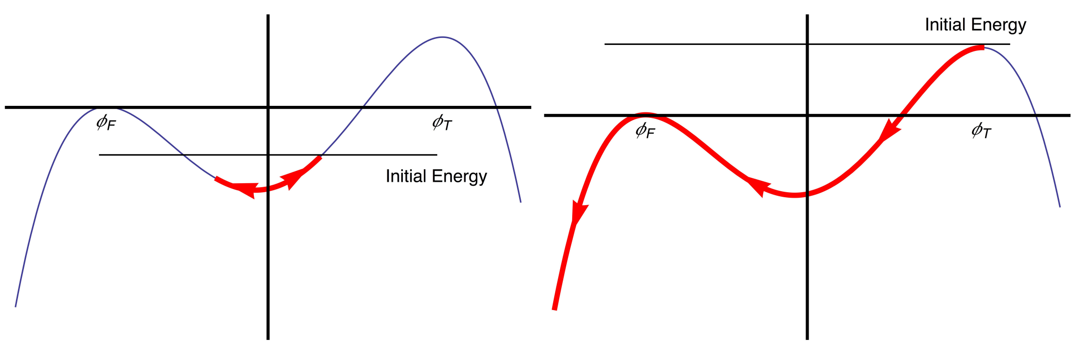

Figure 1.5: Example of initial conditions that lead to an undershoot situation (image on left) and an overshoot situation (image on right).

proof, Coleman's argument suggests a numerical technique that has become known as the *shooting method.* In particular, one chooses some initial point $\phi(0)$ and drops the particle there with zero initial velocity and watches the particle evolve for a very long time. If the particle ends up overshooting the false vacuum we move the initial point farther down the potential while if the particle does not reach the false vacuum, we move the initial location father up. We then repeat the process until we have found an initial location that satisfies our requirements for precision.

This brings us to a note worth mentioning. In any numerical approach there is necessarily some inherent precision issues. In the particular case of the shooting method, one must first decide how long to wait for the particle to reach the false vacuum. For points near the correct starting location it may take very long for the particle to reach ϕ_F or it may only reach ϕ_F asymptotically. As a result, one will never be able to find the correct starting location but by making the time we observe the system for sufficiently large, we can approximate the initial condition arbitrarily well.

Strengths and Weaknesses of the Shooting Method

One of the main strengths of the shooting method is that it works equally well in potentials that satisfy the thin wall approximation as in those that do not. This is very important since those that do not admit thin wall solutions are particularly difficult to analyze analytically since the boundary conditions are partly of Neumann type. Furthermore, as we will see in the next section, the relaxation method is only really applicable in thin wall scenarios so the shooting method is a nice complementary method to keep in mind when solving tunneling problems.

The shooting method has however a glaring shortcoming. Consider a multidimensional field theory with scalar fields ϕ_i with $i = 1, 2, \ldots, N$. Finding the starting location then entails finding the initial value of all of the fields, $\phi_1(0), \phi_2(0), \ldots, \phi_N(0)$ and unless there is some significant symmetry of the problem, using the shooting method becomes unwieldy. The reason is simply that if the trajectory does not end at the false vacuum it is now not a simple matter of overshooting/undershooting anymore. In particular, it is not clear in which direction the initial point must be moved. The problem therefore turns into a multidimensional problem where it is not even clear that a solution must exist.

Fortunately, while the shooting method fails us in these instances, the relaxation method which we discuss next handles these cases with ease.

1.5.2 The Relaxation Method

The relaxation method solves the ordinary differential equations (1.225) by converting them to partial differential equations in two variables [16]. Although this seems like complicating the situation, we will see that in some instances it can help us find numerical solutions to the ordinary differential equations.

Consider a potential with a false vacuum ϕ_F and a true vacuum ϕ_T. Furthermore suppose that the two vacua are nearly degenerate so that we can use the thin wall approximation and therefore that the instanton locally looks like a soliton. Then the problem consists of finding the soliton that interpolates between the two minima. This can of course be framed as the ground state of a $1+1$ dimensional field theory with the boundary conditions $\phi(-\infty) = \phi_T$ and $\phi(+\infty) = \phi_F$ and Lagrangian

$$\mathcal{L} = \frac{1}{2}\partial_\mu \phi \partial^\mu \phi - V(\phi) \tag{1.228}$$

Since the soliton is the ground state for these boundary conditions, any other field configuration that begins at ϕ_T at $\rho = -\infty$ and ends at ϕ_F at $\rho = +\infty$ must by definition contain more energy and will therefore decay into the soliton given a sufficient amount of time. In principle one can therefore begin at $t = 0$ with any such configuration and simply allow it to evolve in time. The configuration is of course not static and will thus radiate away energy until it decays into the appropriate ground state. This is the essential idea of the relaxation method, we simply let our initial condition *relax* into the time independent solution.

There are a few numerical issues however that must be addressed. First of all, in any numerical simulation one cannot specify the boundary conditions at $\pm\infty$. Instead, one must choose a large range in ρ and fix the boundary conditions at the edge of the box. As a rule of thumb, the tension of the wall should be significantly larger than the energy scale implied by the size of the box. Since we don't know the tension a priori, we need to repeat the numerical simulations a few times until we are certain that robust results have been obtained.

Moreover, another effect of the finite box size pertains to the relaxation itself. Although radiation should escape to infinity thereby allowing the initial condition to relax to the soliton, the finite sized box will, due to the Dirichlet boundary conditions, reflect this radiation back in. As a result, the decay will never actually take place. As a work-around, we include in addition to the standard terms in the equations of motion, a friction term that is meant to remove the excess energy

$$\ddot{\phi} - \phi'' + f\dot{\phi} + V'(\phi) = 0. \tag{1.229}$$

Once the field has reached a static solution, such a friction term should not have any effect on the dynamics. In order to ensure that the frictional force does not interfere with the concept of relaxation, one tends to manually turn it off after a certain amount of time. If the solution remains static afterwards, this is a good indication that an acceptable solution has been found.

Strengths and Weaknesses of the Relaxation Method

The main strength of the relaxation method is that it is easily generalized to multidimensional landscapes. One must then in general add a frictional term to each of the equations of motion in order to remove the energy consistently from all fields. This is to be contrasted with the shooting method that miserably fails in such multidimensional scenarios. An example of the use of the relaxation method in a one dimensional field theory can be seen in figure (1.6) as can another example of it being used in a two dimensional field theory. The main drawback with the relaxation method is that it is only applicable in cases where the thin wall approximation can be made. The reason for this is simply that the relaxation method is useful in finding solitonic profiles which only approximate the instanton configuration

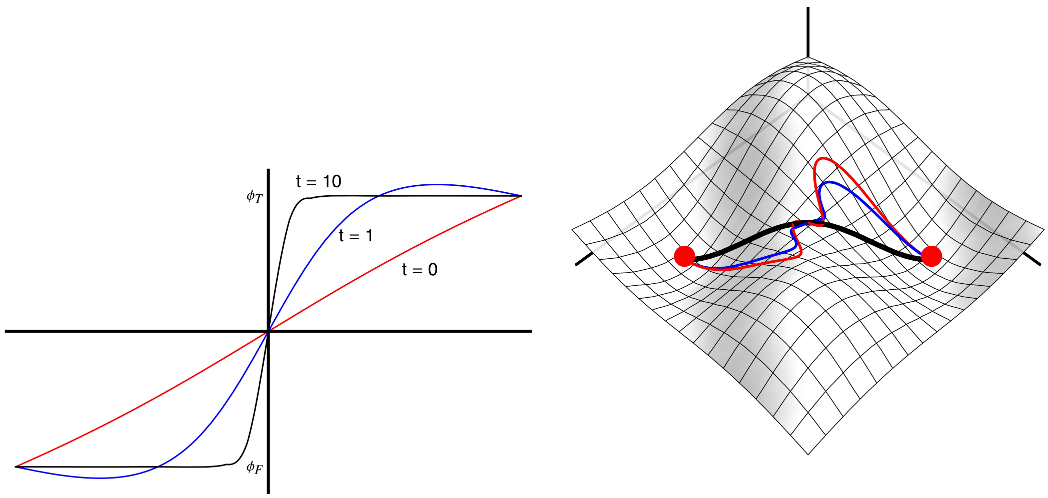

Figure 1.6: (Left) Here we have run the relaxation method for the soliton interpolating between the minima located at $\phi = \pm 1$ of the potential $V(\phi) = (\phi^2 - 1)^2$. As is clear, even an initial condition that is far away from the correct soliton profile will decay to the desired shape rather quickly. (Right) Here we have run the relaxation method for the potential $V(\phi, \psi) = \cos(\phi)\cos(\psi)$. One of the vacuum states is taken to be $\phi = \pi, \psi = 0$ while the other one is $\phi = 2\pi, \psi = \pi$ indicated by red dots in the image. The initial profile in red is far from the correct solitonic profile but very quickly converges to the appropriate form indicated in black. An intermediate profile is shown in blue.

for such nearly degenerate vacua. Furthermore, solving a set of nonlinear partial differential equations tends to be computationally expensive effectively increasing the amount of memory needed by a power of two compared to the original ordinary differential equations due to the increased number of grid points. One also sees a similar increase in computational complexity essentially due to the same reason. Finally, since the energy strictly decreases during relaxation, it is sometimes possible for the field to settle down in a configuration that is a local minimum of the energy although not the global minimum that corresponds to the soliton. The reason for this is that the dynamics is only sensitive to local properties of the field space. As a result one could imagine a field space that supports two static solutions one of which has lower energy than the other. In order to avoid these sorts of issues, it is important to try many different initial conditions when applying the relaxation method to ensure that the solution that one obtains in fact corresponds to that of lowest energy.

Singular Points in the Field Space

As we have seen above, the field space may sometimes contain singular points (we will be concerned with the conifold point below). Using the relaxation method in these instances may be a traitorous endeavor especially when the soliton must pass near these special points [52].

Suppose that the final solution interpolating between ϕ_T and ϕ_F passes very near a singular point in field space. Then, if one uses the relaxation method to find this profile, one must be very careful since the initial condition is not a static solution and will therefore at least initially exhibit dynamics that could potentially draw the profile into the singularity and thereby halt the numerical progress. The natural path to pursue is to insert initial conditions that are close enough to the correct solution that the dynamics during relaxation is not too violent. However, as we do not know the soliton profile a priori, this is not a reasonable approach. Instead, one may insert an artificial hard wall shielding the profile from the singularity. This is accomplished by adding a large step function barrier to the potential

$$V(\phi_1,\phi_2,\ldots,\phi_N) \to V(\phi_1,\phi_2,\ldots,\phi_N)+H\left(r_0-\sqrt{\phi_1^2+\ldots+\phi_N^2}\right)\theta\left(r_0-\sqrt{\phi_1^2+\ldots+\phi_N^2}\right). \tag{1.230}$$

Here we have chosen $\phi = 0$ as the singular point for definiteness and have inserted a wall of height H around the origin of radius r_0. The field profile will then hit this wall after some time. But instead of continuing into the singularity it will bounce back and eventually lay itself against it. After some of the energy has been removed due to the already present frictional terms, one may slowly remove the wall by decreasing r_0. If this is done sufficiently slowly, one may lower the profile near the singular point and once r_0 becomes smaller than the distance of nearest approach of the final soliton it may settle into its final shape. In such a way, one may avoid the singularity. This kind of approach is incredibly useful in analyzing domain wall solutions near the conifold locus of string theory [52]. An example of this approach can be seen in figures (1.7,1.8) below.

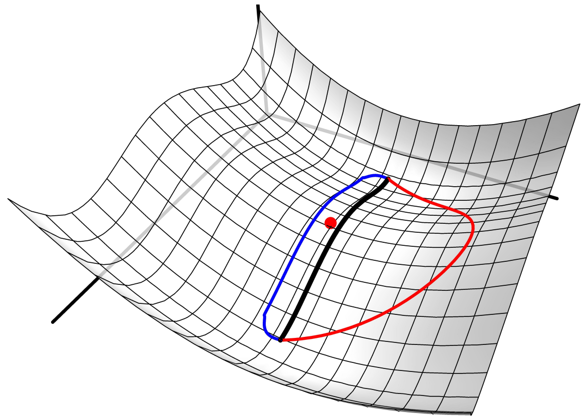

Figure 1.7: Here we illustrate the use of the relaxation method with the origin (labeled by a red dot) taken as a singular point. With a poor choice of initial profile (red curve), the dynamics brings it through the singular point (blue curve).

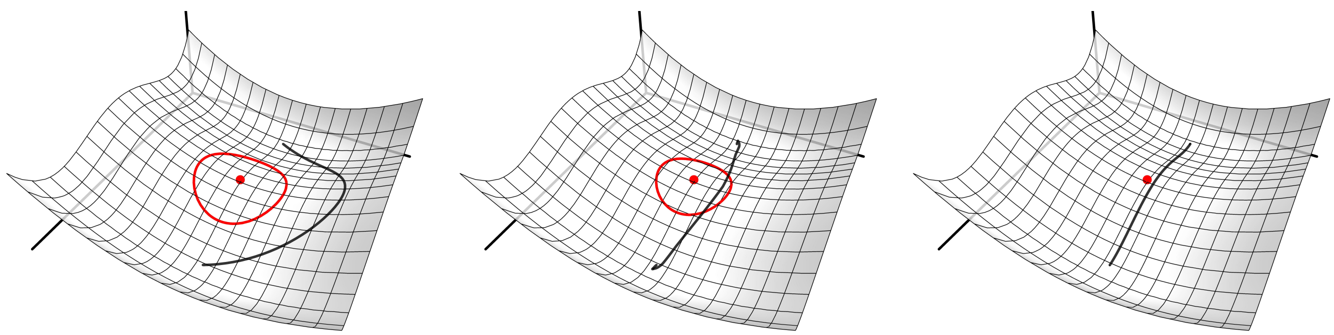

Figure 1.8: Here we have employed the hard wall approach described above. The region around the singular point has been surrounded by a hard wall addition to the potential which over time decreases in size until the profile has been safely lowered near the singular point and taken on its final shape.

Chapter 2

Conifolds and Tunneling in the String Landscape

2.1 Introduction

When compactifying string theory on a Calabi-Yau manifold, there is an inherent ambiguity regarding which Calabi-Yau should be chosen. There are certain discrete choices one must make. However, in addition to these discrete choices, each Calabi-Yau comes with several continuous parameters that are undetermined, the so-called moduli. Once the theory is compactified, these parameters become dynamical in four dimensions and appear in the effective action as massless scalar fields. In order to stabilize these fields and give them a nonzero mass, one can turn on background values for the various p-form fields that also appear in string theory. The precise values of these fields, while quantized, are still undetermined. In general compactifications several hundred components must be specified. Each of these choices can in principle yield a stable configuration of the moduli. As a result, very many potential compactifications are possible. Each of these vacua of string theory leads to distinct low-energy physics. As a result it is very important to understand this *landscape of string theory*.

There are several questions that may be asked about the structure of these solutions. Here we focus on the question of dynamics. While these vacua may appear stable classically, quantum mechanics renders them unstable. Since the aspect that distinguishes these vacua from each other is the choice of flux that is used in the compactification, it seems reasonable that tunneling between them involves the nucleation of a brane that carries the appropriate charge. Here we examine the question of tunneling from a field theoretical perspective where the vacua can be continuously connected via monodromies around the conifold point in the moduli space. We find that the instanton trajectory (or, more precisely, the domain wall profile) is drawn very close to the conifold point. This can be interpreted in terms of brane nucleation as well.

2.2 Flux Compactification of One Parameter Models

2.2.1 The Superpotential, Kähler Potential, and Scalar Potential

Type IIB string theory contains two different 3-form field strengths, F_3 in the R-R sector and H_3 in the NS-NS sector. By turning on nontrivial background configurations for these, one generates a superpotential for the effective four dimensional theory that depends on the complex structure moduli

$$W(z) = \int \Omega \wedge (F_3 - \tau H_3). \tag{2.1}$$

Here Ω is the holomorphic 3-form on the Calabi-Yau, τ is the axio-dilaton, and the integral is taken over the entire Calabi-Yau. This is of course a rather formal looking expression, and in order to make explicit contact with physics one must first find a way to write this in terms of computable functions. As a first step toward doing precisely this, let us introduce a set of 3-cycles on the Calabi-Yau, $\mathcal{C}_I$ with $I = 1, 2, \ldots, 2(1 + h^{1,2})$. Let us also introduce the Poincaré dual basis of 3-forms C_I so that for every closed 3-form α, we have

$$\int_{\mathcal{C}_I} \alpha = \int C_I \wedge \alpha, \tag{2.2}$$

where the latter integral is over the entire Calabi-Yau. Let us introduce the intersection form, Q_{IJ}, which tells us how the various cycles intersect each other

$$Q_{IJ} = \int C_I \wedge C_J. \tag{2.3}$$

Here the integral is over the entire Calabi-Yau. Clearly the form of Q depends on the choice of basis for H_3 although in any basis it must be anti-symmetric since the wedge product of the two 3-forms is itself anti-symmetric. Let us now expand the holomorphic 3-form Ω in terms of this basis

$$\Omega = \Omega_I C_I. \tag{2.4}$$

We also define the *periods* of the Calabi-Yau as the integrals of Ω over the various 3-cycles

$$\Pi_I = \int_{\mathcal{C}_I} \Omega. \tag{2.5}$$

Using the expression for Ω in this basis, we have

$$\Pi_I = \int_{\mathcal{C}_I} \Omega = \Omega_J \int C_I \wedge C_J = Q_{IJ}\Omega_J. \tag{2.6}$$

This implies that Ω can be written in terms of the periods as

$$\Omega = (Q^{-1}_{IJ}\Pi_J)C_I. \tag{2.7}$$

The two 3-forms F_3 and H_3 can similarly be expanded in this basis

$$F_3 - \tau H_3 = Q^{-1}_{IJ}(F_J - \tau H_J)C_I. \tag{2.8}$$

Here we have defined the quantities F_I and H_I as the amount of flux over each of the 3-cycles

$$F_I = \int_{\mathcal{C}_I} F_3 = \int C_I \wedge F_3 \tag{2.9}$$

$$H_I = \int_{\mathcal{C}_I} H_3 = \int C_I \wedge H_3. \tag{2.10}$$

Using these expressions, we then find that the superpotential is given by

$$\begin{aligned} W &= \int \Omega \wedge (F_3 - \tau H_3) \\ &= (Q^{-1}_{IJ}\Pi_J)(Q^{-1}_{KL})(F_L - \tau H_L) \int C_I \wedge C_K \\ &= (Q^{-1}_{IJ}\Pi_J)(Q^{-1}_{KL})(F_L - \tau H_L) Q_{IK} \qquad (2.11) \\ &= (F_I - \tau H_I) Q^{-1}_{IJ} \Pi_J. \qquad (2.12) \end{aligned}$$

In general any basis of 3-cycles is admissible. However it will be beneficial for our purposes to focus on a particular choice of cycles for which the intersection form takes a particularly concise form. This is the *symplectic basis* where the cycles come in pairs of so-called $\mathcal{A}$-cycles and $\mathcal{B}$-cycles. The intersection form then takes the form

$$Q = \begin{pmatrix} & & & & & -1 \\ & & & & 1 & \\ & & & \cdot & & \\ & & \cdot & & & \\ & -1 & & & & \\ 1 & & & & & \end{pmatrix}. \tag{2.13}$$

In this case we can organize the values F_I and H_I into two vectors F and H and the periods into a vector Π

$$\Pi(z) = \begin{pmatrix} \Pi_N(z) \\ \Pi_{N-1}(z) \\ . \\ . \\ \Pi_0(z) \end{pmatrix}, \tag{2.14}$$

so that the superpotential can be written as

$$W = (F - \tau H) \cdot \Pi(z). \tag{2.15}$$

In addition to the superpotential, we would also like to understand the structure of the Kähler potential and ultimately the full scalar potential that governs the dynamics of the moduli in four dimensions. The Kähler potential is given by

$$K_{cs} = -\log\left(i \int \Omega \wedge \bar{\Omega}\right). \tag{2.16}$$

In terms of the periods, this becomes

$$K_{cs} = -\log\left(i\Pi_i^*(\bar{z})Q_{ij}^{-1}\Pi_j(z)\right) = -\log\left(i\Pi^\dagger Q^{-1}\Pi\right). \tag{2.17}$$

In addition to this, one also has Kähler potentials for the axio-dilaton and the overall volume modulus

$$K_{ad} = -\log\left(-i(\tau - \bar{\tau})\right) \tag{2.18}$$

$$K_{vm} = -3\log\left(-i(\rho - \bar{\rho})\right). \tag{2.19}$$

The total potential is then $K = K_{cs} + K_{ad} + K_{vm}$. From the Kähler potential, one can derive the Kähler connection and metric in the usual way. This then ultimately provides us with an expression for the scalar potential. For our purposes it takes the *no-scale* form[1]

$$V = \frac{e^{K_{cs}}}{16\tau_I \rho_I^3} \left(K^{i\bar{j}} D_i W \bar{D}_{\bar{j}} \bar{W} \right) \tag{2.20}$$

where the sum runs over the complex structure moduli and the axio-dilaton $(i, \bar{j} = 0)$. Flux compactifications cannot stabilize the volume modulus ρ. As a result, we will assume that it is stabilized by some other mechanism. The prefactor of ρ_I^{-3} above is therefore simply an overall constant and does not affect the dynamics of the other fields at all.

Now, how can one determine the components F_I and H_I that go into defining the flux compactification? There are only two constraints on these components. First of all, they must be integers since the field strengths satisfy generalized Dirac quantization conditions. Secondly, they must satisfy the tadpole condition

$$\int H_3 \wedge F_3 \leq L \quad \rightarrow \quad F_I Q^{-1}_{IJ} H_J \leq L \tag{2.21}$$

where L is an upper bound on the D3 charge that can be carried by the 3-form fields that in some circumstances can be derived by considering the system from the perspective of F-theory (a generalized version of type IIB string theory). This concludes the discussion about the fluxes. We now turn to the question: how can one find the periods for a certain Calabi-Yau?

[1]This means that the terms $K^{\rho\bar{\rho}} D_\rho W \bar{D}_{\bar{\rho}} \bar{W}$ and $-3|W|^2$ cancel in the expression for the potential.

2.2.2 Picard-Fuchs Equations

The 3-form Ω belongs to the cohomology group $H^{3,0}$. Under variations of the complex structure, Ω picks up a component in $H^{2,1}$. Continuing in this way one finds

$$\begin{aligned}
\Omega &\in H^{3,0} && (2.22)\\
\partial_i\Omega &\in H^{3,0}\oplus H^{2,1} && (2.23)\\
\partial_i\partial_j\Omega &\in H^{3,0}\oplus H^{2,1}\oplus H^{1,2} && (2.24)\\
\partial_i\partial_j\partial_k\Omega &\in H^{3,0}\oplus H^{2,1}\oplus H^{1,2}\oplus H^{0,3} && (2.25)\\
\partial_i\partial_j\partial_k\partial_l\Omega &\in H^{3,0}\oplus H^{2,1}\oplus H^{1,2}\oplus H^{0,3} && (2.26)
\end{aligned}$$

Notice that for each derivative the cohomology class picks up a new linearly independent component. This is true until all of the distinct classes have already been enumerated. Once this has happened, we find that the set of derivatives of Ω is no longer linearly independent as far as cohomology classes go. In particular, a certain linear combination of these forms must be exact

$$\alpha_{ijkl}\partial_i\partial_j\partial_k\partial_l\Omega+\beta_{ijk}\partial_i\partial_j\partial_k\Omega+\gamma_{ij}\partial_i\partial_j\Omega+\delta_i\partial_i\Omega+\epsilon\Omega=d\eta. \tag{2.27}$$

In general, the coefficients above may depend on the complex structure moduli and are therefore functions on the moduli space but otherwise independent of the coordinates on the Calabi-Yau itself. We now integrate this entire expression over any of the 3-cycles $\mathcal{C}_I$. The right-hand side integrates to zero since it is exact and the cycles have no boundary. We therefore obtain a differential equation for the periods of the Calabi-Yau

$$\alpha_{ijkl}\partial_i\partial_j\partial_k\partial_l\Pi_J+\beta_{ijk}\partial_i\partial_j\partial_k\Pi_J+\gamma_{ij}\partial_i\partial_j\Pi_J+\delta_i\partial_i\Pi_J+\epsilon\Pi_J=0. \tag{2.28}$$

These are the Picard-Fuchs equations. In this analysis we will focus on one parameter models for which $h^{1,2} = 1$. As a result, the Picard-Fuchs equations become ordinary differential equations in the complex variable z. They are of fourth order so that they have four independent solutions which is necessary since there are $\dim H_3 = \dim H^3 = h^{3,0} + h^{2,1} + h^{1,2} + h^{0,3} = 2(1 + h^{1,2}) = 4$ independent 3-cycles for which we can define periods. More precisely we will focus on the "generic family of compact one-parameter models" of [28, 52] for which the Picard-Fuchs equation takes the form

$$\left[\delta^4 - z(\delta + \alpha_1)(\delta + \alpha_2)(\delta + \alpha_3)(\delta + \alpha_4)\right] \Pi_I(z) = 0. \tag{2.29}$$

Here, we have defined the differential operator $\delta = zd/dz$. Different choices for the parameters α_i correspond to different Calabi-Yau moduli spaces. In particular, if we set $\alpha_1 = 1/5, \alpha_2 = 2/5, \alpha_3 = 3/5$, and $\alpha_4 = 4/5$ we obtain the periods for the mirror-quintic. These equations are generally solved by the Meijer G functions.

Now, there are four linearly independent solutions to this equation and a priori it is not clear which linear combinations of them to take for the various periods. Of course, different combinations can be related to different choices of the basis of 3-cycles on the Calabi-Yau manifold. Since we will be interested in the symplectic basis we choose the solutions to the Picard-Fuchs equation to represent this same choice [28, 52]. In order to find this linear combination of solutions, one analyzes the monodromy matrices for the Meijer G functions around the three points[2]: $z = 0, z = 1$, and $z = \infty$ [28, 52]. One can then tune the linear combinations until the monodromy matrices take on the same form as they do in the symplectic basis. We will get back to this issue below when we discuss how to compute the periods in *Mathematica*. For now, let us just assume that the appropriate linear combination has been found and that $\Pi_i(z)$ refers to the periods in the symplectic basis.

The monodromy behavior of the periods in the symplectic basis around the conifold

[2]These three points correspond to the large complex structure point ($z = 0$), the conifold point ($z = 1$), and the Landau-Ginzburg point ($z = \infty$). We will only be concerned with with conifold point in what follows.

point, $z = 1$ is given by

$$\begin{aligned}
\Pi_3 &\rightarrow \Pi_3 \\
\Pi_2 &\rightarrow \Pi_2 \\
\Pi_1 &\rightarrow \Pi_1 \\
\Pi_0 &\rightarrow \Pi_0 + \Pi_3. \qquad (2.30)
\end{aligned}$$

Here we take Π_3 as the period over the collapsing cycle. Under such a monodromy, the superpotential actually changes

$$W = (F - \tau H) \cdot \Pi \rightarrow (F - \tau H) \cdot T\Pi \qquad (2.31)$$

where T is a monodromy matrix that encodes the monodromy behavior in (2.30). For fixed fluxes it is not quite clear what it would mean to perform one of these monodromies. In particular it may be surprising that the superpotential (and also therefore the scalar potential) is not single-valued. In an attempt to make sense of this, we notice that rather than having the monodromy matrix act on the periods above, we may allow it to act to the left on the fluxes

$$(F - \tau H) \rightarrow (F - \tau H)T. \qquad (2.32)$$

In terms of components, this implies that (for $G_i = F_i - \tau H_i$)

$$\begin{aligned}
G_0 &\rightarrow G_0 + G_3 \\
G_1 &\rightarrow G_1 \\
G_2 &\rightarrow G_2 \\
G_3 &\rightarrow G_3.
\end{aligned}$$

As a result, one may think of the various sheets as potentials arising from flux compactifications with different fluxes. This prescription therefore allows us to study tunneling phenomena in field theoretic terms without having to resort to discussing brane nucleation explicitly[3]. This is precisely the perspective that we will take below. Using the relaxation method, we will attempt to numerically find the domain wall that interpolates between two supersymmetric vacua. In order to speed up the computations, we will need to pre-compute the periods on a grid. We turn to this analysis next.

2.2.3 Numerical Computation of Periods

Numerical computation of the Kähler potential K, Kähler metric $K_{z\bar{z}}$, superpotential W, and the flux potential V require the use of Meijer functions that solve the fourth-order Picard-Fuchs ODE. *Mathematica* has built-in Meijer functions, however these evaluate too slowly for analytical computations. Instead, we generate a table of look-up values for these functions on a grid running from $(-5.01, 4.99)$ in both the $\mathrm{Re}(z)$ and $\mathrm{Im}(z)$ directions. The grid spacing is 0.05 between each vertex.

The numerical Meijer functions for our models are defined using the built-in ones as follows

$$\begin{aligned}
U_0 &= c\,\texttt{MeijerG}[\{\{\texttt{1}-\alpha_1,\texttt{1}-\alpha_2,\texttt{1}-\alpha_3,\texttt{1}-\alpha_4\},\{\}\},\{\{\texttt{0}\},\{\texttt{0},\texttt{0},\texttt{0}\}\},-\texttt{z}],\\
U_1 &= \frac{c}{2\pi i}\texttt{MeijerG}[\{\{\texttt{1}-\alpha_1,\texttt{1}-\alpha_2,\texttt{1}-\alpha_3,\texttt{1}-\alpha_4\},\{\}\},\{\{\texttt{0},\texttt{0}\},\{\texttt{0},\texttt{0}\}\},\texttt{z}],\\
U_2^- &= \frac{c}{(2\pi i)^2}\texttt{MeijerG}[\{\{\texttt{1}-\alpha_1,\texttt{1}-\alpha_2,\texttt{1}-\alpha_3,\texttt{1}-\alpha_4\},\{\}\},\{\{\texttt{0},\texttt{0},\texttt{0}\},\{\texttt{0}\}\},-\texttt{z}],\\
U_3 &= \frac{c}{(2\pi i)^3}\texttt{MeijerG}[\{\{\texttt{1}-\alpha_1,\texttt{1}-\alpha_2,\texttt{1}-\alpha_3,\texttt{1}-\alpha_4\},\{\}\},\{\{\texttt{0},\texttt{0},\texttt{0},\texttt{0}\},\{\}\},\texttt{z}],
\end{aligned}$$

where the α-parameters are the ones that appear in the Picard-Fuchs equation and define the class of Calabi-Yaus considered. The constant c is given by

$$c = \frac{1}{\Gamma(\alpha_1)\Gamma(\alpha_2)\Gamma(\alpha_3)\Gamma(\alpha_4)}.$$

[3]Note that this only works for fluxes that are related via these particular monodromy relations.

It is also useful to compute look-up tables for the derivatives of these functions:

$$
\begin{aligned}
\partial_z U_0 &= c\,\texttt{MeijerG}[\{\{-\alpha_1,-\alpha_2,-\alpha_3,-\alpha_4\},\{\}\},\{\{\texttt{0}\},\{-\texttt{1},-\texttt{1},-\texttt{1}\}\},-\texttt{z}],\\
\partial_z U_1 &= -\frac{c}{2\pi i}\texttt{MeijerG}[\{\{-\alpha_1,-\alpha_2,-\alpha_3,-\alpha_4\},\{\}\},\{\{\texttt{0},-\texttt{1}\},\{-\texttt{1},-\texttt{1}\}\},\texttt{z}],\\
\partial_z U_2^- &= \frac{c}{(2\pi i)^2}\texttt{MeijerG}[\{\{-\alpha_1,-\alpha_2,-\alpha_3,-\alpha_4\},\{\}\},\{\{\texttt{0},-\texttt{1},-\texttt{1}\},\{-\texttt{1}\}\},-\texttt{z}],\\
\partial_z U_3 &= -\frac{c}{(2\pi i)^3}\texttt{MeijerG}[\{\{-\alpha_1,-\alpha_2,-\alpha_3,-\alpha_4\},\{\}\},\{\{\texttt{0},-\texttt{1},-\texttt{1},-\texttt{1}\},\{\}\},\texttt{z}].
\end{aligned}
$$

Initially, we arrange for the branch-cuts to lie along the real axis from $(-\infty,0]$ and $[1,\infty)$. To do this, we must define

$$
U_2 = \begin{cases} U_2^-, & \text{if } \mathrm{Im}(z) < 0,\\ U_2^- - U_1, & \text{if } \mathrm{Im}(z) \geq 0 \end{cases} \tag{2.33}
$$

and similarly for $\partial_z U_2$.

Let the look-up tables constructed from the above definitions be `U0, U1, U2, U3, dU0, dU1, dU2`, and `dU3`. These arrays contain just the values of the Meijer functions at the grid points. To form the interpolating function on the grid for say, U_0 one must form a table associating each entry in `U0` to its corresponding grid point. One can then run *Mathematica*'s `Interpolation` function on this table. Usually this is one of the final steps after computing the table of values for a function of interest such as the flux potential.

The periods in the symplectic basis Π_j are encoded in the look-up tables `P0`, `P1`, `P2`, `P3` where

$$
\begin{aligned}
\texttt{P3} &= m_2\texttt{U1} + m_4\texttt{U3},\\
\texttt{P2} &= \texttt{3U1} - m_4\texttt{U2},\\
\texttt{P1} &= -\texttt{U1},\\
\texttt{P0} &= \texttt{U0}.
\end{aligned} \tag{2.34}
$$

The m_i are given in terms of the parameters α_i that specify the model under consideration as

$$m_2 = 4\left(\sin(\pi\alpha_1)^2 + \sin(\pi\alpha_2)^2\right), \quad m_1 = 1 - m_2, \tag{2.35}$$

$$m_4 = 16\sin(\pi\alpha_1)^2\sin(\pi\alpha_2)^2, \quad m_3 = -m_4. \tag{2.36}$$

The computation of all the other functions of interest in terms of the canonical periods now follows.

As we will see below, the numerical simulations will drive us near the conifold point. As a result, it will be important to know the form of the potential etc. in this regime. We turn to this now.

2.3 Near-Conifold Potential and Numerical Data

In general, a conifold locus in the moduli space represents Calabi-Yaus that develop various singular points due to the collapse of certain cycles. In the one-parameter examples, there is a single conifold point and a single cycle that degenerates while the periods of the other cycles become constant [2].

Due to the paired intersections of cycles in a Calabi-Yau, the collapsing cycle's partner develops interesting behavior in the moduli space (despite going to a constant at the conifold point). Call the collapsing cycle $\mathscr{A}$ and the intersecting cycle $\mathscr{B}$. Making a closed loop in moduli space around the conifold point, one finds that there is an ambiguity involved in determining what happens to the $\mathscr{B}$-cycle. From the perspective of the periods, a loop around the conifold point sends $\Pi_{\mathscr{B}} \to \Pi_{\mathscr{B}} + \Pi_{\mathscr{A}}$. This implies that

$$\Pi_{\mathscr{A}} = \xi + \pi_{\mathscr{A}}(\xi), \quad \Pi_{\mathscr{B}} = \frac{\xi}{2\pi i}\log\frac{\xi}{\Lambda_0^3} + \pi_{\mathscr{B}}(\xi), \tag{2.37}$$

where the functions $\pi_{\mathscr{A}}$ and $\pi_{\mathscr{B}}$ are $O(\xi^2)$ and $O(1)$, respectively. The monodromy of the

$\mathscr{B}$-cycle period is captured by the behavior of log in the expression above. The constant Λ_0^3 arises from cutting off the conifold geometry and gluing it into the bulk Calabi-Yau at $r \sim \Lambda_0$ where r is the radial coordinate for the singular conifold.

Given the above expressions, we can work out the behavior of the Kähler potential, Kähler metric, superpotential, and the flux potential in the near-conifold limit. We will first do this while ignoring corrections from strong warping.

2.3.1 The Kähler Potential and its Derivatives

The complex structure Kähler potential for the one-parameter models is

$$K_{cs} = -\log\left(i\left(\overline{\Pi}_3\Pi_0 - \Pi_3\overline{\Pi}_0 + \overline{\Pi}_1\Pi_2 - \Pi_1\overline{\Pi}_2\right)\right). \tag{2.38}$$

In our notation, the collapsing cycle is given by $\Pi_{\mathscr{A}} = \Pi_3$, and its intersecting partner is $\Pi_{\mathscr{B}} = \Pi_0$. Plugging in the near-conifold behavior of these cycles and sweeping up all of the $O(1)$ dependence into a function $k(\xi)$ gives

$$K_{cs} = \log\left(\frac{|\xi|^2}{2\pi}\log\frac{\Lambda_0^6}{|\xi|^2} + k\right) \to -\log k, \tag{2.39}$$

where the expression after the arrow indicates the limit of the Kähler potential when we neglect terms of order $O(\xi)$.

The derivative is then

$$K_\xi = e^{K_{cs}}\left(\frac{\bar{\xi}}{2\pi}\left(\log\frac{\Lambda_0^6}{|\xi|^2} - 1\right) - k_\xi\right) \to -\frac{k_\xi}{k}. \tag{2.40}$$

And the Kähler metric is

$$K_{\xi\bar{\xi}} = |K_\xi|^2 + e^{K_{cs}}\left(\frac{1}{2\pi}\left(\log\frac{\Lambda_0^6}{|\xi|^2} - 2\right) - k_{\xi\bar{\xi}}\right) \to \frac{1}{2\pi k}\log\frac{\Lambda_0^6}{|\xi|^2} + \kappa(\xi), \tag{2.41}$$

where $\kappa(\xi) \sim O(1)$. The near conifold Kähler metric possesses a logarithmic singularity at the conifold point.

In order to include the effects of strong warping for very small $|\xi|$, we modify the expression for the Kähler metric above by introducing the warp correction term

$$K_{\xi\bar{\xi}} \approx \frac{1}{2\pi k} \log \frac{\Lambda_0^6}{|\xi|^2} + \frac{K_1}{k} + \frac{C_1}{k|\xi|^{4/3}}, \tag{2.42}$$

where C_1 is taken to be very small, reflecting that we are working with a large (but finite) volume Calabi-Yau manifold. Note also that we have replaced $\kappa = K_1/k$ in the above as it is more convenient to work with in the final expression for the flux potential.

2.3.2 The Superpotential and its Derivatives

The superpotential is as above

$$W = F \cdot \Pi - \tau H \cdot \Pi = A + \tau B. \tag{2.43}$$

Recall that we can use the $SL(2,\mathbb{Z})$ invariance of type IIB supergravity to ensure that H_3 always vanishes. This means that while A has non-trivial monodromy near the conifold point, B does not since the flux multiplying Π_0 is set to zero.

The near-conifold behavior of these functions is easily computed

$$A = \frac{F_{\mathscr{A}}\xi}{2\pi i} \log \frac{\xi}{\Lambda_0^3} + a(\xi) \to a(\xi), \quad B = b(\xi), \tag{2.44}$$

where a and b are $O(1)$ and depend on the choice of the fluxes associated to the other cycles (including the $\mathscr{B}$-cycle). We also have

$$A_\xi = \frac{F_{\mathscr{A}}}{2\pi i} \left(\log \frac{\xi}{\Lambda_0^3} + 1 \right) + a_\xi \to \frac{F_{\mathscr{A}}}{2\pi i} \log \frac{\xi}{\Lambda_0^3}. \tag{2.45}$$

Thus, the derivatives $D_\xi W$ and $D_\tau W$ of the superpotential take the following form near the conifold

$$D_\xi W \approx \frac{F_{\mathscr{A}}}{2\pi i} \log \frac{\xi}{\Lambda_0^3} + A_1 - \tau B_1, \tag{2.46}$$

and

$$D_\tau W \approx \sqrt{k}(A_2 + \bar{\tau} B_2). \tag{2.47}$$

2.3.3 The Flux Potential Near the Conifold

The leading behavior of the flux potential in ξ is determined by the behavior of A in the superpotential above. Recall that the flux potential is given by

$$V = \frac{e^{K_{cs}}}{16\tau_I \rho_I^3} \left(K^{\xi\bar{\xi}} |D_\xi W|^2 + K^{\tau\bar{\tau}} |D_\tau W|^2 \right). \tag{2.48}$$

Inserting the expressions for the Kähler potential, metric, and superpotential near the conifold, we have

$$V = \frac{1}{16\tau_I \rho_I^3} \left(\left(\frac{1}{2\pi} \log \frac{\Lambda_0^6}{|\xi|^2} + K_1 + \frac{C_1}{|\xi|^{4/3}} \right)^{-1} \left| \frac{F_{\mathscr{A}}}{2\pi i} \log \xi + A_1 - \tau B_1 \right|^2 + |A_2 + \bar{\tau} B_2|^2 \right), \tag{2.49}$$

where C_1 is a small constant (its order of magnitude mainly reflecting the large volume of the compactification manifold) and Λ_0 the cut-off characterizing where the singular conifold is glued into the bulk Calabi-Yau geometry.

2.3.4 Mirror Quintic Near-Conifold Numerical Data

Our numerical simulations have been carried out for vacua arising from flux compactification on the mirror quintic. Given the fluxes $F = (3, -6, -9, -1)$ and $H = (-1, 0, -7, 0)$, the parameters in the near-conifold flux potential (2.49) are

$$\begin{aligned} K_1 &= 0.524211, \\ A_1 &= 13.1691 + 17.3632\, i, \\ B_1 &= 0.209511 + 0.000277995\, i, \\ A_2 &= -9.55217 + 7.75481\, i, \\ B_2 &= -2.26182\, i. \end{aligned} \tag{2.50}$$

The choice of F flux implies that $F_{\mathscr{A}} \equiv F_3 = -1$.

The mirror quintic period data near the conifold is approximated as follows: for the period functions that are regular near the conifold, we used *Mathematica* to compute them in terms of Meijer G functions and find their expansions to first order around the conifold point. The period Π_0 picks up a monodromy on sending $\xi \to e^{2\pi i}\xi$. We captured this behavior, the $O(1)$ and $O(z)$ behavior by fitting a function of the appropriate form to a numerically generated period function. The fit is good for $|\xi| \sim 0.04$ for $\Lambda_0^3 \sim 1$. The result is

$$\begin{aligned} \Pi_3 &\to \xi \equiv -0.355878\,(z-1)i, \\ \Pi_2 &\to 6.19501 - 7.11466\, i - (2.33032 + 2.85683\, i)\xi, \\ \Pi_1 &\to 1.29357\, i + 0.423645\,\xi, \\ \Pi_0 &\to \frac{\xi}{2\pi i}\log(-i\xi) + 1.07128 - 0.0630147\, i\,\xi. \end{aligned}$$

We now turn to finding supersymmetric vacua of the theory.

2.4 Finding Vacua

Supersymmetric vacua are points for which $D_z W = D_\tau W = 0$. Note that in principle we should also have $D_\rho W \sim W = 0$. However, since we are not stabilizing the volume modulus anyway, we consider solutions to the first two conditions to be supersymmetric. The condition $D_\tau W = 0$ is simplest to solve. In particular, using the form of the Kähler potential for the axio-dilaton from (2.19) we have

$$\begin{aligned} K_\tau &= \partial_\tau K = -\frac{1}{\tau - \bar{\tau}} && (2.51) \\ K_{\tau\bar{\tau}} &= \partial_\tau \bar{\partial}_{\bar{\tau}} K = \frac{1}{|\tau - \bar{\tau}|^2} && (2.52) \\ K^{\tau\bar{\tau}} &= \frac{1}{K_{\tau\bar{\tau}}} = |\tau - \bar{\tau}|^2. && (2.53) \end{aligned}$$

We can therefore compute the covariant derivative with respect to the axio-dilaton explicitly

$$D_\tau W = \partial_\tau W + K_\tau W = -\frac{1}{\tau - \bar{\tau}} (F - \bar{\tau} H) \cdot \Pi \tag{2.54}$$

Setting this equal to zero gives us an expression for the axio-dilaton in terms of z

$$\bar{\tau} = \frac{F \cdot \Pi}{H \cdot \Pi}. \tag{2.55}$$

We can then use this result in the expression for $D_z W = 0$ to obtain a single equation for the complex structure parameter z. Unfortunately, the resulting equation for z is far too complicated to solve analytically except for in certain regimes (such as in the near conifold limit). In order to find a generic vacuum one must therefore resort to numerics.

Since we ultimately wish to analyze the tunneling trajectories (or more precisely the domain wall profiles) for two vacua that are separated by a monodromy around the conifold point, it may be necessary to sort through several choices of fluxes before a satisfactory set of vacua can be found. Two such vacua are obtained by setting the fluxes as follows.

- Choosing $F = (3, -6, -9, -1)$ and $H = (-1, 0, -7, 0)$ results in a vacuum at $z = 0.463 - 0.124i$.

- Choosing $F = (2, -6, -9, -1)$ and $H = (-1, 0, -7, 0)$ results in a vacuum at $z = 0.229 - 0.363i$.

Notice that these two choices of flux are precisely related via the monodromy relations in (2.33). Now that we have found two vacua related in the appropriate way, we continue to study the domain wall that interpolates between them.

2.5 Numerical Conifunneling

In this section we apply the numerical relaxation method to find domain wall solutions in degenerate vacua—these solutions are excellent approximations to instantons with weakly non-generate vacua. We postpone discussing the physical interpretation of our solutions to the next section. Our goal is to look for instantons between vacua that reside on separate sheets of the flux potential. In our construction, such vacua are associated with the monodromy transformations around the conifold point. If we take the perspective of the monodromies acting on the fluxes, the instantons describe tunneling between different flux compactifications.

It will turn out that the bounce solution connecting these flux vacua *generically* passes very close to the conifold point. The instanton solution is driven there by the presence of non-trivial kinetic terms despite the seeming lack of an obvious path in the potential.

Seeing this behavior numerically requires knowledge of both the Kähler metric and the potential in both the bulk (i.e. far away from the conifold point and near the vacua), and near the conifold point in the field space. In the bulk where an analytical form for the potential and metric are unavailable, we use look-up tables for the relevant functions. Near the conifold point however, analytical expressions for the potential and metric are available. In principle one could imagine glueing these two regimes together. However, relaxation is easier to implement when we split the problem into two parts: relaxation in the bulk and relaxation near the conifold point.

2.5.1 Equations of Motion and Setup

Our goal is to find domain wall solutions using the relaxation method for this system given an action

$$\mathcal{L} = -\left(K_{z\bar{z}}\partial_\mu z \partial^\mu \bar{z} + K_{\tau\bar{\tau}}\partial_\mu \tau \partial^\mu \bar{\tau}\right) + V(z,\tau) \tag{2.56}$$

where z is the complex structure modulus and τ is the axio-dilaton. We assume that the Kähler moduli fields are frozen by some mechanism and that they do not contribute to the dynamics, so we will simply treat them as constants. Hence, we have a system with four real fields. It is convenient to choose the following parameterization

$$re^{i\theta} \equiv z - 1\ ,\ \ \tau \equiv u + iv \tag{2.57}$$

where $\phi \equiv \{r, \theta, u, v\}$ are all real dynamical fields which we have collected into a vector ϕ for notational simplicity. In the same vein, we also define

$$K_{z\bar{z}} \equiv \frac{1}{2} f(r,\theta) \tag{2.58}$$

and remind the reader that

$$K_{\tau\bar{\tau}} = \frac{1}{2}\frac{1}{4v^2}. \tag{2.59}$$

We are looking for domain wall solutions which are effectively 1+1 dimensional, hence we can choose (x,t) as coordinates. Ignoring gravity, the equations of motion are

$$\begin{aligned}
f(\ddot{r}-r'') + \frac{1}{2}(\dot{r}^2 - r'^2) - \frac{1}{2}\partial_r(r^2 f)(\dot{\theta}^2 - \theta'^2) + \partial_\theta f(\dot{\theta}\dot{r} - \theta' r') + \partial_r V &= 0 \\
fr^2(\ddot{\theta}-\theta'') + \frac{1}{2}r^2\partial_\theta f(\dot{\theta}^2 - \theta'^2) - \frac{1}{2}\partial_\theta f(\dot{r}^2 - r'^2) + \partial_r(fr^2)(\dot{r}\dot{\theta} - r'\theta') + \partial_\theta V &= 0 \\
-\frac{1}{2v^3}(\dot{v}\dot{u} - v'u') + \frac{1}{4v^2}(\ddot{u} - u'') + \partial_u V &= 0 \\
-\frac{1}{4v^3}(\dot{v}^2 - v'^2) + \frac{1}{4v^3}(\dot{u}^2 - u'^2) + \frac{1}{4v^2}(\ddot{v} - v'') + \partial_v V &= 0
\end{aligned} \tag{2.60}$$

with dots and primes denoting time and space derivatives.

Domain wall solutions, $\phi_*(x)$, are static solutions to the set of differential equations (2.60) with boundary conditions

$$\phi_*(x \to -\infty) = \phi_1 \ , \ \phi_*(x \to \infty) = \phi_2 \tag{2.61}$$

where ϕ_1 and ϕ_2 are the locations of the minima.

We solve (2.60) on a finite 1-dimensional grid, with a domain $\{x_{min}, x_{max}\}$ where the domain's size is much larger than $1/m$, m being the characteristic mass of the domain wall[4]. In practice, we choose the size of the domain to be a balance between accuracy and computational efficiency. Once a solution is found, we vary the size of the domain to ensure that the results are robust.

We insert a test solution at some initial time t_0, $\phi_0(x,t_0)$. In addition to possessing the correct boundary conditions, we fix the first derivatives at the boundaries to be identically

[4]This is not known in advance of course, but one can make a good guess at a value just after a few iterations of our prescription.

zero at all time (i.e. Dirichlet boundary conditions)

$$\dot{\phi}(x_{max}, t) = \dot{\phi}(x_{min}, t) = 0. \tag{2.62}$$

Given these boundary conditions, we then guess several initial profiles for $r_0(x, t_0)$ and $\theta_0(x, t_0)$ that interpolate between the two vacuum positions. Using these test profiles we find the corresponding *minimum* points of a given r and θ for $u_0(x, t_0)$ and $v_0(x, t_0)$, which we can find by solving for[5]

$$\frac{\partial V}{\partial u}(u_0, v_0) = 0\ ,\ \frac{\partial V}{\partial v}(u_0, v_0) = 0. \tag{2.63}$$

The total energy functional of the system is the integral of the Hamiltonian over the domain[6]

$$E[\phi(x)] = \int_{x_{\min}}^{x_{\max}} dx \left[\frac{1}{2} f(\dot{r}^2 - r'^2 + r^2\dot{\theta}^2 - r^2\theta'^2) + \frac{1}{8v^2}(\dot{u}^2 - u'^2 + \dot{v}^2 - v'^2) + V(r, \theta, u, v)\right]. \tag{2.64}$$

The true domain wall solution, if it exists, minimizes the total energy of the system

$$E[\phi(x)] \geq E[\phi_*(x)]. \tag{2.65}$$

Hence any deviation from the true solution means that there is additional energy in the system, which manifests itself as scalar radiation as the fields seek to relax to their true minimum energy configuration. In a perfect world, the radiation propagates to spatial infinity, never to be seen again. However, our fixed boundary conditions act as a rigid barrier at finite distance, and hence radiation will bounce back from this barrier and remain in the

[5] This choice for u_0 and v_0 is motivated by the fact that we expect that in the actual domain wall solution u and v do not deviate radically from this global minimum solution. However, they do deviate in general, which we can easily see by their equations of motion (2.60): the spatial derivatives must be supported by a non-zero derivative of the potential.

[6] We have suppressed two spatial dimensions – the energy functional is formally infinite if integrated over these suppressed dimensions.

system. To remove this radiation, we introduce friction terms into the equations of motion

$$\ddot{\phi} + \phi'' + ... = 0 \rightarrow \ddot{\phi} + \phi'' + ... + \lambda(t)\dot{\phi} = 0, \tag{2.66}$$

allowing the fields to relax into the true minimum energy configuration (i.e. a domain wall). Note that we allow the friction term to be a function of time; we will say a bit more about how we engineer the friction term later. In principle, the friction term turns itself off once the static solution has been found. We check for the robustness of our solution by manually turning off the friction term.

The test solutions themselves are not very important. In practice, we find that a well chosen initial profile may speed up the computation marginally, but most guesses find identical static solutions in the end. More insidious however, is the possibility that there exist multiple static solutions which are *not* the minimum energy solution ϕ_*. To test for that, we choose several different initial profiles with different initial total energy and check that they all relax to the correct solution.

In addition, there may be *no* solution. The simpler case of this possibility is that the total energy becomes negative after some time. Since our potential is bounded from below and positive, $V > 0$, this never happens. More difficult to detect is the possibility that the field approaches, but never quite converges to, a static configuration. In this case, the system never completely relaxes and long code run times may be mistaken for a true solution. We can check for this by taking the time derivative of the total energy, but in practice we never encounter such a situation.

In the following sections, we separate the field space into two regimes: far away from the conifold point $r > 0.1$ which we call the *bulk* and the near conifold regime where $r < 0.1$. The cut-off at $r = 0.1$ is arbitrary, motivated by the fact that we lack accurate numerical data for the potential below this point. Near the conifold point, the calculation of the potentials is tractable analytically. Note that the numerical bulk potential does not include the effects of warping, but since the data is only really accurate down to $r = 0.1$ and strong warping is not expected to be important until $r \ll 1$, this is not a problem.

In summary, we find that in the bulk relaxation phase, the field profile for r relaxes towards the conifold point rapidly, reaching $r < 0.1$ where we do not possess numerical data for the potential. To investigate the near conifold behavior, we use our analytic potentials and find that the field profiles do indeed continue to be driven to near $r = 0$, but then making a turn-around back into the bulk. While deep inside the near conifold regime, we find that θ makes a rapid transition across the sheets, hence tunneling across a monodromy transition. We dub this behavior, where the fields are driven towards the conifold point in order to transition into a new flux configuration *conifunneling*.

2.5.2 Relaxation in the Bulk

We first look for domain wall solutions between two supersymmetric vacua related by a conifold monodromy in the bulk. We choose the fluxes before and after the monodromy according to

$$F_1 = (3, -6, -9, -1) \quad \rightarrow \quad F_2 = (2, -6, -9, -1) \tag{2.67}$$

$$H_1 = (-1, 0, -7, 0) \quad \rightarrow \quad H_2 = (-1, 0, -7, 0). \tag{2.68}$$

The potentials at each corresponding sheet in z-space are generated using numerically computed Meijer functions. The vacuum positions are to rather high precision

$$z_1 = 0.4628 - 0.1237i \tag{2.69}$$

$$z_2 = 0.2286 - 0.3631i. \tag{2.70}$$

We use coordinates (r, θ) around the conifold point to unwrap the potential and stitch the data together across the sheets. From this, we generate the effective super and Kähler potentials. The vacua positions in these coordinates are then, with $\theta = 0$ being the branch cut,

$$\phi_1 = (r_1 = 0.55, \theta_1 = -2.92, u_1 = -3.41, v_1 = 4.22) \tag{2.71}$$

$$\phi_2 = (r_2 = 0.85, \theta_2 = 3.58, u_2 = -3.37, v_2 = 4.17). \tag{2.72}$$

The vacuum positions for $\tau = u + iv$ are found using conditions (2.63). We use the following test profile

$$\theta(x, t_0) = \frac{2(\theta_2 - \theta_1)}{\pi} \tan^{-1}\left(e^{x/\delta}\right) + \theta_1 \tag{2.73}$$

$$r(x, t_0) = \frac{2(r_{min} - r_1)}{\pi} \tan^{-1}\left(e^{(x-x_1)/\Delta_1}\right) + \frac{2(r_2 - r_{min})}{\pi} \tan^{-1}\left(e^{(x-x_2)/\Delta_2}\right) + r_1 \tag{2.74}$$

where Δ, δ are parameters which control the initial test thickness of the walls, $x_1 < x_2$ control the location of the walls, while r_{min} sets the radial turn-around point (see figure 2.1).

We then run relaxation simulations, using uniform and constant friction for all 4 dynamical fields, varying both the initial test profiles and the magnitude of the friction (ranging from $\lambda = 0.1$ to $\lambda = 10$) to ensure that our general conclusions are robust. Generically, the field profile for r rapidly relaxes to near the conifold point $r < 0.1$ where we do not possess good numerical data for the bulk flux potential (see figure 2.2), hence the simulation breaks down at this point. As a result, we must complement our analysis in the bulk with one that focuses on the near conifold regime.

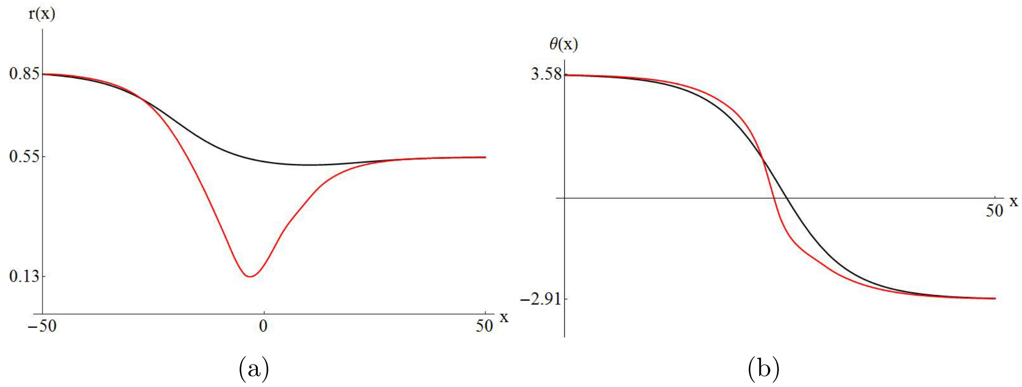

Figure 2.1: Initial (blue) and final (red) profiles for the complex structure field r (left) and θ (right) in the bulk relaxation phase. We stopped the simulation at the final configuration, $r < 0.1$ even though the fields are still not static (indeed they are highly dynamical) since we do not have numerical data for the potentials. Nevertheless, it is clear that the path between the two vacua is rapidly relaxing to the conifold point. We will replace the numerical potential with a near-conifold analytical potential in the next section.

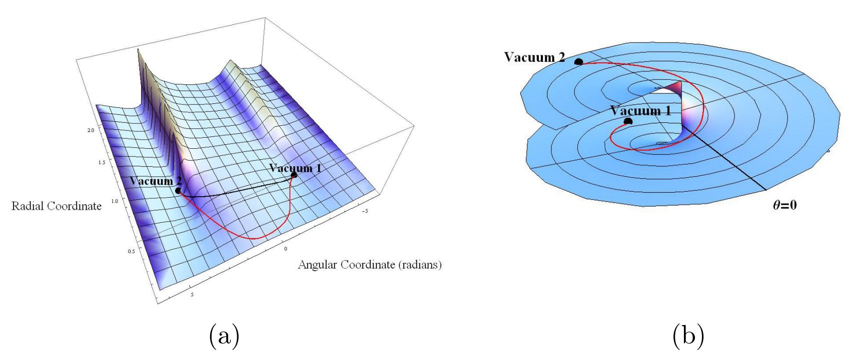

Figure 2.2: Figures showing the path of the complex structure (r, θ). On the left, we superimposed the initial (black) and final (red) profiles of the bulk relaxation phase over the reduced potential $V(r, \theta, u_{\min}(r, \theta), v_{\min}(r, \theta))$, where $u_{\min}$ and $v_{\min}$ are global minima for τ found using (2.63). On the right, we suppress the structure of the potential, but instead plot the final path in polar coordinates. The two sheets are joined at $\theta = 0$ with $r = 0$ being the conifold point. It is clear from this picture that the path traverses close to the conifold point as it wanders down the "funnel".

2.5.3 Results from Relaxation in the Vicinity of the Conifold Point

In order to investigate the behavior of the solutions near the conifold point, we use the analytical approximation described above

$$V_{nc} = \frac{1}{16\tau_I \rho_I^3}\left(\left(\frac{1}{2\pi}\log\frac{\Lambda_0^6}{|0.35r|^2} + K_1 + \frac{C_1}{|0.35r|^{4/3}}\right)^{-1}\left|\frac{F_{\mathscr{A}}}{2\pi i}\log 0.35r + A_1 - \tau B_1\right|^2 + |A_2 + \bar{\tau}B_2|^2\right). \tag{2.75}$$

Note that this is simply equation (2.49), with the rescaling $|\xi| = 0.35r$ for consistency with the notation we are using in this section. The parameters of this near conifold potential are derived assuming that the two vacua are associated by the monodromy described by (2.67). The values for the various parameters were given in (2.50) for the mirror quintic. This

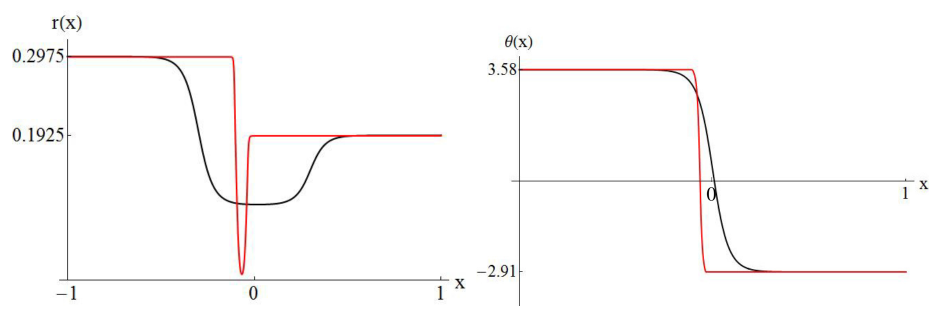

(a) (b)

Figure 2.3: Initial (blue) and final (red) profiles for the complex structure field r (left) and θ (right) in the near-conifold relaxation phase. In the final configuration, a static solution is achieved and hence is a true domain wall solution. The complex structure modulus funnels very close to the conifold point, the proximity depending on how strong the warping is. In terms of the r and θ fields, it is clear that a very sharp θ transition occurs when the field is near the conifold point $r \ll 1$. This indicates that there are three clear phases in the entire process—a shrinking of the 3-cycle associated with the formation of the conifold, a monodromy transition as θ tunnels into the next sheet, and then a return of the 3-cycle to near its original size.

approximation becomes almost exact near the conifold $r < 0.1$, but breaks down in the bulk. The key feature that is lost is the existence of the original vacua. To stabilize the vacuum positions, we drill Gaussian supersymmetric vacua into the potential

$$\tilde{V} = V_{nc} + V_1 + V_2 \tag{2.76}$$

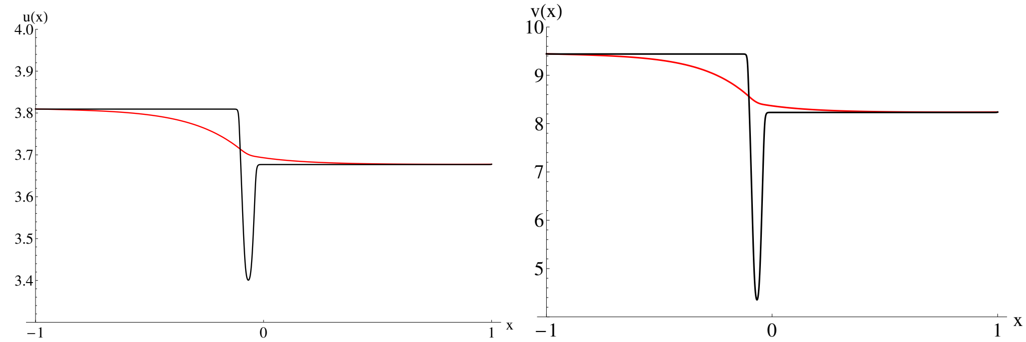

(a) (b)

Figure 2.4: The *final* (red) profiles for the axio-dilaton field u (left) and v (right), and the global minima (black) u_{min} (left) and v_{min} (right) in the near-conifold relaxation phase. In the final configuration, a static solution is achieved and hence is a true domain wall solution. It is clear from the equations of motion (2.60) that u_{min} and v_{min} are not static solutions. The actual final static domain wall solutions are mildly localized. The global minimum solution exhibits a sharp feature as expected from the highly localized nature of the complex structure z domain wall solution.

with

$$V_i = -V_{nc}(r_i, \theta_i, u_i, v_i)e^{[-(\theta-\theta_i)^2-(r-r_i)^2]/\sigma^2} \tag{2.77}$$

where σ is the width of the Gaussian holes. At these vacuum positions, $V_i = 0$. The positions of the holes are matched to the actual vacuum positions for their respective flux configurations, as given in (2.71). Note that we do not drill holes in the τ directions; we simply solve for the minima of τ via equation (2.63) as in section 2.5.2. Since the behavior of the domain wall will be dominated by the near conifold regime, we do not try to reproduce the shape of the potentials beyond this modification. As long as the solution conifunnels towards $r \to 0$ when it is at $r > 0.1$ we are satisfied with the overall bulk behavior.

Nevertheless, there remain two subtleties involved in choosing the exact coefficient for the strong warping factor C_1. First, in principle it may depend on τ, although such a dependence will not greatly effect the behavior of τ. Second, the exact numerical value of this coefficient is treated as a free parameter related to the overall volume of the Calabi-Yau manifold. Consistency requires that the parameter be chosen small enough so as not to have any effects on the bulk of the moduli space. For the purpose of our numerical simulation, we choose C_1 such that the warping term is subdominant when $r \approx r_{1,2}$ i.e.

$$C_1 \ll \left(\frac{1}{2\pi} \log \frac{\Lambda_0^6}{|0.35r|^2} + K_1 \right) |0.35r|^{4/3} \text{ at } r = r_1, r_2. \tag{2.78}$$

Again, we use the test solutions (2.73) and (2.74), varying the test parameters to ensure robustness of our conclusions (figures 2.3 and 2.4). However, due to the strong warping term $r^{-4/3}$ in the flux potential, instead of inserting constant friction terms for all our field equations, we use instead an exponentially damping friction

$$\lambda_\phi(t) = \lambda_\phi(t_0) e^{-\alpha(t-t_0)} \tag{2.79}$$

where α is some parameter which governs how rapidly friction is turned off[7]. The static

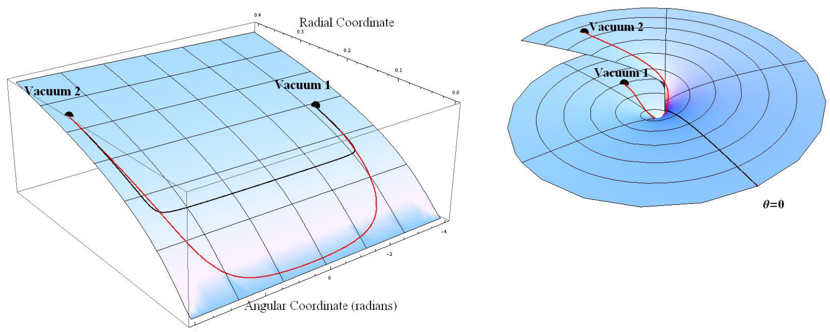

(a) (b)

Figure 2.5: Figures showing the path of the complex structure (r, θ). On the left, we superimposed the initial (black) and final (red) profiles of the near conifold relaxation phase over the "reduced" analytic near-conifold potential $V_{nc}(r, \theta, u_{\min}(r,\theta), v_{\min}(r,\theta))$, where $u_{\min}$ and $v_{\min}$ are global minima for τ found using (2.63). On the right, we plot the final path in polar coordinates, suppressing the gaussian vacuum holes but keeping the structure of the potential near the conifold visible – the strong warping term $r^{-4/3}$ suppresses the potential deep inside the conifold point, resulting in a potential that looks like a true "funnel". The two sheets are joined at $\theta = 0$ with $r = 0$ being the conifold point. The final static path falls deep into the funnel but reemerges on the other side of the monodromy—the conifold funnels the path across the monodromy, hence our moniker *conifunneling*.

[7]We also imposed a hard cut-off of the friction when we check for stability after a solution is obtained. In addition to this, we employ the hard wall regulator discussed in the numerical methods section that allows the profile to avoid the conifold point.

solutions are shown in figure 2.5. The solution relaxes towards the conifold point as we have seen in the previous section using the bulk potential. However, instead of falling into an abyss, the domain wall solution passes very close to the conifold point, and then turns back up into the bulk. In other words, a stable static domain wall solution exists between two vacua related by a monodromy transformation. Moreover, the domain wall passes very close to the conifold point—the exact proximity being determined by the coefficient in front of the strong warping term $r^{-4/3}$ in the Kähler metric. The smaller the coefficient, the later the turn-around occurs[8].

2.6 The Physics of Conifunneling

Despite trying to find a tunneling path through non-singular parts of the Calabi-Yau moduli space, numerical relaxation drove our solutions into the vicinity of the conifold point. These instantons represent conifunneling. Relaxation was only able to succeed due to the crucial effects of strong warping, analyzed in [47, 43, 44], and described both in general and for the conifold above in the section on warping. In this section we interpret conifunneling from a geometrical perspective.

2.6.1 Geometric Interpretation

Figure 2.6 shows the value of the tension integrand in terms of five separate terms: kinetic terms in each field and the flux potential term. We can see that the kinetic terms in τ are very small, which means the dynamics are mostly in the complex structure moduli, z[9]. In particular, the dynamics separates into three distinct parts: radial changes toward and away from the conifold point occur in the beginning and the end of the transition, while

[8]We note that although both $\log r$ and $r^{-4/3}$ blow up as $r \to 0$, the rate at which this blow up occurs is crucial in determining whether the domain wall will turn around sufficiently quickly.

[9]This means that we would have got similar results if we had reduced the problem from 4D to 2D and only focused on z. But it is not obvious that τ would essentially act as a spectator field, so we included it in the analysis for completeness.

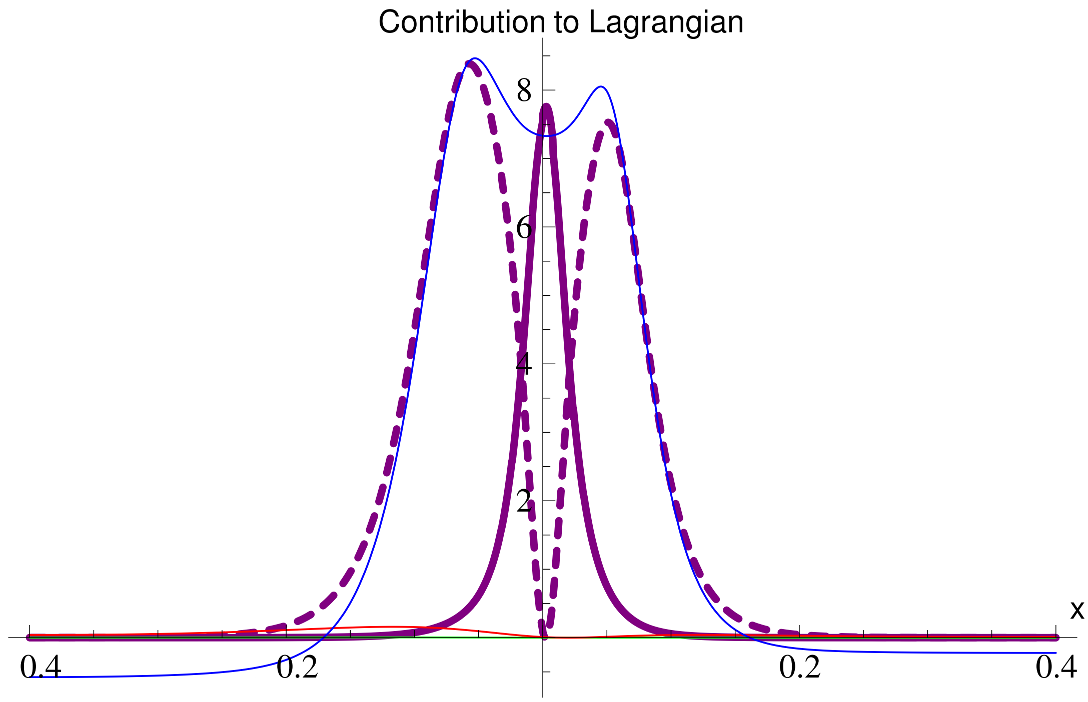

Figure 2.6: The action integrand (Lagrangian) broken up into contributions from five terms. The thin-blue line is the potential term, the dashed-purple line is the kinetic term in r, the solid-purple line is the kinetic term in θ. Kinetic terms in the two components of τ are colored red and green, and barely contribute. Note that the potential dips below zero for the two vacua, this is an artifact of our procedure for drilling these vacua in the near-conifold potential.

angular changes around the conifold occur in the middle. The two vacua are connected by a monodromy transformation, namely, a change of $\Delta\theta \sim 2\pi$. We just need to determine the most economical way to perform this transformation. Namely, minimizing the tension with 3 terms,

$$\sigma = \sigma_1 + \sigma_m + \sigma_2 \ , \tag{2.80}$$

where σ_m is the tension for a monodromy transformation in the vicinity of a point in the moduli space—i.e. keeping close to some geometrical configuration $\mathcal{M}_*$ for the Calabi-Yau. The first term σ_1 comes from deforming the Calabi-Yau from vacuum 1 to the geometry $\mathcal{M}_*$, and σ_2 from deforming $\mathcal{M}_*$ back to vacuum 2.

For our case, σ_m is essentially the action integral in the θ direction,

$$\sigma_m = \int \sqrt{2V - 2V_0}\sqrt{K_{z\bar{z}}}\, r\, d\theta \ , \tag{2.81}$$

and σ_1, σ_2 are like integration in the r direction,

$$\sigma_i = \int \sqrt{2V - 2V_0}\sqrt{K_{z\bar{z}}}\, dr \ . \tag{2.82}$$

These expressions illustrate that taking the fixed geometry $\mathcal{M}_*$ to be very near the conifold minimizes σ_m. However, σ_1 and σ_2 grow in this same limit. As a result, there is some optimal $\mathcal{M}_*$ whose precise form is determined via the interplay between σ_1, σ_m, and σ_2. However, one thing is clear: since σ_m is minimized near the conifold, one should expect that the profile may at least be drawn somewhat close to the conifold point.

The geometric picture is quite straight-forward. The shrinking 3-cycle near the conifold point is exactly the cycle which we cut and twist in the monodromy transformation. Physically the shrinking 3-cycle (with flux) cannot go to zero size, so eventually it becomes strongly warped and the monodromy happens at the tip of the strongly warped conifold, as shown in figure 2.7. Both shrinking and warping help to reduce σ_m. We can also understand this process in the dual picture, where the flux is changed by nucleating a charged brane instead of monodromy. The fluxes due to F_3 and H_3 change by nucleating a 5-brane. Three legs of this 5-brane will wrap the shrinking cycle leaving two spatial directions for the (2+1)D domain wall in the 4D space-time. As depicted in figure 2.8, the monodromy contribution is replaced by a brane,

$$\sigma_{\rm 4D}^{\rm 2-brane} = \sigma_{\rm 10D}^{\rm 5-brane}(V_{\rm shrinking\ 3-cycle})(\text{volume factor})(\text{warp factor}) \ . \tag{2.83}$$

The volume factor corresponds to the dimensional reduction from the 10D theory string frame to the 4D theory Einstein frame. It is a constant in our case since we have frozen the

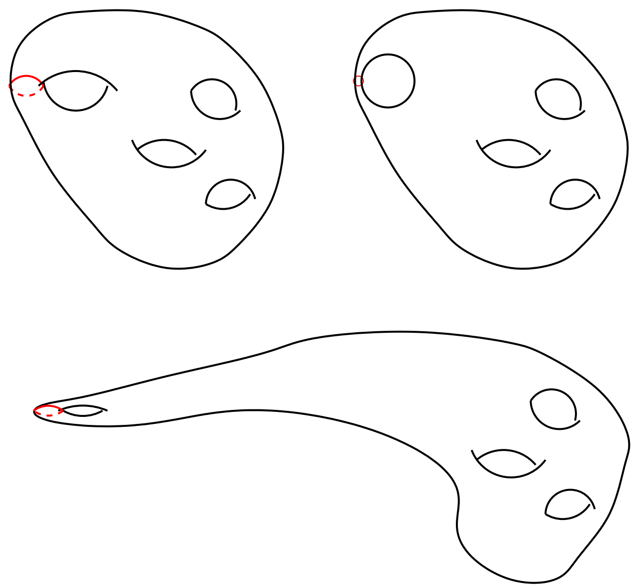

Figure 2.7: Top left is the vacuum configuration of the Calabi-Yau manifold. A monodromy transformation (on the red cycle) contributes less to the action if the 3-cycle is small (top right), and even less if it happens on the tip of the strongly warped conifold (bottom).

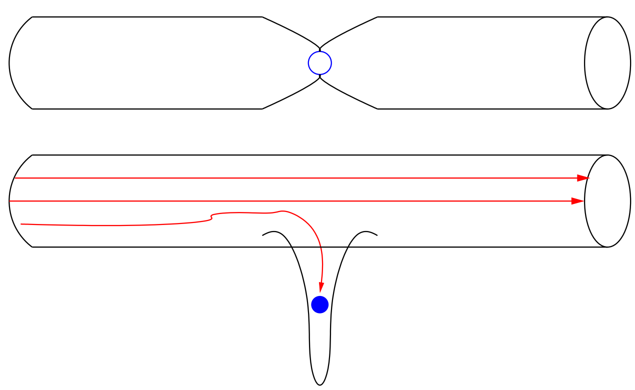

Figure 2.8: The extended horizontal direction represents 4D space-time. The top tube comes with the 3-cycle wrapped by the D5 brane, which wants to shrink. The bottom tube represent the other 3-cycle where the flux is changing, in which the brane is a point like object where the flux line can end. Placing the charge on a locally warped region also reduces 4D tension.

Kähler moduli. It is also easy to see why the shrinking 3-cycle volume and the warp factor help to reduce the effective 4D tension.

Of course, it is very surprising to see that the balance between reducing σ_m and increasing $\sigma_1 + \sigma_2$ happens at such an extreme geometry—a strongly warped Calabi-Yau. In the next section we will provide a more quantitative analysis in this particular case. Here we want to suggest a good intuition for general multi-field tunneling. The roughly equal separate contributions shown in figure 2.6 suggest an equipartition among the three terms σ_1, σ_2, and σ_m that make up the action, (2.80). This is quite natural assuming that the three terms depend on a parameter in the same way (say polynomially or exponentially). What we have is essentially a generalized virial theorem telling us that the three terms should have similar orders of magnitude. Knowing this in advance, we could use this to estimate how big the deformation of the vacuum geometry is.

2.6.2 The Shortest Path

Our numerical results suggest a simple analytical argument for conifunneling. As noted previously, although the axio-dilaton τ changes during tunneling, it contributes very little to the action integral. Therefore the dynamics is similar to a 2D problem in just the complex structure modulus z.

We start from the simplest case with 2D canonical kinetic term in polar coordinates,

$$L = \frac{1}{2}\left(\dot{r}^2 + r^2\dot{\theta}^2\right) - V_{\text{inverse}}(r, \theta) \ . \tag{2.84}$$

Let us first assume that the inverse potential V_{inverse} does not have any special properties near the conifold point (taken to be at the origin, $r = 0$). In this case, minimizing the action is like finding the shortest path, which is of course a straight line. If there are multiple sheets through branch cuts emanating from the conifold point along $\theta = 2\pi n$ there is an additional constraint. When the angular separation between two points is larger than π, a straight line will be obstructed by the branch cut. Therefore the maximum angular separation is π if two vacua are to be connected by a tunneling path.

The strongly warped behavior near the conifold point in our mirror quintic case tells us that we must modify the above with non-canonical kinetic terms

$$L = \frac{K(r)}{2}\left(\dot{r}^2 + r^2\dot{\theta}^2\right) - V_{\text{inverse}}(r,\theta) \ . \tag{2.85}$$

Assuming that the dominant behavior of the Kähler metric is of the form

$$K(r) = r^{2\beta} \ , \tag{2.86}$$

we may change to a more natural set of variables, defining

$$\tilde{r} = \frac{r^{\beta+1}}{\beta+1} \ . \tag{2.87}$$

This yields

$$L = \frac{1}{2}\left(\dot{\tilde{r}}^2 + \tilde{r}^2(\beta+1)^2\dot{\theta}^2\right) - \tilde{V}_{\text{inverse}}(\tilde{r},\theta) \ , \tag{2.88}$$

where

$$\tilde{V}_{\text{inverse}}(\tilde{r},\theta) = V_{\text{inverse}}\left([(\beta+1)\tilde{r}]^{1/(\beta+1)},\theta\right) \ . \tag{2.89}$$

Ignoring the inverse potential, we can see that

$$\Delta\theta_{\max} = \frac{\pi}{\beta+1} \ . \tag{2.90}$$

In our case $\beta = -2/3$, so $\Delta\theta_{\max} = 3\pi$, namely 3/2 of monodromy transformation, is the best we can get. We have confirmed this with numerical simulations.

Also, note that if we did not include the strong warping correction, we would have had

$$K(r) \sim \log r \ , \qquad V(r) \sim \log r \ , \tag{2.91}$$

near $r = 0$. Since $\log r$ diverges slower than any r^β with $\beta < 0$, it should give us roughly $\Delta\theta_{\max} = \pi$. Also the uncorrected V has a logarithmic divergence, which corresponds to an attractive core in the inverse potential. It is also weaker than, for example, $V_{\text{inverse}} = -1/r$. As we saw in the simulation, there is no reason that a path can make $\Delta\theta \sim 2\pi$.

From this point of view, conifunneling happens because the path needs the strong warping correction to the Kähler metric in order to make a monodromy angle change of 2π. For our particular choice of fluxes $F_3 = -1$, this is the minimum amount by which F_0 can change. With $|F_3| > 1$, one might expect to see several vacua on one sheet, which would correspond to changing F_0 by 1 several times. We have not seen such things in any of the examples we have investigated[10]. However, let us for the moment simply assume that there are cases with multiple vacua for $|F_3| > 1$. From our result, it is quite natural to make the following 3 conjectures:

- For angular changes less than π, which means $|\Delta F_0| < |F_3|/2$, tunneling is possible regardless of warping and the path does not get close to the conifold point.
- For angular changes larger than π, which means $|\Delta F_0| > |F_3|/2$, we will see conifunneling.
- For angular changes larger than 3π, which means $|\Delta F_0| > 3|F_3|/2$, there will be no tunneling path.

2.7 Discussion

We have undertaken a detailed study of the flux transitions in type IIB one-parameter models. We have focused throughout on the mirror-quintic for definiteness. Vacua that are related by a monodromy transformation around the conifold point were studied and domain wall

[10]Multiple vacua in a given sheet have been observed in other analyses [37], but τ is treated as a fixed parameter. Our τ is dynamical and we know of no physical reason that requires multiple vacua on a single sheet.

solutions that interpolate between them were found numerically. A general feature is that the domain wall was driven near the conifold point where strong warping effects dominate. A nice geometrical picture associated with this transition was given. In particular, the nucleating brane favors a small cycle so that the effective 4D tension is minimized. Balancing this against the action required to deform to and from this configuration tells us that the cycle must approach some minimal size at which point the monodromy/brane nucleation takes place.

The usual intuition might have suggested that since these flux vacua are near each other in the complex moduli space, it should be simple to construct an appropriately charged brane whose nucleation brings one from one vacuum to another. Our findings suggest that competing effects between the energy required to nucleate a brane wrapping the appropriate cycles and the contraction or growth of these cycles are an essential aspect of the dynamics. Thus, it seems clear that given an initial flux vacuum, finding the most probable tunneling path is more subtle than simply looking at the separation in z-space and concluding that a brane can connect two neighboring vacua. Rather, such a brane would still need to wrap appropriate cycles in order to absorb the appropriate charges, and thus, we expect that the dynamics of these cycles will play a crucial role in determining when such a brane can be nucleated. Because of this, we expect conifunneling to be important in determining how tunneling occurs through a "discretuum" [17] of flux vacua such as that envisioned by Bousso and Polchinski [18].

Chapter 3

Warped Vacuum Statistics

3.1 Introduction

Complex structure moduli in type IIB string theory are stabilized by turning on various p-form fluxes on the internal manifold. This process yields a very large number of stable configurations each of which in principle leads to distinct low-energy predictions. Understanding this *landscape* of string theory is of utmost importance. Above we have seen an in-depth discussion of the dynamics governing these low-energy solutions and found that the conifold point seems to be of distinguished importance [52]. However, another aspect of the vacua that is well studied in the literature is that of statistics [18, 53, 54]. As argued in [18], the existence of very many vacua with closely spaced vacuum energies may take us one step toward understanding the seemingly unnatural value for the cosmological constant. Furthermore, it is reasonable to suspect that the distribution of vacua in moduli space will also have an impact on the dynamics since nearby vacua would be expected to have different tunneling rates than distant ones. As a result, it is valuable to understand various statistical aspects of the distribution of vacua better. Such studies were undertaken in [53] and [54] and later numerically in [32] where they found that the conifold acts as an accumulation point for vacua in the landscape. In fact, in a Monte-Carlo search [32] a significant number of vacua were found as far in as $|\xi| \sim e^{-120}$ where ξ is the complex structure modulus taken to vanish at the conifold point.

Interestingly we also know that it is precisely near the conifold point that the back-reaction of fluxes in the form of warping becomes important. It thus seems natural and necessary to investigate precisely what type of effect warping has on the analysis carried out in [53, 54, 32]. Here we undertake such an analysis.

3.2 Background

Compactifying type IIB string theory on a Calabi-Yau manifold leads to a low-energy effective field theory that contains various scalar fields called moduli. These moduli are related to the smooth ways in which the internal Calabi-Yau manifold can be deformed. Some of these scalar fields, the ones that are related to the complex structure deformations, may be stabilized by turning on various p-form fluxes that naturally appear in the supergravity theory on the internal manifold. This process generates the Gukov-Vafa-Witten superpotential [62]

$$W(z) = \int \Omega_3 \wedge G_3. \tag{3.1}$$

Here the integral is taken over the Calabi-Yau manifold, Ω_3 is its holomorphic $(3,0)$ form, and $G_3 = F_3 - \tau H_3$ is a combination of the the two 3-form field strengths and the axio-dilaton. These are the fluxes that are turned on to yield the superpotential above. As the complex structure is deformed, the value for W changes, something that is indicated by the explicit dependence of W on the complex structure parameter z. Given this superpotential, the scalar potential is given by the usual supergravity form

$$V = e^{K/M_P^2} \left(K^{a\bar{b}} D_a W \bar{D}_{\bar{b}} \bar{W} \right). \tag{3.2}$$

The sum here runs over the complex structure moduli ($a, b = 1, 2, \ldots, h^{2,1}$) as well as the axio-dilaton ($a, b = 0$). Notice that the term $-\frac{3}{M_P^2}|W|^2$ that is usually present in the expression for the potential in supergravity is absent above. This is because for the overall volume modulus ρ, the term $K^{\rho\bar{\rho}}|D_\rho W|^2$ precisely cancels against $-\frac{3}{M_P^2}|W|^2$. This is simply a symptom of the fact that flux compactification can only stabilize the complex structure parameters so that the superpotential ends up independent of the Kähler moduli.

The strategy is now to analyze the minima of the potential in (3.2). In particular we will focus on supersymmetric vacua in the discussion to follow.

3.3 Analytical Distributions

We are ultimately interested in understanding the distribution of vacua near the conifold point. However, a more tractable quantity to compute is the so-called index density defined below. This is closely related to the count of vacua, and in fact approximates the count very well in the cases we discuss. We begin by reviewing past results and then continue with the analysis by adding modifications due to warping.

3.3.1 Counting the Vacua

Here we will review the derivation of the index density given by Douglas and Denef in [54], focusing on areas where our analysis, including the effects of warping, will differ. We will restrict attention to supersymmetric[1] vacua that satisfy $D_a W = 0$ for all complex moduli and the axio-dilaton. The strategy is to consider these equations as constraints on the choice of fluxes and otherwise, simply allow the fluxes to scan. First, assume that fluxes are fixed

[1]Technically supersymmetric vacua must satisfy $D_a W = 0$ for all moduli including those in the Kähler sector. However, since we are not stabilizing the Kähler moduli, we refer to vacua for which $D_a W = 0$ only for the complex structure moduli and the axio-dilaton as supersymmetric.

and consider the function on moduli space given by[2]

$$\delta^{2n+2}(DW(z)) \equiv \delta(D_0W(z))\ldots\delta(D_nW(z))\delta(\overline{D_0W(z)})\ldots\delta(\overline{D_nW(z)}). \tag{3.3}$$

Clearly this provides support only at the locations of the vacua. However, as written each vacuum does not contribute with the same weight. To see this, rewrite equation (3.3) as a sum of delta functions which explicitly spike at the locations of the minima

$$\delta^{2n+2}(DW(z)) = \sum_{\text{vac}} \frac{\delta^{2n+2}(z - z_{\text{vac}})}{|\det D^2W|}. \tag{3.4}$$

Here the determinant arises from expanding the argument of the delta functions near each minimum in much the same way as

$$\delta(f(x)) = \sum \delta(f'(x_{\text{zero}})(x - x_{\text{zero}})) = \sum \frac{\delta(x - x_{\text{zero}})}{|f'(x)|}. \tag{3.5}$$

The matrix denoted D^2W is the $(2n+2)\times(2n+2)$ matrix

$$\begin{pmatrix} \partial_a D_b W & \partial_a \overline{D_b W} \\ \partial_{\overline{a}} D_b W & \overline{\partial_a D_b W} \end{pmatrix}, \tag{3.6}$$

where we let a, b range over the $n = h^{1,2}$ moduli as well as the axio-dilaton. Note that the partial derivatives in the matrix above can be replaced by covariant derivatives at the vacua since there the conditions $D_aW = 0$ render the two expressions equivalent

$$\partial_a D_b W = D_a D_b W - (\partial_a K) D_b W = D_a D_b W \quad \text{at supersymmetric vacua where } D_bW = 0. \tag{3.7}$$

If we then integrate this over the moduli space we find contributions from each vacuum associated with the fixed set of fluxes with weight $|\det D^2W|^{-1}$. Since the value of this

[2] Our conventions for the delta functions and integration measures depending on a complex variable z are given by $\delta^2(z) = \delta(\text{Re } z)\delta(\text{Im } z)$, and $d^2z = d(\text{Re } z)d(\text{Im } z)$.

expression varies over the moduli space, the result of this integration will not reflect the number of vacua but rather some sort of weighted sum of them. To actually count the vacua, we must instead integrate over the delta-functions appropriately weighted

$$\int d^{2n}z d^2\tau \, \delta^{2n+2}(DW(z)) |\det D^2 W|. \tag{3.8}$$

This expression defines the vacuum count for a given set of fluxes. Another useful quantity related to the vacuum count considered in [54] is the index, which involves dropping the absolute values around the determinant of the fermion mass matrix

$$\int d^{2n}z d^2\tau \, \delta^{2n+2}(DW(z)) \det D^2 W. \tag{3.9}$$

This integral then counts the number of positive vacua minus the number of negative vacua, where parity is given by the sign of the determinant of the matrix in equation (3.6). The index therefore provides us with a lower bound to the number of vacua (since the difference between positive and negative vacua is always bounded above by their sum). So far our discussion has focused on a fixed set of fluxes. To count *all* vacua, we must then sum over the fluxes. The fluxes must satisfy the tadpole condition which can be thought of as a consistency condition on how the fluxes can be organized on the internal manifold

$$L = \int_{\mathrm{CY}} F_3 \wedge H_3 \leq L_*. \tag{3.10}$$

Here L_* is the maximum possible value for L. L_* can be derived from F-theory and as a result it will turn out to be useful to lift this discussion from type IIB supergravity to F-theory. To see how this works, recall that the action for type IIB supergravity has an $SL(2,\mathbb{Z})$ symmetry under which the axio-dilaton transforms as

$$\tau \to \frac{a\tau + b}{c\tau + d} \qquad \text{where} \qquad ad - bc = 1. \tag{3.11}$$

By using these transformations, one can restrict the value of the axio-dilaton to lie in the region[3]

$$-1/2 \leq \mathrm{Re}(\tau) \leq 1/2 \qquad \text{and} \qquad |\tau| > 1. \tag{3.12}$$

This should be familiar as the fundamental domain for the complex structure parameter of a torus. It is thus natural to ask if one can incorporate the dynamics of the axio-dilaton by considering some new theory which naturally lives in 12 dimensions which is then compactified on a space that is locally the direct product of a Calabi-Yau threefold and a two torus. This is in fact possible, and the theory one must consider is called F-theory. More precisely, the internal manifold $\mathcal{M}$ is taken as an elliptically fibered Calabi-Yau four-fold, whose base consists of the original three-fold and fibers are given by the auxiliary 2-torus whose complex structure parameter is given by the axio-dilaton τ. In general F-theory compactifications, the four-fold does not have to be a global direct product bundle of a three-fold and a torus (as is true for any fiber bundle) and in fact below we consider precisely such a nontrivial bundle.

We decompose the holomorphic 4-form of the Calabi-Yau four-fold on which F-theory is to be compactified in terms of the holomorphic 3-form from the type IIB Calabi-Yau three-fold and the holomorphic 1-form defined on the torus

$$\Omega_4 = \Omega_1 \wedge \Omega_3. \tag{3.13}$$

If we consider the two 1-cycles $\mathcal{A}$ and $\mathcal{B}$ on the torus, we can define the two 1-forms α and β dual to the cycles $\mathcal{A}$ and $\mathcal{B}$ such that $\int_{\mathcal{A}} \gamma = \int_{T^2} \alpha \wedge \gamma$ and $\int_{\mathcal{B}} \gamma = \int_{T^2} \beta \wedge \gamma$ for all closed 1-forms γ. Then, as long as we define our holomorphic 1-form Ω_1 as

$$\Omega_1 = \alpha - \tau\beta, \tag{3.14}$$

[3]In particular one would use the transformations $\tau \to \tau + 1$ and $\tau \to -1/\tau$ multiple times to accomplish this.

we will have $\tau = \int_{\mathcal{A}} \Omega_1 / \int_{\mathcal{B}} \Omega_1$ as we want for the complex structure of the torus. Furthermore, if we write the flux 4-form that appears in F-theory in terms of those from type IIB as $G_4 = \beta \wedge F_3 - \alpha \wedge H_3$, we can write the left-hand side of the tadpole condition as

$$\frac{1}{2} \int_{\mathcal{M}} G_4 \wedge G_4 = - \int_{T^2} \alpha \wedge \beta \int_{CY_3} F_3 \wedge H_3. \tag{3.15}$$

If we normalize the F-theory torus volume so that $\int_{T^2} \alpha \wedge \beta = -1$, this exactly reproduces the tadpole condition in the type IIB picture. With $K = \dim H^3_{CY_3}$ we've lumped the $2K$ fluxes $F_0, \ldots, F_{K-1}, H_0, \ldots, H_{K-1}$ into the $2K$ components of G_4. Also note that with this definition of the flux 4-form, we can write the usual type IIB superpotential as

$$W = \int_{\mathcal{M}} \Omega_4 \wedge G_4. \tag{3.16}$$

As a result, we have made explicit the correspondence between type IIB supergravity and F-theory. We continue by choosing a particular basis of 3-forms on the CY_3 $\{\Sigma_i\}$ with $i = 1, 2, \ldots, \dim H^3_{CY_3}$, and denote the intersection form in this basis as Q_{ij} so that

$$\int_{CY_3} \Sigma_i \wedge \Sigma_j = Q_{ij}. \tag{3.17}$$

We can extend $\{\Sigma_i\}$ to a basis of 4-forms of $\mathcal{M}$ by wedging them with the 1-forms α and β on the torus, $\{\alpha \wedge \Sigma_a, \beta \wedge \Sigma_a\}$. In this basis, we denote the components of the field strength G_4 by N_a with $a = 0, 1, \ldots 2K - 1$, and the intersection form in the full 4 (complex) dimensional space by η_{ab}. Then, the tadpole condition in equation (3.10) can be written in terms of the components of the two fluxes ($F = F^i \Sigma_i$ and $H = H^i \Sigma_i$) as

$$L = \frac{1}{2} N^a \eta_{ab} N^b = F^i Q_{ij} H^j \leq L_* \tag{3.18}$$

We should then sum only over the fluxes that satisfy this inequality. We can accomplish this by summing over all fluxes while including a step function that enforces the inequality.

$$\text{Index} = \sum_{\text{Fluxes}} \theta(L_* - L) \int d^{2n}z d^2\tau \, \delta^{2n+2}(DW(z)) \det D^2W \tag{3.19}$$

We write the step function as an integral over a delta function[4],

$$\theta(L_* - L) = \int_{-\infty}^{L_*} \delta(L - \widetilde{L}) d\widetilde{L} \tag{3.20}$$

yielding

$$\text{Index} = \sum_{\text{Fluxes}} \int_{-\infty}^{L_*} d\widetilde{L} \int d^{2n}z d^2\tau \, \delta(L - \widetilde{L})\delta^{2n+2}(DW(z)) \det D^2W. \tag{3.21}$$

By treating the fluxes $N_0, \ldots, N_{2K-1}$ as continuous, we can approximate this sum by an integral,

$$\text{Index} = \int_{-\infty}^{L_*} d\widetilde{L} \int d^{2K}N \int d^{2n}z d^2\tau \, \delta(L - \widetilde{L})\delta^{2n+2}(DW(z)) \det D^2W. \tag{3.22}$$

It is natural to define the *index density* in moduli (and axio-dilaton) space by

$$\mu_I(z, \tau) = \int_{-\infty}^{L_*} d\widetilde{L} \int d^{2K}N \, \delta(L - \widetilde{L})\delta^{2n+2}(DW(z)) \det D^2W. \tag{3.23}$$

Upon integrating over τ, z, this will then equal the total index. We now pursue the logic of [53, 54] and rewrite this index density in terms of geometric properties of the moduli space. A first step in doing this is to change basis from $\{\alpha \wedge \Sigma_a, \beta \wedge \Sigma_a\}$ to the set of linearly independent 4-forms $\{\Omega_4, D_a\Omega_4, D_0D_i\Omega_4\} \cup \{c.c\}$ where a ranges over the complex moduli as well as the axio-dilaton while i ranges only over the moduli. This proposed basis consists of $4(n+1)$ elements where n denotes the number of complex moduli in our theory, which

[4] Note that in [54] the step-function is expressed in terms of a contour integral over an exponential $e^{\alpha L_*}$. Our expression in terms of a delta function proves to be more useful for the analysis incorporating warping effects.

agrees with the $2K$ elements of the original basis. This new basis satisfies

$$\begin{aligned}
\int_{\mathcal{M}} \Omega_4 \wedge \bar{\Omega}_4 &= e^{-K(\tau,z)} && (3.24)\\
\int_{\mathcal{M}} D_a\Omega_4 \wedge \bar{D}_{\bar{b}}\bar{\Omega}_4 &= -e^{-K(\tau,z)}K_{a\bar{b}} && (3.25)\\
\int_{\mathcal{M}} D_0 D_i\Omega_4 \wedge \bar{D}_{\bar{0}}\bar{D}_{\bar{j}}\bar{\Omega}_4 &= e^{-K(\tau,z)}K_{\tau\bar{\tau}}K_{i\bar{j}}, && (3.26)
\end{aligned}$$

with all other combinations vanishing. We now manipulate this new basis in a way to produce one that is orthonormal. First, by rescaling all of our basis elements by the factor $e^{K(\tau,z)/2}$, the new basis won't have any of the extra exponentials in their inner products:

$$\begin{aligned}
\int_{\mathcal{M}} e^{K(\tau,z)/2}\Omega_4 \wedge e^{K(\tau,z)/2}\bar{\Omega}_4 &= 1 && (3.27)\\
\int_{\mathcal{M}} e^{K(\tau,z)/2}D_i\Omega_4 \wedge e^{K(\tau,z)/2}\bar{D}_{\bar{j}}\bar{\Omega}_4 &= -K_{i\bar{j}} && (3.28)\\
\int_{\mathcal{M}} e^{K(\tau,z)/2}D_0 D_i\Omega_4 \wedge e^{K(\tau,z)/2}\bar{D}_{\bar{0}}\bar{D}_{\bar{j}}\bar{\Omega}_4 &= K_{\tau\bar{\tau}}K_{i\bar{j}}, && (3.29)
\end{aligned}$$

And because of the properties of the covariant derivative, that is that it transforms covariantly under Kähler transformations, we can accomplish these changes by rescaling the holomorphic four-form by this same factor:

$$\Omega_4 \to e^{K(\tau,z)/2}\Omega_4. \tag{3.30}$$

For notational simplicity we will redefine Ω_4 to represent this rescaled version. When we want to explicitly refer to the actual holomorphic 4-form, we will denote it as $\widehat{\Omega}_4$:

$$\Omega_4 = e^{K(\tau,z)/2}\widehat{\Omega}_4. \tag{3.31}$$

Finally, we can consider any linear combination of the basis above. In particular, we consider the set $\mathcal{B} = \{\Omega_4, D_A\Omega_4, D_{\underline{0}}D_I\Omega_4\} \cup \{c.c.\}$ where $D_A \equiv e^a_A D_a$, and the vielbeins e^a_A satisfy

$e^a_A e^{\bar{b}}_{\bar{B}} K_{a\bar{b}} = \delta_{A\bar{B}}$, as usual. Our new basis is orthonormal:

$$\int_{\mathcal{M}} \Omega_4 \wedge \bar{\Omega}_4 \;=\; 1 \tag{3.32}$$

$$\int_{\mathcal{M}} D_A\Omega_4 \wedge \bar{D}_{\bar{B}}\bar{\Omega}_4 \;=\; -\delta_{A\bar{B}} \tag{3.33}$$

$$\int_{\mathcal{M}} D_{\underline{0}} D_I \Omega_4 \wedge \bar{D}_{\underline{\bar{0}}} \bar{D}_{\bar{J}} \bar{\Omega}_4 \;=\; \delta_{I\bar{J}}. \tag{3.34}$$

The 4-form flux G_4 in the new basis is given by

$$G_4 = \overline{X}\Omega_4 - \overline{Y}^A D_A\Omega_4 + \overline{Z}^I D_{\underline{0}} D_I \Omega_4 + \text{c.c.} \tag{3.35}$$

with $X, Y^{\bar{A}}, Z^{\bar{I}}, \overline{X}, \overline{Y}^A, \overline{Z}^I$ being the coefficients of G_4 in this basis. We have chosen the signs in front of the various coefficients for later convenience. Note that G_4 does not depend on the complex structure moduli or axio-dilaton, which implies that the coefficients $X, Y^{\bar{A}}, Z^{\bar{I}}, \overline{X}, \overline{Y}^A, \overline{Z}^I$ must themselves depend on z^i and τ in such a way as to cancel the dependences arising from Ω_4 and its derivatives in the expression for G_4 above. Since G_4 does not depend on the complex structure of the Calabi-Yau or the axio-dilaton, we can relate these coefficients to various combinations of derivatives acting on the superpotential.

In particular

$$\begin{aligned}
W &= \int \Omega_4 \wedge G_4 = X && (3.36)\\
D_A W &= \int D_A \Omega_4 \wedge G_4 = Y_A && (3.37)\\
D_{\underline{0}} D_{\underline{0}} W &= 0 && (3.38)\\
D_{\underline{0}} D_I W &= \int D_{\underline{0}} D_I \Omega_4 \wedge G_4 = Z_I && (3.39)\\
D_I D_J W &= \int D_I D_J \Omega_4 \wedge G_4 = \mathcal{F}_{IJK} \overline{Z}^K && (3.40)\\
\overline{D}_{\overline{I}} D_J W &= \delta_{\overline{I}J} X && (3.41)\\
\overline{D}_{\overline{0}} D_{\underline{0}} W &= X && (3.42)\\
\overline{D}_{\underline{\overline{0}}} D_I W &= 0. && (3.43)
\end{aligned}$$

Note that we have defined the coefficients $\mathcal{F}_{IJK} = i \int_{CY} \Omega_3 \wedge D_I D_J D_K \Omega_3 = i \int_{CY} \Omega_3 \wedge \partial_I \partial_J \partial_K \Omega_3$. Also, note that W denotes the rescaled superpotential; when we want to explicitly refer to the original one, we will once again place a hat on top of it $(\widehat{W})$. We briefly divert our attention to deriving these expressions for the components of G_4.

- $W = X$

  By the definition of the superpotential, we have

$$\begin{aligned}
W &= \int_{\mathcal{M}} G_4 \wedge \Omega_4 \\
&= \int_{\mathcal{M}} \left(\overline{X} \Omega_4 - \overline{Y}^A D_A \Omega_4 + \overline{Z}^I D_{\underline{0}} D_I \Omega_4 + \text{c.c.} \right) \wedge \Omega_4 = X && (3.44)
\end{aligned}$$

  In the last step we used the orthonormality of the basis.

- $D_A W = Y_A$

Since G_4 is independent of the moduli, we can move the covariant derivative inside the integral so that it only hits Ω_4.

$$D_A W = \int_{\mathcal{M}} G_4 \wedge D_A \Omega_4 \tag{3.45}$$

Then inserting the expression for G_4 in the new basis and again using the orthonormality of the basis ($\int_{\mathcal{M}} \overline{D}_{\bar{B}} \overline{\Omega}_4 \wedge D_A \Omega_4 = -\delta_{\bar{B}A}$), we obtain

$$\begin{aligned} D_A W &= \int_{\mathcal{M}} \left(\overline{X} \Omega_4 - \overline{Y}^A D_A \Omega_4 + \overline{Z}^I D_{\underline{0}} D_I \Omega_4 + \text{c.c.} \right) \wedge D_A \Omega_4 \\ &= -Y^{\bar{B}} \int_{\mathcal{M}} \overline{D}_{\bar{B}} \overline{\Omega}_4 \wedge D_A \Omega_4 = +Y_A \end{aligned} \tag{3.46}$$

- $D_{\underline{0}} D_{\underline{0}} W = 0$

  Once again, since G_4 is independent of the moduli, we have

$$D_{\underline{0}} D_{\underline{0}} W = \int_{\mathcal{M}} G_4 \wedge D_{\underline{0}} D_{\underline{0}} \Omega_4 \tag{3.47}$$

  Now $D_{\underline{0}} \Omega_4$ is a $(0,1) \wedge (3,0)$-form (where we highlight the order of the form in the fiber and on the base respectively) since

$$D_{\underline{0}} \Omega_4 = (D_{\underline{0}} \Omega_1) \wedge \Omega_3 \in H^{0,1} \wedge H^{3,0}. \tag{3.48}$$

  In fact, we see that

$$D_\tau \widehat{\Omega}_1 = (\partial_\tau + K_\tau)(\alpha - \tau\beta) = K_\tau (\alpha - \overline{\tau}\beta) = K_\tau \overline{\widehat{\Omega}}_1 \tag{3.49}$$

  where we have used $K_\tau = -1/(\tau - \overline{\tau})$. Using the fact that the vielbein $e^0_{\underline{0}} = 1/K_\tau$, we have

$$D_{\underline{0}} \Omega_4 = \overline{\Omega}_1 \wedge \Omega_3, \tag{3.50}$$

As a result, the expression under investigation reduces to

$$D_{\underline{0}} D_{\underline{0}} \Omega_4 = \left(D_{\underline{0}} \overline{\Omega}_1\right) \wedge \Omega_3. \tag{3.51}$$

However we know that $D_{\underline{0}} \overline{\Omega}_1 = 0$, so the identity holds.

- $D_{\underline{0}} D_I W = Z_I$

  This identity follows from orthonormality:

$$D_{\underline{0}} D_I W = \int_{\mathcal{M}} G_4 \wedge D_{\underline{0}} D_I \Omega = \int_{\mathcal{M}} \left(\overline{X}\Omega_4 - \overline{Y}^A D_A \Omega_4 + \overline{Z}^I D_{\underline{0}} D_I \Omega_4 + \text{c.c.}\right) \wedge D_{\underline{0}} D_I \Omega = Z_I \tag{3.52}$$

- $D_I D_J W = \mathcal{F}_{IJK} \overline{Z}^K$

  We will again use the definition for G_4

$$D_I D_J W = \int_{\mathcal{M}} \left(\overline{X}\Omega_4 - \overline{Y}^A D_A \Omega_4 + \overline{Z}^I D_{\underline{0}} D_I \Omega_4 + \text{c.c.}\right) \wedge D_I D_J \Omega_4 \tag{3.53}$$

It is useful to note that $D_A D_B \Omega_4$ is a (2,2)-form. In fact, given the nature of our Calabi-Yau 4-fold, essentially factorizing into a 3-fold and a torus, this (2,2)-form can be decomposed as $(2,2) = (1,0) \wedge (1,2) \oplus (0,1) \wedge (2,1)$. To see this, note that $D_A \Omega_4$ could in principle be a mixture of a $(3,1) \oplus (4,0)$, but the (4,0) component vanishes:

$$\int_{\mathcal{M}} D_A \Omega_4 \wedge \overline{\Omega}_4 = D_A \left(\int_{\mathcal{M}} \Omega_4 \wedge \overline{\Omega}_4\right) - \int_{\mathcal{M}} \Omega_4 \wedge D_A \overline{\Omega}_4 = 0. \tag{3.54}$$

The second term here vanishes since $\overline{\Omega}_4$ varies holomorphically with respect to the moduli space coordinates while the first term vanishes due to the definition of the covariant derivative and the Kähler potential:

$$D_A \left(\int_{\mathcal{M}} \Omega_4 \wedge \overline{\Omega}_4\right) = D_A e^{-K} = \partial_A e^{-K} + K_A e^{-K} = -K_A e^{-K} + K_A e^{-K} = 0. \tag{3.55}$$

Similarly $D_A D_B \Omega_4$ could in principle have $(2,2) \oplus (3,1) \oplus (4,0)$ structure. However,

$$\int_{\mathcal{M}} D_A D_B \Omega_4 \wedge \overline{\Omega}_4 = D_A \left(\int_{\mathcal{M}} D_B \Omega_4 \wedge \overline{\Omega}_4 \right) - \int_{\mathcal{M}} D_B \Omega_4 \wedge D_A \overline{\Omega}_4 = 0 \tag{3.56}$$

implying that there is no $(4,0)$ component. Furthermore

$$\int_{\mathcal{M}} D_A D_B \Omega_4 \wedge \overline{D}_{\overline{C}} \overline{\Omega}_4 = D_A \left(\int_{\mathcal{M}} D_B \Omega_4 \wedge \overline{D}_{\overline{C}} \overline{\Omega}_4 \right) - \int_{\mathcal{M}} D_B \Omega_4 \wedge D_A \overline{D}_{\overline{C}} \overline{\Omega}_4 \tag{3.57}$$

the first term on the left-hand-side is equal to $D_A \delta_{B\overline{C}} = 0$. The second term becomes

$$\delta_{A\overline{C}} \int_{\mathcal{M}} D_B \Omega_4 \wedge \overline{\Omega}_4 = 0 \tag{3.58}$$

which shows that there is no $(3,1)$ component in $D_A D_B \Omega_4$ either and therefore that it is completely contained in $H^{2,2}$. Because of the direct product nature of the four-fold, one can further break this up as

$$D_A D_B \Omega_4 \in H^{1,0} \wedge H^{1,2} \oplus H^{0,1} \wedge H^{2,1}. \tag{3.59}$$

Now, $D_I D_J \Omega_4$ is precisely a $(1,0) \wedge (1,2)$-form since the covariant derivatives only act on the 3-fold factor. The only pieces of the integral in (3.53) that can yield a non-zero result must then be of the form $(0,1) \wedge (2,1)$, which are thus proportional to $D_{\underline{0}} D_I \Omega_4$. This leaves us with

$$D_I D_J W = \overline{Z}^K \int_{\mathcal{M}} D_{\underline{0}} D_K \Omega_4 \wedge D_I D_J \Omega_4. \tag{3.60}$$

The D_K and $D_{\underline{0}}$ derivatives commute, so we have

$$D_I D_J W = \overline{Z}^K D_K \left(\int_{\mathcal{M}} D_{\underline{0}} \Omega_4 \wedge D_I D_J \Omega_4 \right) - \overline{Z}^K \int_{\mathcal{M}} D_{\underline{0}} \Omega_4 \wedge D_K D_I D_J \Omega_4. \tag{3.61}$$

The first term on the right-hand-side vanishes due to orthonormality since $D_{\underline{0}}\Omega_4$ is a (3,1)-form while $D_I D_J \Omega_4$ is a $(1,0)\wedge(1,2)$-form. Factorizing $\Omega_4 = \Omega_1 \wedge \Omega_3$, we see that $D_{\underline{0}}\Omega_4 = \overline{\Omega}_1 \wedge \Omega_3$. The integral over the torus will simply yield a factor of $-i$ (recall that Ω_1 refers to the rescaled holomorphic 1-form on the torus, so the usual factor of $e^{-K(\tau,\bar{\tau})}$ is absent), leaving us with

$$D_I D_J W = i\overline{Z}^K \int_{\mathcal{CY}} \Omega_3 \wedge D_K D_I D_J \Omega_3. \tag{3.62}$$

Pulling out all scaling factors and vielbeins, and explicitly writing out the covariant derivatives, we see that the resulting derivatives can all be converted to partials. This allows us to rearrange the ordering and finally gives

$$D_I D_J W = i\overline{Z}^K \int_{\mathcal{CY}} \Omega_3 \wedge \partial_I \partial_J \partial_K \Omega_3 = \mathcal{F}_{IJK}\overline{Z}^K \tag{3.63}$$

where we have defined the coefficients $\mathcal{F}_{IJK} = i\int_{\mathcal{CY}} \Omega_3 \wedge \partial_I \partial_J \partial_K \Omega_3$.

- $\bar{D}_{\bar{A}} D_B W = \delta_{\bar{A}B} X$

First consider

$$\bar{D}_{\bar{a}} D_b \widehat{W} \;=\; \bar{\partial}_{\bar{a}}(\partial_b + K_b)\widehat{W} = (\bar{\partial}_{\bar{a}}\partial_b + K_{b\bar{a}} + K_b \bar{\partial}_{\bar{a}})\widehat{W} = K_{\bar{a}b}\widehat{W} \tag{3.64}$$

The first and last term vanish since $\widehat{W}$ is holomorphic in the moduli. Then, since $W = X$, by reintroducing the scaling factor $e^{K/2}$ and the vielbeins, we have

$$\bar{D}_{\bar{A}} D_B W = \delta_{\bar{A}B} X. \tag{3.65}$$

- $\bar{D}_{\bar{\underline{0}}} D_I W = 0$

We can easily see this by noting that the outer derivative is a regular partial derivative and that this commutes with the inner derivative. Then, since $\hat{W}$ is holomorphic in τ,

$\bar{\partial}_{\bar{0}}$ sends the expression to zero.

We now return to our main analysis. With the expressions (3.36-3.43) we can then rewrite all of our expressions in terms of these new functions on moduli space. For the tadpole condition we obtain

$$L = \frac{1}{2} N\eta N = \frac{1}{2}\int G_4 \wedge G_4 = |X|^2 - |Y|^2 + |Z|^2, \tag{3.66}$$

where $|Y|^2 = \overline{Y}^A Y^{\bar{A}} \delta_{\bar{A}A}$, etc. The index density then becomes

$$\mu_I(z,\tau) = \int_{-\infty}^{L_*} d\widetilde{L} \int d^2X\, d^{2n+2}Y\, d^{2n}Z\, J\, |\det g|\, \delta(\widetilde{L} - |X|^2 + |Y|^2 - |Z|^2)\delta^{2n+2}(Y_A)\, |X|^2$$
$$\times \det \begin{pmatrix} \overline{X}\delta_{IJ} - \frac{Z_I \overline{Z}_J}{X} & \mathcal{F}_{IJK}\overline{Z}^K \\ \overline{\mathcal{F}}_{IJK} Z^K & X\delta_{IJ} - \frac{\overline{Z}_I Z_J}{\overline{X}} \end{pmatrix} \tag{3.67}$$

Here J is the Jacobian obtained in changing variables from N_a to X, Y_A, Z_I, which we will determine explicitly below. We have included an additional factor of $|\det g|$ which comes from transforming both the delta functions and the determinant to the new variables, and note that factors of e^K cancel between the delta functions and the determinant.

Let us now compute the Jacobian $|J|$. In the original basis, the components of G_4 were given by N_a. We can now write the N_a in the new basis

$$N = \eta^{-1}\left(\overline{X}\Pi - \overline{Y}^A D_A \Pi + \overline{Z}^I D_{\underline{0}} D_I \Pi + \text{c.c.}\right). \tag{3.68}$$

Here the Πs are the periods of the rescaled holomorphic 4-form and are related to the usual ones by a factor of $e^{K/2}$.We can see from this expression that the change of basis is achieved by the application of the matrix

$$M = \eta^{-1}(\Pi, -D_A\Pi, D_0 D_I \Pi, c.c.). \tag{3.69}$$

If we use the convention that $d^2z = \frac{1}{2i}dz \wedge d\bar{z}$, we find that the appropriate Jacobian is

$$J = 2^{2(n+1)}|\det M| = 4^{n+1}|\det \eta|^{-1/2}|\det M^\dagger \eta M|^{1/2}. \tag{3.70}$$

We have $M^\dagger \eta M = \mathrm{diag}(1, -\mathbf{1}_{n+1}, \mathbf{1}_n, 1, -\mathbf{1}_{n+1}, \mathbf{1}_n)$, which follows from our choice of an orthonormal basis of 4-forms. This implies that the Jacobian is given by

$$J = 4^{n+1}|\det \eta|^{-1/2}. \tag{3.71}$$

The final expression is then (after explicitly integrating over Y_A),

$$\begin{aligned}\mu_I(z,\tau) = 4^{n+1}|\det \eta|^{-1/2} \int_{-\infty}^{L_*} d\tilde{L} \int d^2X\, d^{2n}Z\, |\det g|\, \delta(\tilde{L} - |X|^2 - |Z|^2)|X|^2 \\ \times \det \begin{pmatrix} \overline{X}\delta_{IJ} - \frac{Z_I \overline{Z}_J}{X} & \mathcal{F}_{IJK}\overline{Z}^K \\ \overline{\mathcal{F}}_{IJK}Z^K & X\delta_{IJ} - \frac{\overline{Z}_I Z_J}{\overline{X}} \end{pmatrix}.\end{aligned} \tag{3.72}$$

We can explicitly integrate over the phases, leaving only integrals over the magnitudes $|X|$ and $|Z|$, showing that the tadpole delta function fixes the region of integration to lie on a circle of radius $\sqrt{\widetilde{L}}$ in the $|X|, |Z|$ plane. There is therefore no need to integrate over negative $\widetilde{L}$s, and furthermore the remaining finite integral can be evaluated. Following this approach, one can show that the index density has a nice geometrical interpretation [54]:

$$\mu_I(z,\tau) = \det(R + \omega\mathbb{I}), \tag{3.73}$$

where R is the curvature 2-form on the moduli space and ω is the Kähler form. For the case of one complex modulus (and the axio-dilaton), this reduces to

$$\mu_I = -\pi^2|\det \eta|^{-1/2}\omega_0 \wedge R_1 \tag{3.74}$$

where ω_0 is the Kähler form on the axio-dilaton side while R_1 is the curvature form on the moduli space side. In order to obtain this, one must use a relationship between the Kähler and curvature forms on the axio-dilaton moduli space: $R_0 = -2\omega_0$.

3.3.2 Incorporating Warping

The analysis above neglected the back-reaction of the fluxes on the geometry. These effects become pronounced when one approaches the conifold locus essentially since one of the cycles that carries flux collapses there. A complete treatment of warped Calabi-Yau geometry involves using the machinery of generalized complex geometry [55, 45, 56]. However, a rough method that produces the appropriate functional behavior induced by warping near the conifold will suffice for our purposes. This behavior can be derived by taking the warped Kähler potential to be approximated by [42]

$$e^{-\widetilde{K}} = \int e^{-4A}\,\Omega \wedge \bar{\Omega}, \tag{3.75}$$

where $e^{-4A} = 1 + e^{-4A_0}/c$ is the warp factor, with e^{-4A_0} capturing the significant warping at the conifold while c is a constant related to the overall volume of the Calabi-Yau manifold. One can roughly divide up the Calabi-Yau manifold into two regions, one that corresponds to the part near the tip of the conifold and another one that corresponds to the rest of the manifold that we will call the bulk. In the bulk, the warp correction is negligible so that $e^{-4A} \to 1$ there. As a result, we can write

$$e^{-\widetilde{K}} \approx \int_{\text{Bulk}} \Omega \wedge \bar{\Omega} + \int_{\text{Conifold}} \left(1 + \frac{e^{-4A_0}}{c}\right) \Omega \wedge \bar{\Omega}. \tag{3.76}$$

In general, we will use tildes to denote quantities that include warp corrections. The warp-corrected Kähler metric has been shown to have the near-conifold form [52, 47, 44, 43]

$$\widetilde{K}_{\xi\bar{\xi}} \approx \frac{K_1}{k} - \frac{1}{2\pi k}\log\xi + \frac{C_w}{k|\xi|^{4/3}} = K_{\xi\bar{\xi}} + \widehat{K}_{\xi\bar{\xi}}, \tag{3.77}$$

where ξ is the local coordinate around the conifold point, $k = \lim_{\xi,\bar{\xi}\to 0} e^{K(\xi,\bar{\xi})}$ and K_1 is a constant (to leading order) associated with the Kähler metric's expansion around the conifold. The hatted quantity in the rightmost expression corresponds to the warp correction to the original, unwarped Kähler metric. The constant C_w is on the order of the inverse volume of the Calabi-Yau, capturing the suppression of the warping effects at large volume.

We find by integrating the expression for the Kähler metric in (3.77), that up to shifts by functions holomorphic and antiholomorphic in ξ, we have

$$
\begin{aligned}
\widetilde{K} &\approx K + 9C_w|\xi|^{2/3} = K + \widehat{K}, && (3.78)\\
\widetilde{K}_\xi &\approx K_\xi + 3C_w\frac{\bar{\xi}^{1/3}}{\xi^{2/3}} = K_\xi + \widehat{K}_\xi. && (3.79)
\end{aligned}
$$

To take warping into account in computing the vacuum count and index, we follow the basic logic laid out above while incorporating various necessary modifications. First, we continue to define quantities such as X, Y, and Z without making any reference to the warping. This is perfectly fine since those are simply geometric quantities defined on the Calabi-Yau itself. As a result, the logic for converting the step function $\theta(L_* - L)$ into an integral is unchanged. What does change however, are the expressions within the delta-functions and the determinant of the fermion mass matrix. More precisely, the positions of the vacua are now determined by the conditions $D_AW + \widehat{K}_AW = 0$, where the second term is the correction due to warping. Thus, the delta-functions must now read

$$\delta^{2n+2}(Y_A + \widehat{K}_AX), \tag{3.80}$$

and the quantities appearing in the fermion mass matrix now have to incorporate warp corrections: $\left(D_A + \widehat{K}_A\right)\left(D_B + \widehat{K}_B\right)W$. Note that at a vacuum we have the equivalence $\partial_A(D_BW + \widehat{K}_BW) \equiv \left(D_A + \widehat{K}_A\right)\left(D_B + \widehat{K}_B\right)W$, and in general we will make use of similar equivalences in what follows. We have:

$$\begin{aligned} D_{\underline{0}}(D_I + \widehat{K}_I)W &\equiv Z_I, & (3.81)\\ \left(D_I + \widehat{K}_I\right)\left(D_J + \widehat{K}_J\right)W &\equiv \mathcal{F}_{IJK}\overline{Z}^K + \widehat{K}_{IJ}X + \widehat{K}_J Y_I, & (3.82)\\ \left(D_I + \widehat{K}_I\right)\overline{\left(D_J + \widehat{K}_J\right)W} &\equiv \left(\delta_{I\bar{J}} + \widehat{K}_{I\bar{J}}\right)\overline{X}. & (3.83) \end{aligned}$$

The first expression is a direct consequence of equation (3.39) together with the fact that there is no τ dependence in the warping correction

$$\begin{aligned} D_{\underline{0}}(D_I + \widehat{K}_I)W &= D_{\underline{0}}D_I W + D_{\underline{0}}(\hat{K}_I W)\\ &= Z_I + \widehat{K}_I D_{\underline{0}} W = Z_I. & (3.84) \end{aligned}$$

The second expression is easily obtained by distributing the various derivatives and tossing away terms proportional to $(D_J + \hat{K}_J)W$ which vanish at the vacua.

$$\begin{aligned} \left(D_I + \widehat{K}_I\right)\left(D_J + \widehat{K}_J\right)W &= D_I D_J W + D_I(\hat{K}_J W) + \hat{K}_I(D_J + \hat{K}_J)W\\ &= D_I D_J W + \hat{K}_{IJ}W + \hat{K}_J D_I W\\ &= \mathcal{F}_{IJK}\bar{Z}^K + \hat{K}_{IJ}X + \hat{K}_J Y_I & (3.85) \end{aligned}$$

Finally, the third expression above is obtained by again distributing the derivatives and tossing away terms proportional to $\overline{\left(D_J + \widehat{K}_J\right)W}$ as well as recognizing that $D_I\bar{W} = 0$.

$$\begin{aligned} \left(D_I + \widehat{K}_I\right)\overline{\left(D_J + \widehat{K}_J\right)W} &= D_I\bar{D}_{\bar{J}}\bar{W} + D_I(\overline{\hat{K}_J W}) + \hat{K}_I\overline{\left(D_J + \widehat{K}_J\right)W}\\ &= \delta_{I\bar{J}}\bar{W} + \hat{K}_{I\bar{J}}\bar{W}\\ &= \left(\delta_{I\bar{J}} + \widehat{K}_{I\bar{J}}\right)\overline{X}. & (3.86) \end{aligned}$$

Upon making these substitutions in order to include warping and then integrating over the

Y_A we find the index density

$$\mu_I = 4^{n+1}|\det\eta|^{-1/2}\int_{-\infty}^{L_*} d\tilde{L}\int d^2X\, d^{2n}Z\,|\det g|\,\delta\left(\tilde{L}-\alpha|X|^2-|Z|^2\right)|X|^2 \quad (3.87)$$

$$\times \det\begin{pmatrix} \overline{X}\mu_{I\bar{J}}-\frac{Z_I\overline{Z}_{\bar{J}}}{X} & \mathcal{F}_{IJK}\overline{Z}^K+\sigma_{IJ}X \\ \overline{\mathcal{F}}_{\overline{IJK}}Z^{\bar{K}}+\bar{\sigma}_{\overline{IJ}}\overline{X} & X\mu_{\bar{I}J}-\frac{\overline{Z}_{\bar{I}}Z_J}{\overline{X}} \end{pmatrix} \quad (3.88)$$

where $\alpha = 1-\widehat{K}_I\overline{\widehat{K}}^I$, $\mu_{I\bar{J}} = \delta_{I\bar{J}}+\widehat{K}_{I\bar{J}}$, and $\sigma_{IJ} = \widehat{K}_{IJ}-\widehat{K}_I\widehat{K}_J$.

In order to compute this density, it proves helpful to consider the special case of one complex modulus as well as the axio-dilaton. In this particular case, we obtain the expression

$$\mu_I \propto \int_{-\infty}^{L_*} d\widetilde{L}\int d^2X\, d^{2n}Z\,|\det g|\,\delta\left(\widetilde{L}-\alpha|X|^2-|Z|^2\right)\left(|Z|^4+(\mu^2-|\sigma|^2)|X|^4-(2\mu+|\mathcal{F}|^2)|X|^2|Z|^2\right) \quad (3.89)$$

Here $\mathcal{F}=\mathcal{F}_{111}$ is the only component of $\mathcal{F}_{IJK}$ in the case of a single complex modulus and similarly for the other indexed quantities. Note, that we have eliminated a few terms that will integrate to zero because they depend explicitly on the phases of X, Z. Far from the conifold, α approaches 1 since the warping corrections can then be neglected. However, when one moves toward the conifold, α gets progressively smaller until at some critical value it equals zero, and then the warping correction drives α negative. As long as α is positive, the tadpole delta function fixes the range of integration so that $|X|$ and $|Z|$ lie on a finite ellipse. Upon computing the integral, one therefore obtains a finite value for the index. However, when α goes to zero, this ellipse becomes increasingly stretched until for $\alpha = 0$, the range of integration for $|X|$ becomes unconstrained. At this point, the integral above for the index density diverges. Then, as α goes negative, this divergence persists as the ellipse turns into a hyperbola. Naively, this suggests that there should be an infinite number of vacua within a finite disk surrounding the conifold point. This is in stark disagreement with numerical Monte-Carlo searches which find a finite density near the conifold (we discuss such numerical simulations in detail below). However, a more careful analysis that we carry out next takes into account the finite bound on the fluxes and yields a finite result.

3.3.3 Finite Fluxes

One major difference between the analysis above and numerical simulations is the range of the fluxes. In numerical simulations fluxes are necessarily kept within a finite range, while in the derivation above, arbitrarily large ones were included. To derive a theoretical distribution that mirrors the effects seen in numerical studies, it is best to include a bound on the fluxes. This complicates the final expression for the theoretical distribution but, of course, the finite bound is physically well motivated since the supergravity approximation breaks down for large enough fluxes. In the absence of warping, the finite range does not lead to dramatic differences from naively taking the bound to infinity, but as we will see, this limit is more involved when warping is included.

Suppose that we bound our fluxes by the range $N_i \in [-\Lambda, \Lambda]$. The N_a and X, Y, Z variables are related by

$$X = N_a \Pi_a \tag{3.90}$$

$$Y_A = N_a D_A \Pi_a \tag{3.91}$$

$$Z_I = N_a D_0 D_I \Pi_a. \tag{3.92}$$

Here the Π's are the periods of the rescaled holomorphic form, as before. We would thus expect the ranges on X, Y, Z to be moduli dependent. Let us separate the phase and magnitude of X, Y, Z. Although in principle, the ranges of the phases may have a complicated dependence on both the moduli and the magnitudes $|X|, |Y|, |Z|$, we will neglect this subtlety and suppose that they range over the usual $[0, 2\pi]$. As a result, we can easily integrate these variables out, leaving us with the integrals over the magnitudes. We would expect to have these range over the values

$$|X| \in [0, \Lambda f_X(\xi,\tau)] \tag{3.93}$$

$$|Y_A| \in [0, \Lambda f_Y(\xi,\tau)] \tag{3.94}$$

$$|Z_I| \in [0, \Lambda f_Z(\xi,\tau)] \tag{3.95}$$

for particular functions on moduli space f_X, f_Y, and f_Z. Let us consider f_X. The largest value that $|X|$ will take corresponds to the fluxes N_a taking one of their two extreme values of $\pm\Lambda$; which of the two possibilities maximizes $|X|$ depends on the near conifold behavior of the periods. We must choose the eight signs for the eight fluxes N_a in such a way that we maximize the expression

$$f_X = \max\left(\left|\sum_a \pm\Pi_a(\xi,\tau)\right|\right). \tag{3.96}$$

Since the periods are all finite in the near conifold limit, the ξ dependence decouples. However, the value for f_X will still be τ dependent. As far as f_Y and f_Z are concerned, the idea is the same except for the fact that the ξ dependence can't be neglected due to logarithmic divergences. In particular, we find that

$$f_X = f_X(\tau) \tag{3.97}$$

$$f_Y = f_Y^1(\tau)|1 - f_Y^2(\tau)\log(\xi)| \tag{3.98}$$

$$f_Z = f_Z^1(\tau)|1 - f_Z^2(\tau)\log(\xi)|. \tag{3.99}$$

Here we have defined functions only of the axio-dilaton $f_X, f_Y^1, f_Y^2, f_Z^1, f_Z^2$. Now consider a fixed point in moduli space ξ as well as a fixed value for τ. Then the upper limits on these integrals will involve particular constants multiplying the flux cutoff Λ. Integrating over the variables Y_0 in the expression for the index density, the delta function $\delta\left(Y_0\right)$ fixes $Y_0 = 0$, leaving us with

$$\begin{aligned}\mu_I \quad &\propto \quad \int_{-\infty}^{L_*} d\widetilde{L} \int_0^{f_X \Lambda} |X| d|X| \int_0^{f_Y \Lambda} |Y| d|Y| \int_0^{f_Z \Lambda} |Z| d|Z| \, |\det g| \, \delta(\widetilde{L} - \alpha |X|^2 - |Z|^2) \\ &\times \quad \delta^2 \left(Y_1 + \widehat{K}_\xi X \right) \left(|Z|^4 + \left(\mu^2 - |\sigma|^2 \right) |X|^4 - \left(2\mu + |\mathcal{F}|^2 \right) |X|^2 |Z|^2 \right). \end{aligned} \tag{3.100}$$

The remaining delta function constraints come from the tadpole condition and the supersymmetry condition $D_\xi W + \widehat{K}_\xi W = 0$, equivalent to $Y_1 + \widehat{K}_\xi X = 0$. Satisfying these constraints will place complicated restrictions on the upper and lower bounds of the remaining integrals. Let us first examine the region of integration imposed by the supersymmetry constraint $Y_1 + \widehat{K}_\xi X = 0$:

- When $|X|$ is at its lower bound of 0, the constraint is trivial to satisfy by also setting $|Y_1| = 0$. Thus, the lower bound of $|X|$ is unchanged.

- However, when $|X| > 0$, there will be points in the moduli space where the warping correction to the Kähler connection is rather large so that $\left| \widehat{K}_\xi X \right| > f_Y \Lambda$. At such points, the supersymmetry constraint cannot be satisfied and so the delta function imposing the constraint $Y_1 = -\widehat{K}_\xi X$ must vanish. We thus see that the upper bound of $|X|$ is restricted in such cases to $f_Y \Lambda / \left| \widehat{K}_\xi \right|$. Solving the delta function constraint for Y_1 requires that the upper bound of the $|X|$ integral be taken to be $|X|_\Lambda = \min \left(\Lambda f_X, \Lambda f_Y / \left| \widehat{K}_\xi \right| \right)$.

Note that in our scheme for bounding the fluxes, the upper limits of integration for $|X|, |Y|$ and $|Z|$ all scale with the cutoff Λ in the same way. So, simply taking the limit as $\Lambda \to \infty$ won't affect the analysis. From our scheme's perspective, it is only in the strictly infinite case where the naive divergence reappears as discussed at the end of section 3.3.2. (One could imagine more complicated schemes for bounding the fluxes, treating X, Y, and Z independently, allowing for a set of limits that recover the divergent results of the naive approach. Such a scheme would increase the difficulty of relating the numerical and theoretical analyses, as investigated in the unwarped case in [53, 54, 32] and also summarized above.

Given the new limits of integration on $|X|$, we can freely integrate out the delta function fixing the value of Y_1:

$$\begin{aligned}\mu_I \;\propto\; & \int_{-\infty}^{L_*} d\widetilde{L} \int_0^{|X|_\Lambda} |X| d|X| \int_0^{f_Z\Lambda} |Z| d|Z| \, |\det g| \, \delta\left(\widetilde{L} - \alpha|X|^2 - |Z|^2\right) \\ \times \;& \left(|Z|^4 + \left(\mu^2 - |\sigma|^2\right)|X|^4 - \left(2\mu + |\mathcal{F}|^2\right)|X|^2|Z|^2\right). \qquad (3.101)\end{aligned}$$

To simplify our notation, let us change variables to $u = |X|^2$ and $v = |Z|^2$. The density can then be written as

$$\mu_I \propto \int_{-\infty}^{L_*} d\widetilde{L} \int_0^{u_\Lambda} du \int_0^{f_Z^2\Lambda^2} dv \, |\det g| \, \delta\left(\widetilde{L} - \alpha u - v\right) \left(v + \left(\mu^2 - |\sigma|^2\right) u^2 - \left(2\mu + |\mathcal{F}|^2\right) uv\right) \qquad (3.102)$$

where $u_\Lambda = |X|^2_\Lambda = \min\left(\Lambda^2 f_X^2, \Lambda^2 f_Y^2 / \left|\widehat{K}_\xi\right|^2\right)$

It is useful to consider the two cases $\alpha > 0$ and $\alpha < 0$, separately.

The case $\alpha > 0$

The delta function in (3.102) arising from the tadpole condition is $\delta(\widetilde{L} - \alpha u - v)$. This constrains the value of v to be $\widetilde{L} - \alpha u$. However, since v must itself lie in a certain interval, this indirectly also constrains the region of integration on the $\widetilde{L}/u$-plane. In the sections to follow we will adhere to the notation $X^{\pm}_{\text{up}}, X^{\pm}_{\text{down}}$ for the upper (up) and lower (down) limit of integration for the variable X in the case of positive (+) and negative (−) α.

Let us first determine the lower bounds on $\widetilde{L}$ and u:

- Since u, v and α are all both positive, the tadpole delta function fixes $\widetilde{L}$ to be positive as well. As a result, we don't have to integrate over negative $\widetilde{L}$s and therefore restrict the lower limit of integration for $\widetilde{L}$ to be zero:

$$\widetilde{L}^{+}_{\text{down}} = 0. \qquad (3.103)$$

- If the upper bound $v_{\text{up}} = f_Z^2\Lambda^2$ on v is too small so that $v_{\text{up}} < \widetilde{L}$ for a fixed $\widetilde{L}$, then the delta function cannot be satisfied for arbitrarily small u. As a result, the lower limit on u must then be taken to be $\left(\widetilde{L} - f_Z^2\Lambda^2\right)/\alpha$. If instead $v_{\text{up}} \geq \widetilde{L}$ then it is consistent to take the lower bound on u to be 0. In order to incorporate both of these possibilities, we take the lower bound on u to be

$$u^+_{\text{down}} = \max\left(0, \frac{\widetilde{L} - f_Z^2\Lambda^2}{\alpha}\right). \tag{3.104}$$

Now for the upper bounds:

- For large values of $\widetilde{L}$ the values that u and v must take on in order to satisfy the tadpole delta function become large as well. As a result, if the upper limit L_* for $\widetilde{L}$ is too large, the delta function may vanish identically for all values of u and v. It may therefore be necessary to cutoff the upper integration bound for $\widetilde{L}$. In particular we will set

$$L^+_{\text{up}} = \min\left(L_*, L_\Lambda\right) \qquad \text{where } L_\Lambda = \alpha u_\Lambda + f_Z^2\Lambda^2. \tag{3.105}$$

- If, at a fixed $\widetilde{L}$, we had $\alpha u_\Lambda > \widetilde{L}$, then since the lower bound on v is 0, this places an upper bound on u of $\widetilde{L}/\alpha$. If the inequality is reversed, then the upper bound on u is u_Λ. So, in general the upper bound on u is

$$u^+_{\text{up}} = \min\left(u_\Lambda, \widetilde{L}/\alpha\right). \tag{3.106}$$

Various possible regions of integration in the $\widetilde{L}/u$-plane are illustrated in figure 3.1.

Using the bounds described above and integrating over v yields

$$\mu_I^+ \propto \int_0^{L^+_{\text{up}}} d\widetilde{L} \int_{u^+_{\text{down}}(\widetilde{L})}^{u^+_{\text{up}}(\widetilde{L})} du |\det g| \left(\left(\widetilde{L} - \alpha u\right)^2 + \beta u^2 + \gamma u\left(\widetilde{L} - \alpha u\right)\right) \tag{3.107}$$

where and $\beta = \mu^2 - |\sigma|^2$ and $\gamma = -2\mu - |\mathcal{F}|^2$. Then, expanding everything out and integrating over u, we obtain

$$\mu_I^+ \propto \int_0^{L_{\text{up}}^+} d\widetilde{L} |\det g| \Bigg(\widetilde{L}^2 \left(u_{\text{up}}^+ - u_{\text{down}}^+\right) + \frac{\gamma - 2\alpha}{2} \widetilde{L} \left(\left(u_{\text{up}}^+\right)^2 - \left(u_{\text{down}}^+\right)^2 \right) \\ + \frac{\alpha^2 + \beta - \alpha\gamma}{3} \left(\left(u_{\text{up}}^+\right)^3 - \left(u_{\text{down}}^+\right)^3 \right) \Bigg)$$

where the $\widetilde{L}$ dependence of u_{up} and u_{down} has been suppressed in the last line.

In order to integrate over $\widetilde{L}$, we must separate the integral above into two parts since u_{up}^+ and u_{down}^+ are different functions of $\widetilde{L}$. Let $\mathscr{I}_{\text{up}}^+$ be the portion of the integral involving terms containing powers of u_{up}^+ and $\mathscr{I}_{\text{down}}^+$ be the portion of the integral containing u_{down}^+. Note that we will remove the $|\det g|$ factor from these integrals. Focusing first on $\mathscr{I}_{\text{up}}^+$ we see that for[5] $0 < \widetilde{L}/\alpha < u_{\text{up}}^+ (L_*)$, we can replace instances of $u_{\text{up}}^+ \left(\widetilde{L}\right)$ in the integral with $\widetilde{L}/\alpha$, while if $u_{\text{up}}^+ (L_*) < \widetilde{L}/\alpha$, then $u_{\text{up}}^+ = u_\Lambda$, which is independent of $\widetilde{L}$. So $\mathscr{I}_{\text{up}}^+$ splits into integrals over the two regions:

$$\begin{aligned} \mathscr{I}_{\text{up}}^+ &= \int_0^{\alpha u_{\text{up}}^+(L_*)} d\widetilde{L} \left(\frac{1}{\alpha} + \frac{\gamma - 2\alpha}{2\alpha^2} + \frac{\alpha^2 + \beta - \alpha\gamma}{3\alpha^3} \right) \widetilde{L}^3 \\ &+ \int_{\alpha u_{\text{up}}^+(L_*)}^{L_{\text{up}}^+} d\tilde{L} \left(\widetilde{L}^2 u_\Lambda + \frac{\gamma - 2\alpha}{2} \widetilde{L} u_\Lambda^2 + \frac{\alpha^2 + \beta - \alpha\gamma}{3} u_\Lambda^3 \right) \end{aligned} \tag{3.108}$$

Integrating yields

$$\begin{aligned} \mathscr{I}_{\text{up}}^+ = &\left(\frac{1}{\alpha} + \frac{\gamma - 2\alpha}{2\alpha^2} + \frac{\alpha^2 + \beta - \alpha\gamma}{3\alpha^3} \right) \frac{\alpha^4 \left(u_{\text{up}}^+ (L_*)\right)^4}{4} \\ &+ \frac{\left(\left(L_{\text{up}}^+\right)^3 - \alpha^3 \left(u_{\text{up}}^+ (L_*)\right)^3 \right) u_\Lambda}{3} + \frac{\gamma - 2\alpha}{4} \left(\left(L_{\text{up}}^+\right)^2 - \alpha^2 \left(u_{\text{up}}^+ (L_*)\right)^3 \right) u_\Lambda^2 \\ &+ \frac{\alpha^2 + \beta - \alpha\gamma}{3} \left(L_{\text{up}}^+ - \alpha u_{\text{up}}^+ (L_*)\right) u_\Lambda^3 \end{aligned} \tag{3.109}$$

For the integral $\mathscr{I}_{\text{down}}^+$, we consider the regions $0 < \widetilde{L} < f_Z^2 \Lambda$ and $f_Z^2 \Lambda < \widetilde{L}$. In the first

[5]Note that we could have considered $u_{\text{up}}^+ \left(L_{\text{up}}^+\right)$ instead of $u_{\text{up}}^+ (L_*)$ as the upper part of the interval. However, recall that L_{up}^+ is the smaller of either L_* or L_Λ. If $L_* > L_\Lambda$, $u_{\text{up}}^+ \left(L_{\text{up}}^+\right) = u_{\text{up}}^+ (L_\Lambda) = u_\Lambda$ since from the definition of L_Λ, the inequality $u_\Lambda < L_\Lambda/\alpha$ always holds.

case, $u^+_{\text{down}} = 0$ in which case this entire portion of the integral vanishes, while in the second, $u^+_{\text{down}} = \left(\widetilde{L} - f_Z^2\Lambda\right)/\alpha$. If $L_* < f_Z^2\Lambda^2$ then the entirety of $\mathscr{I}^+_{\text{down}} = 0$, so we have

$$\begin{aligned}\mathscr{I}^+_{\text{down}} &= -\theta\left(L_* - f_Z^2\Lambda^2\right)\int_{f_Z^2\Lambda^2}^{L^+_{\text{up}}} d\widetilde{L}\Bigg(\frac{1}{\alpha}\left(\widetilde{L}^3 - f_Z^2\Lambda^2\widetilde{L}^2\right) + \frac{\gamma-2\alpha}{2\alpha^2}\left(\widetilde{L}^3 - 2f_Z^2\Lambda^2\widetilde{L}^2 + f_Z^4\Lambda^4\widetilde{L}\right)\\ &\quad + \frac{\alpha^2+\beta-\alpha\gamma}{3\alpha^3}\left(\widetilde{L}^3 - 3f_Z^2\Lambda^2\widetilde{L}^2 + 3f_Z^4\Lambda^4\widetilde{L} - f_Z^6\Lambda^6\right)\Bigg)\\ &= -\theta\left(L_* - f_Z^2\Lambda^2\right)\int_{f_Z^2\Lambda^2}^{L^+_{\text{up}}} d\widetilde{L}\Bigg(\left(\frac{1}{\alpha} + \frac{\gamma-2\alpha}{2\alpha^2} + \frac{\alpha^2+\beta-\alpha\gamma}{3\alpha^3}\right)\widetilde{L}^3\\ &\quad - f_Z^2\Lambda^2\left(\frac{1}{\alpha} + \frac{\gamma-2\alpha}{\alpha^2} + \frac{\alpha^2+\beta-\alpha\gamma}{\alpha^3}\right)\widetilde{L}^2\\ &\quad + f_Z^4\Lambda^4\left(\frac{\gamma-2\alpha}{2\alpha^2} + \frac{\alpha^2+\beta-\alpha\gamma}{\alpha^3}\right)\widetilde{L} - f_Z^6\Lambda^6\frac{\alpha^2+\beta-\alpha\gamma}{3\alpha^3}\Bigg)\end{aligned} \tag{3.110}$$

Integrating yields

$$\begin{aligned}\mathscr{I}^+_{\text{down}} &= -\theta\left(L_* - f_Z^2\Lambda^2\right)\Bigg(f_Z^8\Lambda^8\left(\frac{1}{12\alpha} - \frac{\gamma-2\alpha}{24\alpha^2} + \frac{\alpha^2+\beta-\alpha\gamma}{12\alpha^3}\right)\\ &\quad - f_Z^6\Lambda^6\frac{\alpha^2+\beta-\alpha\gamma}{3\alpha^3}L^+_{\text{up}} + f_Z^4\Lambda^4\left(\frac{\gamma-2\alpha}{4\alpha^2} + \frac{\alpha^2+\beta-\alpha\gamma}{2\alpha^3}\right)\left(L^+_{\text{up}}\right)^2\\ &\quad - \frac{1}{3}f_Z^2\Lambda^2\left(\frac{1}{\alpha} + \frac{\gamma-2\alpha}{\alpha^2} + \frac{\alpha^2+\beta-\alpha\gamma}{\alpha^3}\right)\left(L^+_{\text{up}}\right)^3 + \left(\frac{1}{4\alpha} + \frac{\gamma-2\alpha}{8\alpha^2} + \frac{\alpha^2+\beta-\alpha\gamma}{12\alpha^3}\right)\left(L^+_{\text{up}}\right)^4\Bigg)\end{aligned} \tag{3.111}$$

Notice that when one ignores warping and the finite fluxes, $\alpha = 1, \widehat{K}_\xi = 0$, and $\Lambda \to \infty$, implying $\beta = 1$, $\gamma = -2 - |\mathcal{F}|^2$, $u^+_{\text{up}}(L_*) = L_*$, and $L^+_{\text{up}} = L_*$. In this case, we must go back to the expression (3.108) and note that the second integral in that expression vanishes since the lower and upper bound of integration are both L_*. Furthermore the integral $\mathscr{I}^+_{\text{down}}$ vanishes due to the θ-function prefactor. The index density in the unwarped case is thus

$$\mu_I^{\text{Unwarped}}(\xi,\tau) = |\det g|\,\mathscr{I}^+_{\text{up}} = |\det g|\,\frac{L_*^4}{4}\left(\frac{6+3\gamma-6+2+2\beta-2\gamma}{6}\right) = |\det g|\,\frac{L_*^4}{4!}(2-|\mathcal{F}|^2) \tag{3.112}$$

This precise combination gives us the curvature tensor as argued in [53, 54]. So, our expression reduces to the correct form in the unwarped, infinite flux case. We now turn our attention to the case where $\alpha < 0$.

The case $\alpha < 0$

Once again, we first establish the lower and upper bounds on $\widetilde{L}$ and u.

Let us begin by analyzing the lower bounds.

- The tadpole delta function fixes $\widetilde{L} = \alpha u + v$. The smallest value that $\widetilde{L}$ can take on therefore corresponds to taking u at its maximum (since $\alpha < 0$) and v at its minimum. As a result, we find

$$L^-_{\text{down}} = \alpha u_\Lambda. \tag{3.113}$$

  Note that this is negative.

- Consider some fixed $\widetilde{L} \leq f_Z^2 \Lambda^2$. If $\widetilde{L} > 0$, then there is always a $v = \widetilde{L}$ to cancel it, and the lower bound for u in this case is 0. However, if $\widetilde{L} < 0$, the fact that $v \geq 0$ implies that for the constraint to hold, we need the lower bound for u to be $\widetilde{L}/\alpha$ (which is positive). So in general, the lower bound for u is

$$u^-_{\text{down}} = \max\left(0, \widetilde{L}/\alpha\right). \tag{3.114}$$

  We now turn to the upper bounds on $\widetilde{L}$ and u.

- The largest $\widetilde{L}$ that could possibly satisfy the tadpole condition $\widetilde{L} = \alpha u + v$ is obtained by taking u at its lower limit of zero and v at its upper limit of $f_Z^2 \Lambda^2$. This gives $\widetilde{L} = f_Z^2 \Lambda^2$. If L_* is smaller than this value, we must keep the upper limit at L_*. Otherwise, it must be modified so that we take

$$L^-_{\text{up}} = \min(L_*, f_Z^2 \Lambda^2). \tag{3.115}$$

- Consider again a fixed $\widetilde{L}$. Then, since u is given by $u = (\widetilde{L} - v)/\alpha$, the largest u that can satisfy the tadpole condition corresponds to taking v as its maximum value (since $\alpha < 0$). This would give $u = (\widetilde{L} - f_Z^2\Lambda^2)/\alpha$. If this falls within the original range of integration, the delta function will vanish identically for large u. We can then restrict the upper bound for u so that

$$u^-_{\rm up} = \min\left(u_\Lambda, \left(\widetilde{L} - f_Z^2\Lambda^2\right)/\alpha\right) \tag{3.116}$$

Given these bounds on u and $\widetilde{L}$, we may now integrate over v, eliminating the tadpole delta function to get

$$\mu_I^- \propto \int_{L^-_{\rm down}}^{L^-_{\rm up}} d\widetilde{L} \int_{u^-_{\rm down}(\widetilde{L})}^{u^-_{\rm up}(\widetilde{L})} du\, |\det g| \, \left(\widetilde{L}^2 + (\gamma - 2\alpha)\widetilde{L}u + \left(\alpha^2 + \beta - \alpha\gamma\right) u^2\right). \tag{3.117}$$

Carrying out the u integration yields

$$\begin{aligned} \mu_I^- \;\; &\propto \;\; \int_{L^-_{\rm down}}^{L^-_{\rm up}} d\widetilde{L} |\det g| \left(\widetilde{L}^2\left(u^-_{\rm up} - u^-_{\rm down}\right) + \widetilde{L}\left(\frac{\gamma - 2\alpha}{2}\right)\left(\left(u^-_{\rm up}\right)^2 - \left(u^-_{\rm down}\right)^2\right)\right. \\ &+ \;\; \left.\frac{\alpha^2 + \beta - \alpha\gamma}{3}\left(\left(u^-_{\rm up}\right)^3 - \left(u^-_{\rm down}\right)^3\right)\right) \end{aligned} \tag{3.118}$$

where we have suppressed the $\widetilde{L}$ dependence of $u^-_{\rm up}$, and $u^-_{\rm down}$.

As before, split the integral into two parts, $\mathscr{I}^-_{\rm up}$ and $\mathscr{I}^-_{\rm down}$, involving just the $u^-_{\rm up}$ and $u^-_{\rm down}$ parts, respectively. To compute $\mathscr{I}^-_{\rm up}$ we consider two cases:

- Suppose $L_* < L_\Lambda$, where we recall $L_\Lambda = \alpha u_\Lambda + f_Z^2\Lambda^2$. Note that since $\alpha < 0$, we have that $L_\Lambda < f_Z^2\Lambda^2$, and thus, $L^-_{\rm up} = L_*$ in this case. We also see that $u^-_{\rm up} = u_\Lambda$, and so in this case, the integral $\mathscr{I}^-_{\rm up}$ is simply

$$\mathscr{I}^-_{\rm up} = \int_{L^-_{\rm down}}^{L_*} d\widetilde{L}\left(\widetilde{L}^2 u_\Lambda + \widetilde{L}\left(\frac{\gamma - 2\alpha}{2}\right) u_\Lambda^2 + \frac{\alpha^2 + \beta - \alpha\gamma}{3} u_\Lambda^3\right) \tag{3.119}$$

- Suppose that $L_* > L_\Lambda$. In this case, for $\widetilde{L} < L_\Lambda$, $u^-_{\text{up}} = u_\Lambda$ as before, but when $\widetilde{L} > L_\Lambda$ we have $u^-_{\text{up}} = \left(\widetilde{L} - f_Z^2\Lambda^2\right)/\alpha$. So the integral splits into two parts

$$\begin{aligned}
\mathscr{I}^-_{\text{up}} &= \int_{L^-_{\text{down}}}^{L_\Lambda} d\widetilde{L}\left(\widetilde{L}^2 u_\Lambda + \widetilde{L}\left(\frac{\gamma - 2\alpha}{2}\right)u_\Lambda^2 + \frac{\alpha^2+\beta-\alpha\gamma}{3}u_\Lambda^3\right)\\
&+ \int_{L_\Lambda}^{L^-_{\text{up}}} d\widetilde{L}\left(\widetilde{L}^2\left(\frac{\widetilde{L}-f_Z^2\Lambda^2}{\alpha}\right) + \widetilde{L}\left(\frac{\gamma-2\alpha}{2}\right)\left(\frac{\widetilde{L}-f_Z^2\Lambda^2}{\alpha}\right)^2\right.\\
&+ \left.\frac{\alpha^2+\beta-\alpha\gamma}{3}\left(\frac{\widetilde{L}-f_Z^2\Lambda^2}{\alpha}\right)^3\right) \qquad (3.120)
\end{aligned}$$

These two expressions can be joined if we introduce $L_{\text{mid}} = \min\left(L_*, L_\Lambda\right)$:

$$\begin{aligned}
\mathscr{I}^-_{\text{up}} &= \int_{L^-_{\text{down}}}^{L_{\text{mid}}} d\widetilde{L}\left(\widetilde{L}^2 u_\Lambda + \widetilde{L}\left(\frac{\gamma - 2\alpha}{2}\right)u_\Lambda^2 + \frac{\alpha^2+\beta-\alpha\gamma}{3}u_\Lambda^3\right)\\
&+ \int_{L_{\text{mid}}}^{L^-_{\text{up}}} d\widetilde{L}\left(\widetilde{L}^2\left(\frac{\widetilde{L}-f_Z^2\Lambda^2}{\alpha}\right) + \left(\frac{\gamma-2\alpha}{2}\right)\widetilde{L}\left(\frac{\widetilde{L}-f_Z^2\Lambda^2}{\alpha}\right)^2\right.\\
&+ \left.\frac{\alpha^2+\beta-\alpha\gamma}{3}\left(\frac{\widetilde{L}-f_Z^2\Lambda^2}{\alpha}\right)^3\right) \qquad (3.121)
\end{aligned}$$

The integral in the second line above vanishes if $L_{\text{mid}} = L_*$, since in that case L^-_{up} also is L_*. Carrying out the integral yields (after plugging in $L^-_{\text{down}} = \alpha u_\Lambda$)

$$\begin{aligned}
\mathscr{I}^-_{\text{up}} &= \frac{u_\Lambda}{3}\left(L^3_{\text{mid}} - \alpha^3 u_\Lambda^3\right) + \frac{\gamma-2\alpha}{4}u_\Lambda^2\left(L^2_{\text{mid}} - \alpha^2 u_\Lambda^2\right) + \frac{\alpha^2+\beta-\alpha\gamma}{3}u_\Lambda^3\left(L_{\text{mid}} - \alpha u_\Lambda\right) \qquad (3.122)\\
&+ \frac{1}{4}\left(\frac{1}{\alpha} + \frac{\gamma-2\alpha}{2\alpha^2} + \frac{\alpha^2+\beta-\alpha\gamma}{3\alpha^3}\right)\left(\left(L^-_{\text{up}}\right)^4 - L^4_{\text{mid}}\right) \qquad (3.123)\\
&- \frac{f_Z^2\Lambda^2}{3}\left(\frac{1}{\alpha} + \frac{\gamma-2\alpha}{\alpha^2} + \frac{\alpha^2+\beta-\alpha\gamma}{\alpha^3}\right)\left(\left(L^-_{\text{up}}\right)^3 - L^3_{\text{mid}}\right) \qquad (3.124)\\
&+ \frac{f_Z^4\Lambda^4}{2}\left(\frac{\gamma-2\alpha}{2\alpha^2} + \frac{\alpha^2+\beta-\alpha\gamma}{\alpha^3}\right)\left(\left(L^-_{\text{up}}\right)^2 - L^2_{\text{mid}}\right) \qquad (3.125)\\
&- f_Z^6\Lambda^6\left(\frac{\alpha^2+\beta-\alpha\gamma}{3\alpha^3}\right)\left(L^-_{\text{up}} - L_{\text{mid}}\right) \qquad (3.126)
\end{aligned}$$

The integral $\mathscr{I}^-_{\text{down}}$ vanishes when $\widetilde{L} > 0$ since in that case $u^-_{\text{down}} = 0$. Thus, the only region that contributes is where $L^-_{\text{down}} \leq \widetilde{L} \leq 0$, in which $u^-_{\text{down}} = \widetilde{L}/\alpha$. We have,

$$\mathscr{I}^-_{\text{down}} = -\int_{L^-_{\text{down}}}^{0} d\widetilde{L} \left(\frac{1}{\alpha}\tilde{L}^3 + \frac{\gamma - 2\alpha}{2\alpha^2}\tilde{L}^3 + \frac{\alpha^2 + \beta - \alpha\gamma}{3\alpha^3}\tilde{L}^3 \right) \tag{3.127}$$

which gives

$$\mathscr{I}^-_{\text{down}} = \frac{1}{4}\left(\frac{1}{\alpha} + \frac{\gamma - 2\alpha}{2\alpha^2} + \frac{\alpha^2 + \beta - \alpha\gamma}{3\alpha^3} \right) \alpha^4 u_\Lambda^4 \tag{3.128}$$

where we have again used $L^-_{\text{down}} = \alpha u_\Lambda$.

The full index density is thus

$$\mu_I(\xi, \tau)/\det g = \left(\mathscr{I}^+_{\text{up}} + \mathscr{I}^+_{\text{down}} \right) \theta(\alpha) + \left(\mathscr{I}^-_{\text{up}} + \mathscr{I}^-_{\text{down}} \right) \theta(-\alpha) \tag{3.129}$$

In the unwarped, infinite flux case where a concise geometric result is obtained, one can integrate out the axio-dilaton to obtain an effective density only in terms of the complex moduli. However, in our case this type of integration proves intractable. As a result we will, when comparing with simulations, have to fix a value of the axio-dilaton and compare the un-integrated form of our density. We now turn to a numerical study of this problem.

3.4 Numerical Vacuum Statistics

To perform a numerical study of the distribution of vacua in moduli space near the conifold point, we will randomly choose appropriate fluxes $F = (F_0, F_1, F_2, F_3)$ and $H = (H_0, H_1, H_2, H_3)$ and then solve the conditions $D_\tau W = 0$ and $D_\xi W = 0$ for the moduli space coordinate ξ as well as for the axio-dilaton τ. Here $W = N_i \Pi_i$ is the superpotential, and N is an 8-vector whose first four components are those of F and last four are those of H. We work in a basis such that the vector of 4-fold periods $\Pi = (\Sigma, \tau\Sigma)$, where Σ is the vector of periods on the 3-fold. Near the conifold point, the vector of 3-fold periods takes the form:

$$\Sigma = \sum_{n=0}^{\infty} a_n \xi^n + b\xi \log(-i\xi), \tag{3.130}$$

where the a_n and b are constant vectors associated with the expansion of the periods. Note that in the case of a single complex modulus, the vector $b = (0,0,0,b^0)$, since only Σ_0 has non-trivial logarithmic behavior near the conifold. Also, the local coordinate around the conifold point is proportional to Σ_3, which implies that the vector $a_0 = (0, a_0^2, a_0^1, a_0^0)$. We begin by illustrating this approach in the case where the warping correction is neglected.

3.4.1 Unwarped Analysis

The unwarped Kähler potential is

$$e^{-K} = -i\overline{\Sigma}\cdot Q\cdot\Sigma = -i\left((\overline{a}_n \cdot Q \cdot a_m)\bar{\xi}^n\xi^m + (\overline{b} \cdot Q \cdot a_m)\xi^m\bar{\xi}\log(i\bar{\xi}) + (\overline{a}_n \cdot Q \cdot b)\bar{\xi}^n\xi\log(-i\xi)\right), \tag{3.131}$$

where the term proportional to $\overline{b} \cdot Q \cdot b$ has been dropped since given b and η it vanishes.

For supersymmetric vacua in the unwarped case

$$D_\xi W = N \cdot (\partial_\xi \Pi + \Pi K_\xi) = 0. \tag{3.132}$$

Keeping logarithmic and constant terms gives

$$(F - \tau H) \cdot (a_1 + b\,(\log(-i\xi) + 1)) - (F - \tau H) \cdot a_0 \frac{\overline{a}_0 \cdot Q \cdot a_1}{\overline{a}_0 \cdot Q \cdot a_0} = 0. \tag{3.133}$$

where the fact that $\overline{a}_0 \cdot Q \cdot b = 0$ has been used to simplify the expression. This is an equation of the form

$$\mathcal{A} + \mathcal{B}\log(-i\xi) = 0, \tag{3.134}$$

with

$$\mathcal{A} = (F-\tau H)\cdot b(\overline{a}_0\cdot Q\cdot a_0) + (F-\tau H)\cdot a_1(\overline{a}_0\cdot Q\cdot a_0) - (F-\tau H)\cdot a_0(\overline{a}_1\cdot Q\cdot a_0) \quad (3.135)$$

$$\mathcal{B} = (F-\tau H)\cdot b(\overline{a}_0\cdot Q\cdot a_0). \quad (3.136)$$

The leading-order constraints arising from requiring $D_\tau W = 0$ are

$$\tau = \frac{F\cdot\overline{\Sigma}}{H\cdot\overline{\Sigma}} = \frac{F\cdot\overline{a}_0}{H\cdot\overline{a}_0}. \quad (3.137)$$

This implies that

$$F-\tau H = \frac{(H\cdot\overline{a}_0)F-(F\cdot\overline{a}_0)H}{H\cdot\overline{a}_0}. \quad (3.138)$$

As a result, we can quickly see that

$$|\xi| = |e^{-\mathcal{A}/\mathcal{B}}|. \quad (3.139)$$

Before considering the effects of warp corrections, it is worth determining how close to the conifold vacua may be found in the unwarped scenario. The $D_\xi W = 0$ constraint implies that $|\xi|$ is exponentially suppressed by the ratio of $|\mathcal{A}/\mathcal{B}|$, so if $|\mathcal{A}|$ is even just a couple of orders of magnitude greater than $|\mathcal{B}|$, we should expect to see vacua on the order of e^{-100} units away from the conifold point—indeed, this has been observed in previous studies [32]. In order for $|\mathcal{A}|$ to differ appreciably from $|\mathcal{B}|$ the quantity $|(F-\tau H)\cdot b|$ should be relatively small compared to $|(F-\tau H)\cdot a_0|$ or $|(F-\tau H)\cdot a_1|$. Using the form of the vector b above, this indicates that the fluxes through the collapsing cycle, F_3 and H_3 should be small relative to some of the other fluxes. We now turn to the warped analysis.

3.4.2 Warped Analysis

Introducing warping leads to the corrections (3.78) and (3.79) to the Kähler potential and its derivative. The modification to the near-conifold supersymmetric vacuum condition is then

$$D_\xi W \longrightarrow D_\xi W + 3C_w \frac{\bar{\xi}^{1/3}}{\xi^{2/3}} N \cdot \Pi. \tag{3.140}$$

Now, assuming that C_w is small (i.e. the volume of the 3-fold is large) these new terms will matter only close to $\xi = 0$. The supersymmetry condition thus leads to

$$\mathcal{A} + \mathcal{B} \log(-i\xi) + \mathcal{C} \frac{\bar{\xi}^{1/3}}{\xi^{2/3}} = 0, \tag{3.141}$$

with $\mathcal{A}$ and $\mathcal{B}$ as before and

$$\mathcal{C} = 3\, C_w (F - \tau H) \cdot a_0. \tag{3.142}$$

We will turn to an in-depth analysis of the solutions to these equations in the following section. However, before we get there we want to discuss the rough effects that the additional warping term will have on the distribution.

In the unwarped case, we expect to find vacua at a distance e^{-100} or so away from the conifold. This would require fluxes for which $|\mathcal{A}| \sim 100|\mathcal{B}|$. Furthermore, for fluxes constrained to lie in $(0, 100)$ this hierarchy is about the maximum order of magnitude difference that one would expect. If however, $C_w \sim 10^{-20}$, then for $|\xi| \sim 10^{-100}$, the warp term contribution is on the order of 10^{10}, swamping the logarithmic contribution and requiring fluxes for which $|\mathcal{A}| \sim 10^{10}$ which lies beyond the range we consider.

In the region of strong warping where the logarithmic term is dominated by the warping term, the distance of a vacuum from the conifold point is thus set by $|\mathcal{C}/\mathcal{A}|^3$. Given that $\mathcal{A}$ is at maximum of roughly 100 or so, the constant C_w, and thus, the overall volume of the Calabi-Yau, determines how near the conifold vacua lie. This can dramatically truncate the range—since the assumption of large but finite volume is well satisfied by volumes of order

10^{20}, but in those cases, vacua will not show up much closer than 10^{-60}. We can get vacua at around 10^{-120} by taking a volume of order 10^{40}, but in the absence of warping, vacua as far in as 10^{-200} are expected.

The main message of this argument is that warping pushes the vacua farther away from the conifold point. Thus we expect to find in the next section that the conifold point no longer acts like an accumulation point for vacua.

3.4.3 Monte-Carlo Vacua

For the numerical analysis, we use the Calabi-Yau manifold labeled model 3 in the appendix of [52]. This family of Calabi-Yau can be expressed as a locus of octic polynomials in $\mathbb{WP}^{4,1,1,1,1}$. The corresponding orientifold arises from a certain limit of F-theory compactified on a Calabi-Yau fourfold hypersurface in $\mathbb{WP}^{12,8,1,1,1,1}$, following the methods of [57], and briefly described in [40]. For our purposes, we use the fact that the fourfold has Euler characteristic $\chi = 23328$, which implies that $L_{\max} = \chi/24 = 972$ for the tadpole condition for flux compactification on the corresponding orientifolded 3-fold.

Since the warped form of the near conifold equation is not as simple to solve as in the unwarped case, a slightly more involved approach is necessary. We begin by defining two real variables ρ and θ such that

$$-i\xi = \rho^3 e^{i\theta} \tag{3.143}$$

We take $\rho \geq 0$ and $0 \leq \theta \leq 2\pi$. In terms of these variables, eqn (3.141) and its complex conjugate expression take the forms

$$\mathcal{A} + 3\mathcal{B}\ln(\rho) + i\mathcal{B}\theta + \frac{\mathcal{C}}{\rho}e^{-i\theta} \;=\; 0 \tag{3.144}$$

$$\overline{\mathcal{A}} + 3\overline{\mathcal{B}}\ln(\rho) - i\overline{\mathcal{B}}\theta + \frac{\overline{\mathcal{C}}}{\rho}e^{i\theta} \;=\; 0. \tag{3.145}$$

Multiplying the first equation by $\overline{\mathcal{B}}$ and the second one by $\mathcal{B}$, and then adding and subtracting the two, we find two purely real or imaginary equations. Letting $\mathcal{A} = ae^{i\alpha}$, $\mathcal{B} = be^{i\beta}$, and $\mathcal{C} = ce^{i\gamma}$, we have

$$a\sin(\alpha-\beta) + b\theta + \frac{c}{\rho}\sin(\gamma-\beta-\theta) = 0 \quad (3.146)$$

$$a\cos(\alpha-\beta) + 3b\log(\rho) + \frac{c}{\rho}\cos(\gamma-\beta-\theta) = 0. \quad (3.147)$$

We now solve for ρ in terms of θ and then numerically solve the final equation for θ. It seems natural to solve equation (3.146) for ρ since it is a linear equation. However, this approach fails in the limit $C_w \to 0$ since then $c \to 0$ too. Instead we solve for ρ in equation (3.147). One can rearrange the equation as

$$\rho e^{\Gamma}\log(\rho e^{\Gamma}) = -\frac{ce^{\Gamma}}{3b}\cos(\gamma-\beta-\theta). \quad (3.148)$$

Here we have defined the constant $\Gamma = \frac{a\cos(\alpha-\beta)}{3b}$. This is of the form $x\log(x) = y$ which has the solution $x = y/W(y)$ where $W(y)$ is the Lambert W-function. We therefore find

$$\rho(\theta) = \frac{-c\cos(\gamma-\beta-\theta)}{3bW(-\frac{ce^{\Gamma}}{3b}\cos(\gamma-\beta-\theta))}. \quad (3.149)$$

Consider using this expression for ρ in equation (3.146), which now only depends on θ. Under the assumption that there is only one near conifold vacuum for each set of fluxes, the left-hand side must either start out positive, and go negative or vice versa. To find the zero-crossing, we divide the region $[0, 2\pi]$ into two equal pieces and then determine in which region (if any) equation (3.146) changes sign. If such a region is found, we apply the same method to that region, splitting it into two smaller intervals, continuing in this way until we reach a predetermined level of accuracy.

There are two relevant comments to be brought up here. First, in equation (3.149) it is not clear that the value of ρ is positive, or even real. We must therefore exclude the regions where ρ is either negative or complex. Fortunately, if ρ is real, it is never negative since

$W(x)$ must have the same sign as x. A necessary and sufficient condition for ρ to be real is that the argument of the Lambert W function is greater than or equal to $-1/e$. This means that the relevant region to begin with may not be the entire interval $[0, 2\pi]$. Second, it turns out that the Lambert W function has two real branches for arguments between $-1/e$ and 0. Thus, both of these branches must be considered.

To better compare the numerical and analytical and numerical distributions, we fix τ and then select a random sets of fluxes F and H consistent with our choice of τ and satisfying the tadpole condition, $F \cdot Q \cdot H \leq L_{max}$. For the particular model we consider, $L_{max} = 972$, and we display a run using $\tau = 2i$, and $C_w = 10^{-15}$ against the corresponding analytical prediction in figure 3.2. We plot the vacuum count and integrated analytical distribution as measured around the conifold point using a log scale for the distance from the conifold. As is evident from the figure, the count receives two major contributions: the one farther away from the conifold point is the usual contribution that is present without warping. However, we also see a major contribution much closer to the conifold at a distance roughly on the order of C_w^3. This contribution is due to the strong warping effects and is matched by the cumulative analytical results. Furthermore, notice that the number of vacua found within this critical distance of roughly C_w^3 is negligible. This supports our conjecture that the vacua that would have been present near the conifold point without warping are now either absent or pushed farther away. In other words, the conifold point is no longer an accumulation point of vacua to the same extent that it was without incorporating warping into the story.

3.5 Discussion

We've analyzed the distribution of flux vacua in the vicinity of the conifold point, including the effects of warping, and confirmed our results by a direct numerical Monte Carlo search. In comparison with the well known results, that don't include warping, we find a significant dilution of vacua in close proximity to the conifold, with the proximity scale set by the volume of the Calabi-Yau compactification.

One complication in the analytical approach, relative to the unwarped case, is the need to bound the fluxes – a physically sensible requirement but one that can be avoided in the unwarped analysis, yielding the geometrical result of [53, 54]. In the unwarped story, there is a very nice geometrical form of the distribution in terms of the curvature on moduli space. Given the type of bounding that was necessary above, we cannot determine if a similar interpretation is available to us in this instance.

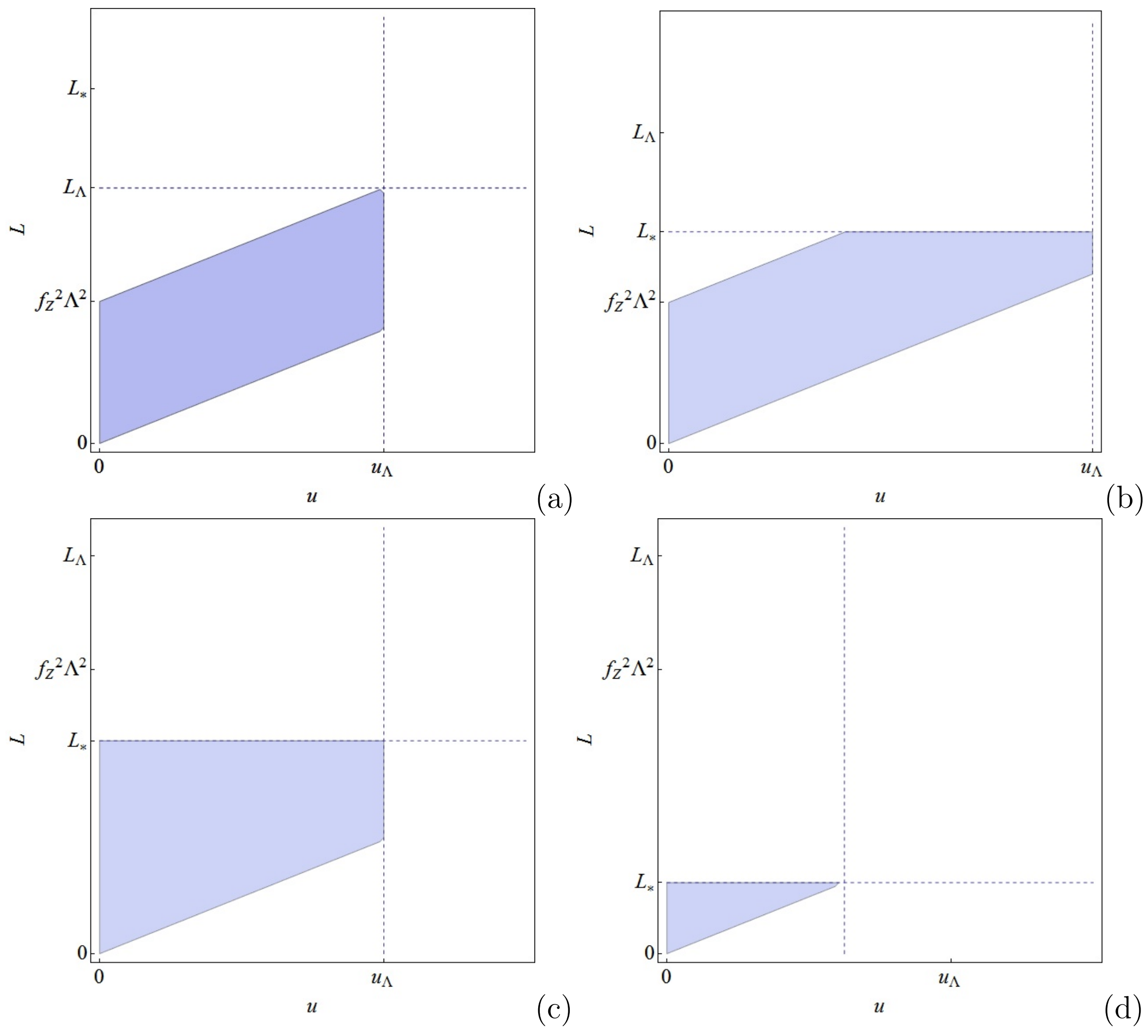

Figure 3.1: Various possible regions of integration for $\alpha > 0$. In (a) $L_* > L_\Lambda$, where $L_\Lambda = \alpha u_\Lambda + f_Z^2\Lambda^2$ and $u_\Lambda = \min\left(\Lambda^2 f_X^2, \Lambda^2 f_Y^2/\widehat{K}_\xi^2\right)$ so the region is cut off at u_Λ. In (b) $f_Z^2\Lambda^2 < L_* < L_\Lambda$. In (c), $L_* < f_Z^2\Lambda^2$, and $u_\Lambda < L_*/\alpha$. Finally, (d) shows a region where $L_* < f_Z^2\Lambda^2$ and $u_\Lambda > L_*/\alpha$.

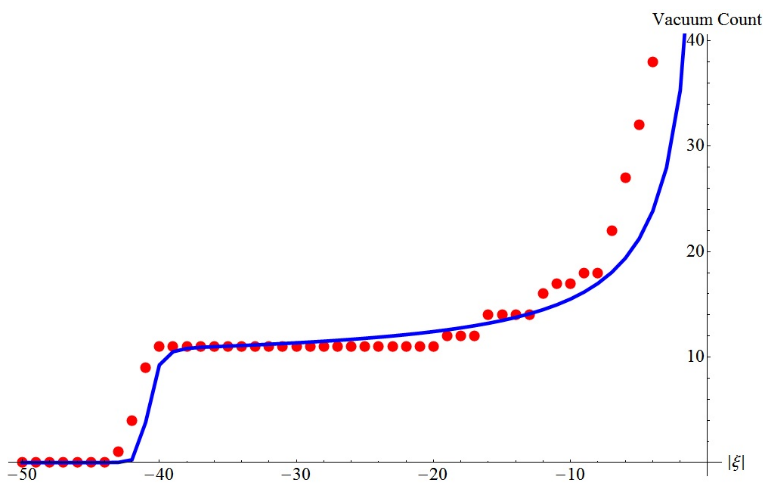

Figure 3.2: A comparison between numerical and analytical distributions. Red circles mark the numerical data while the blue curve is the integrated analytical distribution. Distance from the conifold $|\xi|$ is plotted on a log scale on the horizontal axis, while the vacuum count is plotted on the vertical axis.

Chapter 4

Exploring Spiral Inflation in String Theory

4.1 Introduction

It is widely believed that the early universe underwent a dramatic expansion called *inflation* during which its size increased exponentially. There are many reasons to believe this, most notably the incredibly successful prediction of the anisotropies found in the power spectrum of the cosmic microwave background. Being of such fundamental importance in early universe cosmology it is essential that it is embeddable within the structure of string theory.

There are multiple ways to approach inflation, most notably *slow-roll inflation*. Recently a novel perspective on this kind of inflation was offered under the name *spiral inflation* [58]. Spiral inflation is very interesting from the perspective of string theory since the type of potentials required to sustain it are very natural near the conifold point. Below we will briefly review the ideas behind spiral inflation and then investigate if it can be realized in string theory. Our results are negative in that whenever spiral inflation seems to be realized, the inflation is actually driven by a non-zero vacuum energy. We back this assertion up with a numerical investigation.

4.2 Spiral Inflation

From the perspective of string theory, it is reasonable to suspect that multiple scalar fields participated in the inflationary phase of the universe. However the generalization of the standard slow-roll parameters to the case of multi-field inflation is nontrivial and many proposals have appeared in the literature [58, 59, 60, 61].

One recent proposal [58] is particularly interesting from the perspective of string theory since, as we will see in more detail below, it requires potentials with non trivial monodromies around special points in their field space, a situation that is very natural in string theory. To see how one arrives at such a conclusion, we briefly review the analysis from [58].

4.2.1 Slow-Roll Conditions for Multiple Fields

The analysis of slow-roll inflation begins with the assertion that the Hubble parameter must vary slowly (this will produce an exponential expansion). In other words the relative change of H during one Hubble time, $1/H$, must be small

$$\left|\frac{\dot{H}}{H^2}\right| \ll 1. \tag{4.1}$$

We consider multiple fields $\phi_1, \phi_2, \ldots, \phi_n$ taking on homogeneous configurations $\phi_i(t)$. One can then write the Hubble parameter as

$$H^2 = \frac{8\pi G}{3}\left(\frac{1}{2}\dot{\phi_i}^2 + V(\phi_i)\right). \tag{4.2}$$

This gives

$$2H\dot{H} = \frac{8\pi G}{3}\left(\ddot{\phi_i} + \partial_i V\right)\dot{\phi_i}. \tag{4.3}$$

The equations of motion for the scalar field in the background FRW metric are

$$\ddot{\phi_i} + 3H\dot{\phi_i} + \partial_i V = 0. \tag{4.4}$$

Notice the additional term $3H\dot{\phi}_i$ referred to as the *Hubble friction*. This results from the minimal coupling of the scalar fields to gravity. These equations can then be used to write the expression for $\dot{H}$ as

$$\dot{H} = -4\pi G\dot{\phi}^2. \tag{4.5}$$

The condition that the Hubble parameter changes slowly, (4.1), then gives

$$\left|\frac{\dot{H}}{H^2}\right| \ll 1 \quad \rightarrow \quad \frac{\frac{1}{2}\dot{\phi_i}^2}{\frac{1}{2}\dot{\phi_i}^2 + V(\phi_i)} \ll 1. \tag{4.6}$$

This in turn implies that the dynamics of the field must be potential energy dominated

$$\frac{1}{2}\dot{\phi_i}^2 \ll V(\phi_i). \tag{4.7}$$

So far the analysis for the multiple field case does not differ from the standard single field case. One can then define the first slow-roll parameter ϵ. Traditionally this is written in terms of the potential and its first derivative but that way of writing it actually depends on further conditions that do not have to be satisfied in the multiple field case. As a result we stick with the dynamical definition

$$\epsilon \equiv \frac{\frac{1}{2}\dot{\phi_i}^2}{V(\phi_i)} \ll 1. \tag{4.8}$$

In order to obtain sustained inflation, one must also make sure that ϵ stays small or more precisely that the relative change in ϵ during one Hubble time is small

$$\frac{\dot{\epsilon}}{\epsilon H} \ll 1. \tag{4.9}$$

Using the form for ϵ above, $\dot{\epsilon}$ can be written as

$$\dot{\epsilon} = \ddot{\phi}_i\dot{\phi}_i\frac{\frac{1}{2}\dot{\phi_j}^2 + V}{V^2} + 6H\left(\frac{\frac{1}{2}\dot{\phi_i}^2}{V}\right)^2. \tag{4.10}$$

Using the fact that $\epsilon \ll 1$, i.e. that the potential energy dominates over the kinetic energy, we find

$$\frac{\dot{\epsilon}}{\epsilon H} \ll 1 \quad \rightarrow \quad \eta \equiv \frac{1}{H}\frac{2\ddot{\phi}_i\dot{\phi}_i}{\dot{\phi}_j^{\,2}} \ll 1. \tag{4.11}$$

In other words, the kinetic energy should not change much over a Hubble time. It is this last expression that allows us to depart from the standard slow-roll conditions on the potential when multiple fields are involved. Traditionally, one satisfies (4.11) by setting the acceleration $\ddot{\phi}_i$ to be very small. Together with the equations of motion this would imply that the slope of the potential is proportional to $3H\dot{\phi}_i$. Using the fact that the motion is potential energy dominated this further implies that the slope must be small

$$\partial_i V \approx -3H\dot{\phi}_i \approx -\sqrt{3}\frac{\sqrt{V}}{M_P}\dot{\phi}_i \quad \rightarrow \quad M_P^2\left(\frac{\partial_i V}{V}\right)^2 \sim \frac{\dot{\phi}_i^{\,2}}{V} \ll 1. \tag{4.12}$$

However, in the present context it is clear that there are other ways to maintain small kinetic energy without having a negligible acceleration. In particular, one only needs to ensure that the acceleration is always perpendicular to the motion

$$\ddot{\vec{\phi}} \perp \dot{\vec{\phi}} \quad \rightarrow \quad \ddot{\vec{\phi}} \cdot \dot{\vec{\phi}} \ll H\dot{\phi}_i^{\,2}. \tag{4.13}$$

As a result, no conditions are imposed on the steepness of the potential. Instead the conditions are imposed on the dynamical trajectories that the fields travels on. The conclusion of [58] is therefore that slow-roll inflation may be possible in steep potentials that otherwise would have been overlooked by the standard slow-roll arguments.

4.2.2 Spiral Trajectories and the Global Properties of the Potential

Requiring the acceleration of the field to be orthogonal to its motion but not necessarily small itself means that its trajectory must locally be roughly circular. This is why this type of inflation was referred to as *Spiral Inflation* in [58]. If we choose the center of the circle to lie at $\phi_i = 0$ and furthermore restrict to the case of two scalar fields ϕ_1, ϕ_2, we can (after moving to polar coordinates) parametrize it as $r = \text{const}$ with θ changing during the evolution. In polar coordinates the equations of motion become

$$\ddot{r} + 3H\dot{r} - r\dot{\theta}^2 + \frac{\partial V}{\partial r} = 0 \tag{4.14}$$

$$r^2\ddot{\theta} + 2r\dot{r}\dot{\theta} + 3Hr^2\dot{\theta} + \frac{\partial V}{\partial \theta} = 0. \tag{4.15}$$

It is clear that the only way a stable circular orbit can exist is if the potential in this regime is radially attractive and furthermore if we balance the inward force due to the gradient of the potential against the centrifugal term in the effective potential. Setting $\dot{r} = 0$ above gives

$$r\dot{\theta}^2 = \frac{\partial V}{\partial r}. \tag{4.16}$$

In order for this type of inflation to differ significantly from standard slow-roll in a flat potential, we really want the slope in the orthogonal (i.e. radial) direction to be large enough so that we violate the standard slow-roll condition

$$\frac{\partial V}{\partial r} \sim \frac{V}{M_P}. \tag{4.17}$$

This means that the kinetic energy of the field is given by

$$\frac{1}{2}r^2\dot{\theta}^2 = \frac{1}{2}r\frac{\partial V}{\partial r} \sim \frac{r}{M_P}V. \tag{4.18}$$

We see that balancing the attractive radial force against the centrifugal force necessarily puts the kinetic energy on the order of the potential (up to a factor of r). In order for this orbit to still be potential energy dominated, one must therefore take $r \ll M_P$. One can rearrange the above expression for the kinetic energy as

$$\dot{\theta} = \sqrt{\frac{2V}{rM_P}}. \tag{4.19}$$

The change in θ during one Hubble time is then approximately

$$\Delta\theta = \frac{\dot{\theta}}{H} = \dot{\theta}\sqrt{\frac{3M_P^2}{V}} = \sqrt{6M_P/r} \tag{4.20}$$

Since we must take $r \ll M_P$, we find that $\Delta\theta$ is rather large. In other words, during a single Hubble time, the field will cover a large angular displacement. In order to allow for multiple e-foldings, we must then consider multiple laps around the origin. In order for the acceleration to be orthogonal to the motion of the field, we must take $\ddot{\theta} = 0$. As is clear from the equations of motion for θ, the potential must therefore have a monotonic slope in the angular direction

$$\frac{\partial V}{\partial \theta} = -3Hr^2\dot{\theta}. \tag{4.21}$$

Clearly upon one revolution such a potential cannot return to its original value. As a result, one is forced to consider potentials with multiple connected sheets. As was pointed out in [58] this is very natural in string theory. In [58] one particular model was presented that satisfies all of these constraints. We briefly review that model here. Consider the potential, written in polar coordinates,

$$V(r,\theta) = V_0 + c\theta + \frac{c^2}{9\alpha H^2}\frac{r^\alpha}{R^{\alpha+2}}. \tag{4.22}$$

We can obtain a stable circular orbit by initializing the system according to

$$\begin{aligned} r &= R && (4.23) \\ \dot{\theta} &= -\frac{c}{3HR^2}. && (4.24) \end{aligned}$$

Despite initializing the system in this way, it is possible that the circular trajectory will still decay over time. In particular one must make sure that $r = R$ remains a minimum of the effective potential even as one moves down the monodromy ladder. This can only be the case if the angular momentum is conserved. Fortunately the angular momentum *is* conserved by virtue of balancing the angular tilt against the Hubble friction. This can easily be seen by rewriting the angular equation in terms of the angular momentum $L = r^2\dot{\theta}$

$$\dot{L} + 3HL + \frac{\partial V}{\partial \theta} = 0. \tag{4.25}$$

Thus besides being critical for spiraling, balancing the Hubble friction agains the angular slope also ensures that one can sustain the circular motion. As a result, the model above that was introduced in [58] allows for the circular motion to be sustained indefinitely.

Clearly the monodromy of the potential was an essential part of the story without which a sufficient number of e-foldings could not be achieved. This is particularly interesting from the perspective of string theory since the scalar potential for the complex structure deformation in flux compactifications of string theory on Calabi-Yau manifolds exhibit precisely such monodromies near the conifold locus. We thus turn to studying the near conifold potential of such models to see if one can realize spiral inflation in string theory.

4.3 Potentials in String Theory

The moduli space of string theory consists of two main sectors, the Kähler moduli space and the complex structure moduli space. Out of these, only the complex structure moduli can be stabilized by turning on fluxes on the internal manifold. We imagine that the Kähler sector has already been stabilized in some way and focus on the complex structure moduli space. As a result there will be contributions to the vacuum energy of the potential from the Kähler side of the story. Also different classes of Calabi-Yaus have different values for various parameters. As a result, we will below treat all of the parameters (including the vacuum energy) that go into defining a particular potential as adjustable.

We will focus on one parameter models and take the coordinate on moduli space to be ξ and the axio-dilaton to be τ. The scalar potential is then given by

$$V(\xi,\tau) = \frac{e^K}{16\tau_I \rho_I^3}\left(K^{\xi\bar{\xi}}|D_\xi W|^2 + K^{\tau\bar{\tau}}|D_\tau W|^2\right). \tag{4.26}$$

Here ρ_I is related to the volume of the Calabi-Yau and is thus part of the Kähler moduli. We imagine that it is stabilized in some other way and therefore only acts like a constant here. The superpotential W is given by the Gukov-Vafa-Witten form [62]

$$W = (\vec{\mathcal{F}} - \tau\vec{\mathcal{H}}) \cdot \vec{\Pi}(\xi), \tag{4.27}$$

and the covariant derivatives are computed as always like

$$D_i W = \partial_i W + (\partial_i K) W. \tag{4.28}$$

In these expressions K is the Kähler potential on moduli space and the metric components $K_{\xi\bar{\xi}}$ and $K_{\tau\bar{\tau}}$ are given by applying two derivative to the Kähler potential $K_{i\bar{j}} = \partial_i\bar{\partial}_{\bar{j}}K$. The vectors $\vec{\mathcal{F}} = (\mathcal{F}_0, \mathcal{F}_1, \mathcal{F}_2, \mathcal{F}_3)$ and $\vec{\mathcal{H}} = (\mathcal{H}_0, \mathcal{H}_1, \mathcal{H}_2, \mathcal{H}_3)$ are vectors of the components of the fluxes $\mathcal{F}, \mathcal{H}$ in a certain basis of three-forms. Using modular invariance we set $\mathcal{H}_3 = 0$. The vector $\vec{\Pi} = (\Pi_3, \Pi_2, \Pi_1, \Pi_0)$ is a vector of the periods of the holomorphic three-form Ω in the basis of three-cycles, $\mathcal{C}_i$, that is dual to whatever basis is chosen for the three-forms

$$\Pi_i(\xi) = \int_{\mathcal{C}_i} \Omega. \tag{4.29}$$

We choose the coordinate ξ on the moduli space in such a way that the conifold point, where we take Π_3 as the period over the collapsing cycle, occurs at $\xi = 0$ and furthermore normalize the coordinate so that $\Pi_3 = \xi$ near $\xi = 0$.

4.3.1 Near Conifold Form of the Metric and Potential

We pick a particular basis known as the symplectic basis where the intersection form takes the form

$$Q = \begin{pmatrix} 0 & 0 & 0 & -1 \\ 0 & 0 & 1 & 0 \\ 0 & -1 & 0 & 0 \\ 1 & 0 & 0 & 0 \end{pmatrix} \tag{4.30}$$

Near the conifold point of one parameter models, the periods are given by

$$\Pi_3(z) = \xi \tag{4.31}$$

$$\Pi_2(z) = a_0 + a_1\xi \tag{4.32}$$

$$\Pi_1(z) = b_0 + b_1\xi \tag{4.33}$$

$$\Pi_0(z) = \frac{\xi}{2\pi i}\log(-i\xi) + c_0 + c_1\xi \tag{4.34}$$

We now use these expression to derive the form of the Kähler potential, connection, and metric as well as the superpotential and scalar potential.

Kähler potential, connection, and metric

The Kähler potential (for the complex structure moduli ξ) is given in terms of the periods as

$$K^o = -\log(i\Pi^\dagger Q^{-1}\Pi). \tag{4.35}$$

As $|\xi| \to 0$, this remains regular. The connection $K^o_\xi = \partial_\xi K^o$ also remains regular while the the metric $K^o_{\xi\bar{\xi}} = \partial_\xi \bar{\partial}_{\bar{\xi}} K^o$ develops a logarithmic divergence

$$
\begin{aligned}
K^0 &= -\log(k + \frac{|\xi|^2}{2\pi}\log|\xi|^2) \to -\log k && (4.36)\\
K^0_\xi &= -e^{K^o}\left(k_\xi + \frac{\bar{\xi}}{2\pi}(\log|\xi|^2 + 1)\right) \to -\frac{k_\xi}{k} && (4.37)\\
K^0_{\xi\bar{\xi}} &= \left(|K^o_\xi|^2 - \frac{1}{\pi k} - \frac{k_{\xi\bar{\xi}}}{k}\right) - \frac{1}{2\pi k}\log|\xi|^2 \to \kappa - \frac{1}{2\pi k}\log|\xi|^2. && (4.38)
\end{aligned}
$$

Here we have introduced various regular functions $k(\xi), k_\xi(\xi), k_{\xi\bar{\xi}}(\xi)$, and $\kappa(\xi)$. Since we are interested in the near conifold limit, we will evaluate them all at $\xi = 0$ so that they essentially become model dependent constants.

Since we are working in the near conifold limit we must also consider the back-reaction of the fluxes on the geometry in the form of warping. The warping correction to the Kähler metric is given by [12, 42, 52]

$$K_{\xi\bar{\xi}} = K^o_{\xi\bar{\xi}} + C_w|\xi|^{-4/3}. \tag{4.39}$$

One can integrate these to derive the warping correction to the Kähler connection

$$K_\xi = K^o_\xi + 3C_w\frac{\bar{\xi}^{1/3}}{\xi^{2/3}}. \tag{4.40}$$

The warping correction to the Kähler potential is regular and therefore subleading compared to the terms that are being kept in this approximation. We now move on to the superpotential.

Superpotential

The superpotential is given in terms of the flux components and the periods as

$$W = (\mathcal{F}_i - \tau\mathcal{H}_i)\Pi_i(\xi) \tag{4.41}$$

and is regular as $|\xi| \to 0$ (where regular involves terms like $\xi \log \xi$). The (ordinary) derivative of W is

$$W_\xi = w_\xi + \frac{\mathcal{F}_3}{2\pi i} \log \xi. \tag{4.42}$$

Here we have isolated all of the regular terms from W_ξ in the quantity w_ξ in order to highlight the logarithmic divergence in W_ξ. The covariant derivative of W which is what is used in defining the scalar potential is then given by

$$D_\xi W = W_\xi + K_\xi W = \left(w_\xi - \frac{k_\xi}{k} w \right) + \left(\frac{\mathcal{F}_3}{2\pi i} \log \xi + 3C_w \frac{\bar{\xi}^{1/3}}{\xi^{2/3}} w \right) \tag{4.43}$$

where again we highlight the divergent terms. For simplicity we lump all of the regular terms into a function that we will call ω so that

$$D_\xi W = \omega + \left(\frac{\mathcal{F}_3}{2\pi i} \log \xi + 3C_w \frac{\bar{\xi}^{1/3}}{\xi^{2/3}} w \right) \tag{4.44}$$

The covariant derivative with respect to the axio-dilaton is given by

$$D_\tau W = \frac{1}{\bar{\tau} - \tau} (\mathcal{F}_i - \bar{\tau} \mathcal{H}_i) \Pi_i(\xi) = \frac{M}{\tau - \bar{\tau}}. \tag{4.45}$$

Here we have defined a function M that is regular in ξ. As a result we will treat it as an adjustable parameter (that technically depends on τ). In terms of polar coordinates r, θ we can write

$$D_\xi W = \omega + \frac{\mathcal{F}_3}{2\pi i} \log r + \frac{\mathcal{F}_3}{2\pi} \theta + 3C_w r^{-1/3} e^{-i\theta} w \tag{4.46}$$

The scalar potential

We now have all of the ingredients necessary to construct the full scalar potential. If we write $w = |w|e^{i\theta_w}$ and $\omega = |\omega|e^{i\theta_\omega}$ the square of the covariant derivative becomes

$$\begin{aligned}|D_\xi W|^2 &= |\omega|^2 + \left(\frac{\mathcal{F}_3}{2\pi}\right)^2 (\log r)^2 + \left(\frac{\mathcal{F}_3}{2\pi}\right)^2 \theta^2 + 9C_w^2 r^{-2/3}|w|^2 + \frac{\mathcal{F}_3}{\pi}|\omega|\sin(\theta_\omega)\log r \\ &\quad + \frac{\mathcal{F}_3}{\pi}|\omega|\cos(\theta_\omega)\theta + 6C_w|\omega||w|r^{-1/3}\cos(\theta_\omega + \theta_w - \theta) + \\ &\quad \frac{3\mathcal{F}_3}{\pi}|w|C_w r^{-1/3}\log r \sin(\theta_w - \theta) + \frac{3\mathcal{F}_3}{\pi}|w|C_w r^{-1/3}\theta\cos(\theta_w - \theta). \end{aligned} \tag{4.47}$$

We see that the angular dependence comes in two versions: periodic and non-periodic. Out of these, the periodic dependence will complicate things quite a bit as far as spiral inflation goes. The reason is that since we want to balance the Hubble friction against the angular slope, a varying slope will result in the angular momentum not being conserved and thereby forcing the orbit to move closer to or farther away from the conifold. Although in principle these variations could be very small, it is not clear how one would analyze these terms in any systematic way. As a result, we will focus on the regions where this periodic dependence is subleading. This happens when we take $r \gg C_w^3$. This amounts to neglecting the warping correction to the Kähler connection K_ξ. In this regime the above expression reduces to

$$|D_\xi W|^2 = |\omega|^2 + \left(\frac{\mathcal{F}_3}{2\pi}\right)^2 (\log r)^2 + \left(\frac{\mathcal{F}_3}{2\pi}\right)^2 \theta^2 + \frac{\mathcal{F}_3}{\pi}\omega_I \log r + \frac{\mathcal{F}_3}{\pi}\omega_R\theta \tag{4.48}$$

where we have reverted back to cartesian form $\omega = \omega_R + i\omega_I$. By shifting the angular variable as $\phi = \theta + 2\pi\omega_R/\mathcal{F}_3$ we can absorb the linear term in θ. The scalar potential then takes the form

$$V(r, \phi) = V_0(r) + V_1(r)\phi^2 \tag{4.49}$$

where we have defined the two functions

$$V_0(r) = \alpha + \frac{\beta}{K_{\xi\bar{\xi}}(r)}(\log r + \gamma)^2 \tag{4.50}$$

$$V_1(r) = \frac{\beta}{K_{\xi\bar{\xi}}(r)}. \tag{4.51}$$

The constants α, β, γ are given by

$$\begin{aligned} \alpha &= \frac{|M|^2}{2k\tau_I} \\ \beta &= \frac{1}{2k\tau_I}\left(\frac{\mathcal{F}_3}{2\pi}\right)^2 \\ \gamma &= \frac{2\pi\omega_I}{\mathcal{F}_3}. \end{aligned} \tag{4.52}$$

4.4 Spiraling in String Theory

As spiral inflation requires circular trajectories, one is naturally led to consider multi-sheeted potentials such as those appearing in complex structure moduli space in string theory, (4.49). In order to maximize the time spent inflating, one should initialize the field in a minimum of the effective potential

$$V_{eff} = \frac{L^2}{2r^2} + V(r, \phi). \tag{4.53}$$

Here we briefly neglect the effect of a nontrivial Kähler metric to illustrate the main approach in the argument to follow. By balancing the Hubble friction against the angular tilt, we end up conserving angular momentum. This in turn implies that the centrifugal uplift of the potential is conserved and that a circular orbit may perhaps be sustained for a sufficiently long time.

4.4.1 Spiral Inflation Versus de Sitter Space

Minimizing the effective potential gives

$$\frac{L^2}{r^3} = \frac{\partial V}{\partial r}. \tag{4.54}$$

Since the motion is entirely in the angular direction, this equality can be used to express the kinetic energy in terms of the potential as

$$\frac{L^2}{2r^2} = \frac{1}{2} r \frac{\partial V}{\partial r} \tag{4.55}$$

This is a direct result of spiral inflation. In our case we have a nontrivial Kähler metric, so the effective potential is really

$$V_{eff} = \frac{L^2}{2K_{\xi\bar{\xi}} r^2} + V, \tag{4.56}$$

where the angular momentum is defined as $L = K_{\xi\bar{\xi}} r^2 \dot{\phi}$. Despite this complication, the same logic holds. In particular minimizing V_{eff} results in

$$\frac{L^2}{2K_{\xi\bar{\xi}} r^2} \frac{\frac{\partial}{\partial r}(r^2 K_{\xi\bar{\xi}})}{r^2 K_{\xi\bar{\xi}}} = \frac{\partial V}{\partial r}. \tag{4.57}$$

The kinetic energy is thus in our case given by the more complicated expression

$$\frac{L^2}{2K_{\xi\bar{\xi}} r^2} = \frac{\partial V}{\partial r} \frac{r^2 K_{\xi\bar{\xi}}}{\frac{\partial}{\partial r}(r^2 K_{\xi\bar{\xi}})}. \tag{4.58}$$

So far everything results directly from the spiral condition but in addition to the spiral condition one must always make sure to be potential energy dominated. As a result, one gets a constraint on the potential

$$\frac{r^2 K_{\xi\bar{\xi}}}{\frac{\partial}{\partial r}(r^2 K_{\xi\bar{\xi}})} \cdot \frac{\partial V}{\partial r} \ll V. \tag{4.59}$$

This will be the pitfall of spiral inflation in string theory. It will turn out to be impossible to satisfy this constraint without adding a large constant to V. This of course means that inflation isn't really driven by the spiral nature of the trajectory but rather by a de Sitter like vacuum energy.

Consider any function of the form

$$f(r) = r^n (\log r)^m. \tag{4.60}$$

The derivative of such a function is at least on the same order as $f(r)/r$ as long as n is not too small

$$\frac{\partial f}{\partial r} = n r^{n-1} (\log r)^m + r^n \frac{m(\log r)^{m-1}}{r} = r^{n-1}(\log r)^m (n + \frac{m}{\log r}) = \frac{f(r)}{r}(n + \frac{m}{\log r}). \tag{4.61}$$

Interestingly both the expression involving the Kähler metric, $r^2 K_{\xi\bar{\xi}}$, above and our potential $V(r, \phi)$ consists precisely of such terms. As a result we first of all have that

$$r\frac{\partial}{\partial r}(r^2 K_{\xi\bar{\xi}}) \sim r^2 K_{\xi\bar{\xi}}. \tag{4.62}$$

More precisely, near the conifold point where the warping correction dominates, we have $r(r^2 K_{\xi\bar{\xi}})' = \frac{2}{3}(r^2 K_{\xi\bar{\xi}})$. The condition on the potential from (4.59) therefore becomes

$$r\frac{\partial V}{\partial r} \ll V \tag{4.63}$$

Since the potential also consists of terms polynomial and logarithmic in r, the left-hand side in this expression is on the same order as the potential itself seemingly violating this condition. There is however one caveat. Since any terms independent of r will be annihilated by ∂_r, the left-hand side is just on the same order as the radially dependent terms in V. As a result, the only way to retain a hierarchy such as the one described in equation (4.63) would be to have the potential dominated precisely by the terms independent of r.

$$r\frac{\partial V}{\partial r} \sim \text{radially dependent part of } V \ll V \quad \rightarrow \quad V \sim \text{radially \textit{independent} part of } V. \tag{4.64}$$

In the original model proposed in [58] this could have been accomplished in two independent ways: either by moving far up the monodromy ladder (i.e. setting θ very large) or by choosing a large constant contribution to the potential V_0. However, in our case moving to large values for ϕ won't do us any good since the angular dependence is intrinsically coupled to a radially dependent function $V_1(r)$. As a result the only way for us to retain the hierarchy in (4.59) would be to require the vacuum energy set by the constant α in (4.52) to dominate the value of the potential

$$V(r, \phi) \sim V(0, \phi) = \alpha. \tag{4.65}$$

This means that in order for spiral inflation to work, we must essentially be rolling around in a highly uplifted de Sitter minimum. The inflation is in other words not so much driven by the spiral nature of the trajectory but rather by a vacuum energy that would have yielded standard de Sitter inflation anyway. In fact, the numerical simulations below indicate that when one tries to implement spiral inflation the trajectory quickly begins violating the orthogonality requirement set by the spiral conditions while continuing to inflate due to the presence of a nonzero vacuum energy.

It is possible that examples exist outside of the context of flux compactifications where the potential is not given by terms polynomial or logarithmic in r. In such cases it would be possible that spiral inflation could yield new interesting inflationary scenarios. The schematic form of such a potential is given in fig. (4.2). Regardless of its potential success outside of the context currently being studied, the fact remains that within the realm of flux compactifications in string theory, spiral inflation does not allow inflation to proceed in regimes where regular de Sitter space like inflation could not have already been realized. In order to further strengthen our point, we now turn to a numerical investigation of this topic.

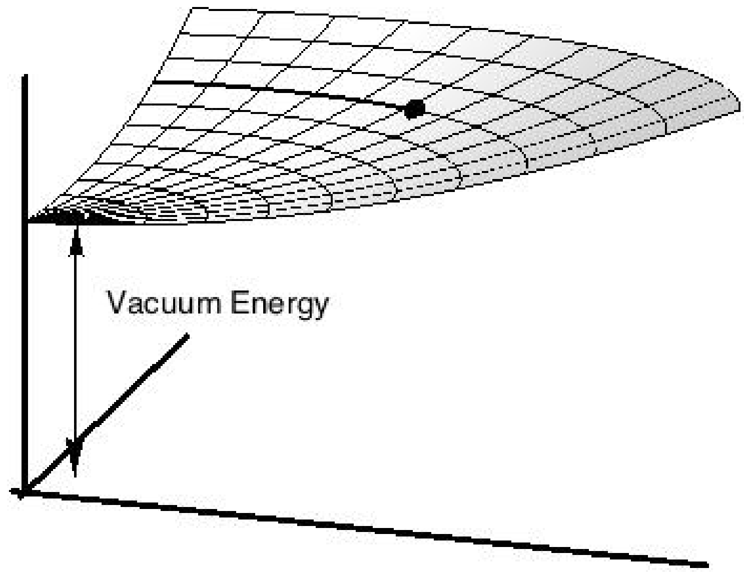

Figure 4.1: The general form of a sheet of the near conifold potential for the complex structure modulus highlighting the need for an uplifted potential.

4.5 Numerical Simulations

In this section we investigate numerically precisely how long spiral inflation can be maintained in the type of potentials encountered in string flux compactifications. The first step toward achieving this is to understand the optimal initial conditions for the field. Since we are looking for circular trajectories, we clearly want to initialize the field without any radial velocity, $\dot{r} = 0$. However, in order to sustain a circular orbit we also need to make sure that $\ddot{r} = 0$ or in other words that we start in a minimum of the effective potential. The worry is of course that as the system begins to evolve, the minimum of the effective potential begins to shift. We can avoid this by conserving angular momentum. This way the centrifugal uplift of the potential will be conserved and the initial radial location will remain a minimum of V_{eff} for longer. This requires us to balance the Hubble friction against the angular tilt of the potential,

$$3HL + \frac{\partial V}{\partial \phi} = 0 \quad \rightarrow \quad \phi = -\frac{3HL}{2V_1(r)} = -\frac{3HL}{2\beta} K_{\xi\bar{\xi}}(r). \tag{4.66}$$

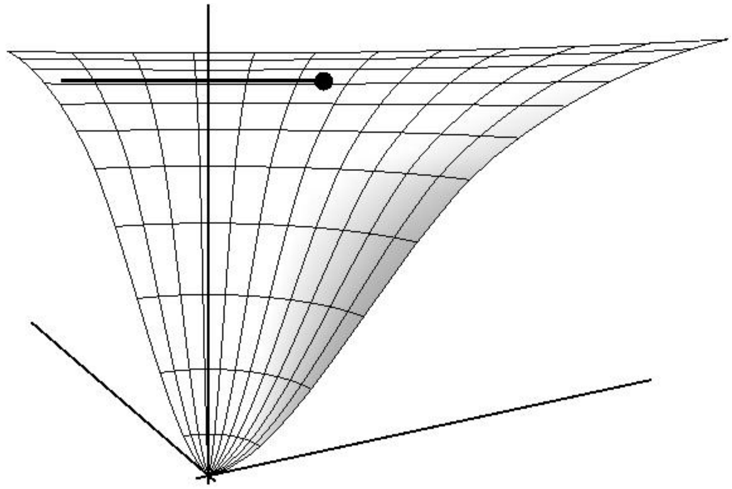

Figure 4.2: A schematic form of a potential that could potentially allow for spiral inflation without relying on a de Sitter like vacuum energy.

The sign here simply tells us that we must move down the potential. Without any loss of generality we can and will take L negative and therefore $\dot{\phi}$ positive. Once L is given, the equations in (4.57) and (4.66) determine the initial conditions of the field. The radial velocity must be taken to be zero and the angular velocity is calculable from the angular momentum. As a result we obtain a one parameter family of initial conditions parameterized by the amount of angular momentum present in the system. One can therefore scan through different values for L and for each value calculate the initial conditions. Once these initial conditions have been specified, it is a simple matter to evolve the system forward numerically to see when exactly the spiral conditions fail. Clearly the equations (4.57) and (4.66) are difficult to solve analytically so we spend some time in the next section solving them numerically.

4.5.1 Initial Conditions

The optimal initial location for the field is given by the simultaneous solution of equations (4.57) and (4.66). Using equation (4.66) in (4.57) gives us an equation for the radial location

$$L^2 = \frac{2K_{\xi\bar{\xi}}(r)^2 r^4}{K'_{\xi\bar{\xi}}(r)r^2 + 2K_{\xi\bar{\xi}}(r)r}\left(-\frac{\beta K'_{\xi\bar{\xi}}(r)}{K_{\xi\bar{\xi}}(r)^2}(\log r+\gamma)^2 + \frac{2\beta}{K_{\xi\bar{\xi}}(r)r}(\log r+\gamma) - \beta K'_{\xi\bar{\xi}}(r)\left(\frac{3HL}{2\beta}\right)^2\right). \tag{4.67}$$

Rather than trying to solve this equation analytically we proceed numerically. One generally finds that the equation has multiple roots. For sufficiently small angular momentum, a single solution exists. Then as the angular momentum is increased, two additional roots appear closer to the conifold point. These two additional solutions then begin to separate. One approaches a limit point near the conifold point while the other root moves farther away from the conifold point until it annihilates the root that was present for small angular momenta. As the angular momentum is increased further, only the near conifold root remains. This process is illustrated in figure 4.3 below. Since each of these roots is a legitimate starting

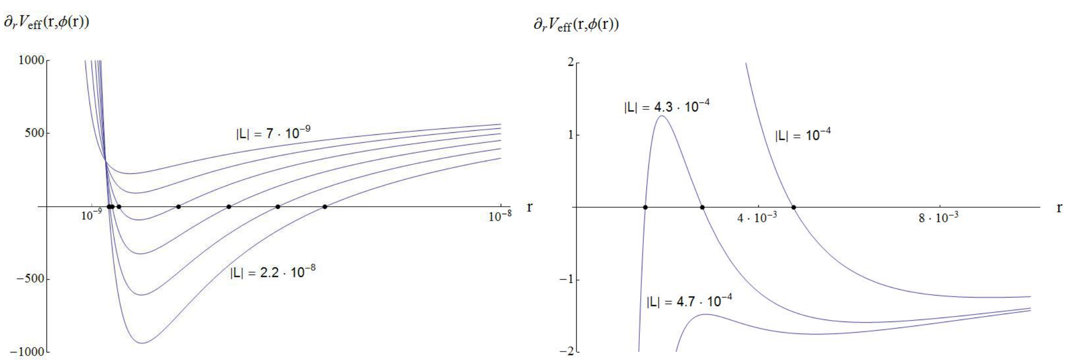

Figure 4.3: $\partial_r V_{eff}$ (evaluated with $\phi = \phi(r)$ where equation (4.66) is satisfied) is here plotted for $C_w = 10^{-5}$. (Left) Two additional solutions appear near the conifold point for sufficiently large L. (Right) One of these solutions moves out to annihilate another one farther out as the angular momentum is increased.

location, we investigate them all in the next section.

4.5.2 Duration of Spiral Inflation

The strategy is to first fix angular momentum and then initialize the field at one of the (up to three different) radial locations given by solving equation (4.67). The angular location is furthermore given by equation (4.66). Once the initial conditions have been specified, we integrate the equations of motion forward numerically. Simulations show that the axio-dilaton does not evolve in any dramatic way. As a result we fix $\tau = 2i$ for the duration of these simulations. For our system, the equations of motion are given by

$$\begin{aligned} K_{\xi\bar{\xi}}(r)r^2\ddot{\phi} + K'_{\xi\bar{\xi}}(r)r^2\dot{r}\dot{\phi} + 2K_{\xi\bar{\xi}}(r)r\dot{r}\dot{\phi} + 3HK_{\xi\bar{\xi}}(r)r^2\dot{\phi} + \frac{\partial V}{\partial \phi} &= 0 \quad (4.68)\\ K_{\xi\bar{\xi}}(r)\ddot{r} + \frac{1}{2}K'_{\xi\bar{\xi}}(r)\dot{r}^2 + 3HK_{\xi\bar{\xi}}(r)\dot{r} - \left(\frac{1}{2}K'_{\xi\bar{\xi}}(r)r^2 + K_{\xi\bar{\xi}}(r)r\right)\dot{\phi}^2 + \frac{\partial V}{\partial r} &= 0. \quad (4.69) \end{aligned}$$

We then track the orthogonality of the acceleration and the velocity. More precisely, we track how quickly the kinetic energy changes. Since our system has a non-canonical metric on the moduli space the relevant quantity to track is

$$\eta = \frac{1}{K_{\xi\bar{\xi}}(r)(\dot{r}^2 + r^2\dot{\phi}^2)}\frac{d}{dt}\left(K_{\xi\bar{\xi}}(r)(\dot{r}^2 + r^2\dot{\phi}^2)\right). \quad (4.70)$$

We repeat this for a set of angular momenta in the range $10^{-10} < |L| < 10^3$ each time solving the equations of motion for each of the possible initial conditions. We generally find that despite being satisfied at $t = 0$ the spiral condition $\eta \ll 1$ becomes violated very quickly. The time dependence during a generic run is displayed in figure 4.4. Furthermore, the number of e-foldings one obtains before the spiral condition fails is far too small as is clear from figure 4.5 where we display the number of e-foldings for each of the up three possible initial conditions. This analysis is repeated for different values for C_w although we here only display the results for $C_w = 10^{-5}$. Interestingly, as we can see in figure 4.6, even after the spiral condition $\eta \ll 1$ fails, the motion continues to be potential energy dominated. This is just a symptom of the fact that we are rolling around in a de Sitter minimum. We also

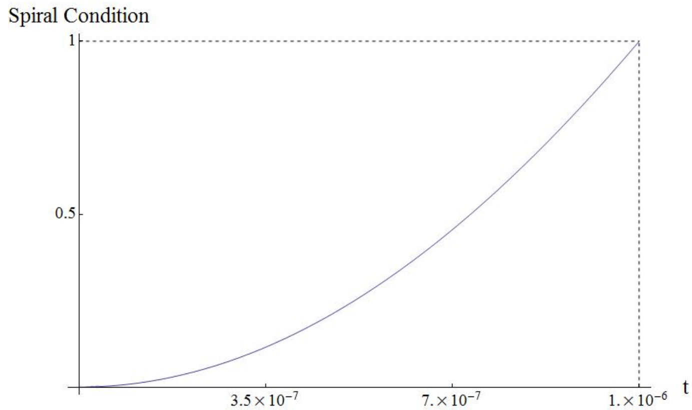

Figure 4.4: Evolution of the absolute value of the spiral condition from equation (4.70) plotted here for $C_w = 10^{-5}$ and $L = 10^{-5}$. This is for the solution nearest the conifold point.

want to bring attention to the fact that the initial angular location tends to be very large. If we interpret the angle as a proxy for how much flux is present in the compactification, we see that one must necessarily move to very large fluxes. This is clearly something we want to avoid for physical reasons since our supergravity approximation relies on these being small. Despite this constraint on the size of the fluxes, we still consider this regime out of completeness of our discussion.

4.6 Discussion

We have investigated the possibility of embedding spiral inflation in string theory. Although at first it seems natural from a stringy perspective since the monodromies that are needed are ubiquitous near the conifold point, we have found that this novel type of inflation is inherently tied to de Sitter inflation in the particular models one encounters in flux compactifications. As a result, even if spiral inflation was realized, the inflation would actually be driven by a vacuum energy. This assertion was backed up by a numerical investigation. In particular it was found that inflation continues due to the vacuum energy even after the spiral condition fails to hold. We thus conclude that while intriguing, the spiral inflation model does not offer any new vantage points in the realm of flux compactifications in string theory.

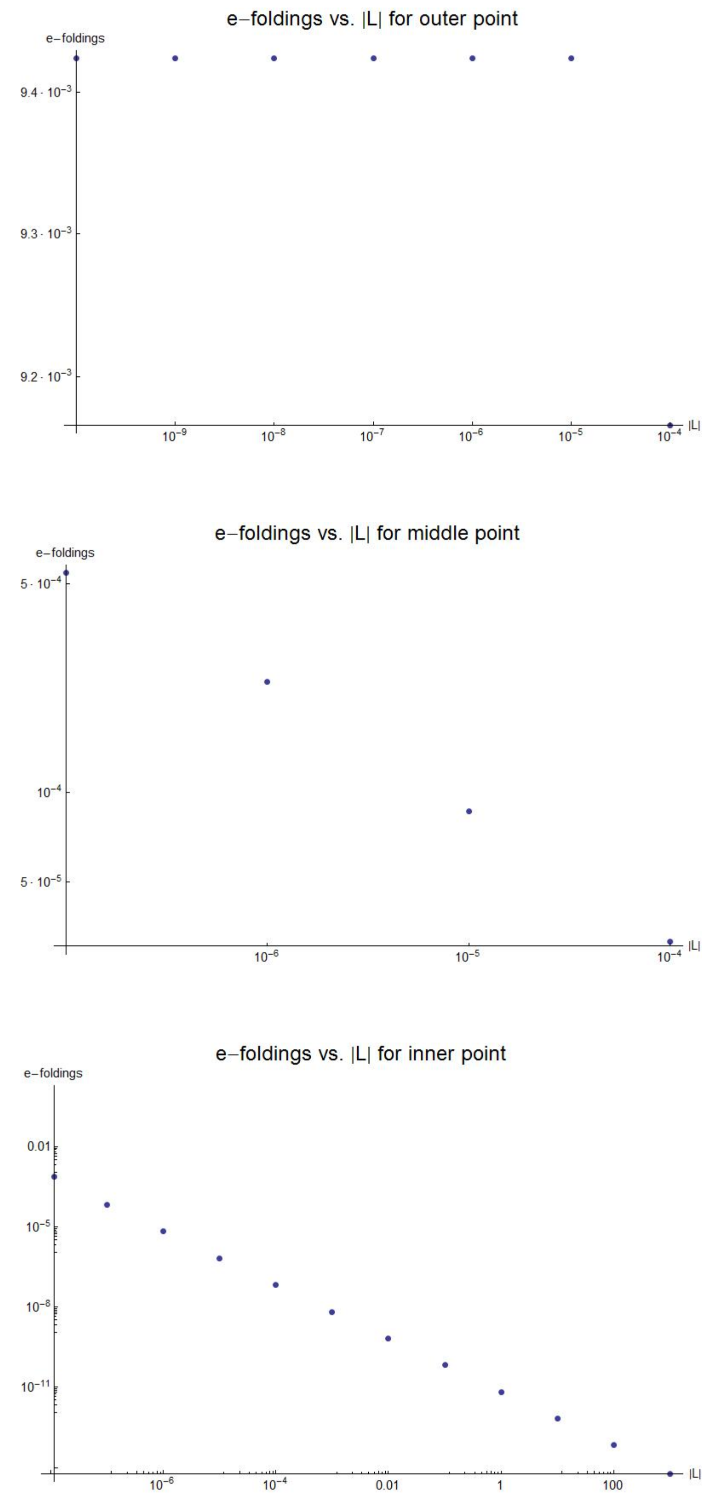

Figure 4.5: Number of e-foldings for various choices of angular momentum $|L|$ for the three possible solutions. Note that the various solutions only exist for a range of $|L|$ (see figure 4.3)

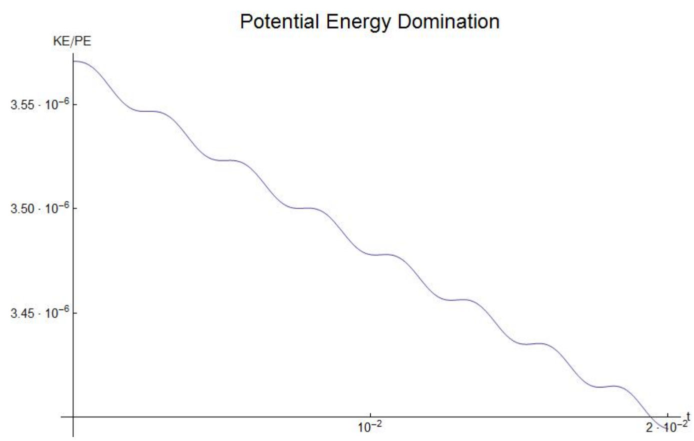

Figure 4.6: Even though the spiral condition in this particular simulation failed at $t = 2.2 \cdot 10^{-4}$, the motion continues to be potential energy dominated for much longer. This reflects the fact that we have a de Sitter like potential, and is not a result of spiral inflation.

Concluding Remarks

It is amazing how powerful the concept of the string really is. The consistency of a relativistic, quantum mechanical string *requires* the existence of gravity and provides us with Einstein's equations. It tells us about the dimensionality of the universe, and shows us that our world must fundamentally be supersymmetric. It gives us gauge theories and D-branes, dualities and string geometry. Despite all of its successes though, string theory remains a highly controversial theory.

The arguments against string theory often involve the fact that the energy scales involved are so large that "it is not falsifiable". This however is not so much a criticism of string theory as it is one of quantum gravity in general since the Planck scale involved is common to any such theory. In fact, being a theory of more than just gravity, string theory actually has a hope of giving testable predictions at much lower energies such as those probed at the LHC. Of course teasing these predictions out of string theory is not a simple task, and to some extent this is where the real issues with string theory lie. As we have discussed in some depth above, the set of low-energy solutions in string theory is all but well understood. This landscape of string theory may contain as many as 10^{500} low-energy vacua each with distinct physical signatures. Clearly there are too many solutions for us to go through one-by-one, and statistical searches therefore become of relevant. In fact even if one could find the precise vacuum that corresponds to our observable universe, the natural follow-up question would be "what happened to the other worlds?".

Barring some sort of super-selection rule that singles out our vacuum as the only admissible one, we will be forced to question how natural our vacuum is both from a dynamical and a statistical perspective. In particular, let us suppose that we find that the physical properties of our vacuum are rather common throughout the landscape but that somehow it is dynamically isolated. Despite being happy with our vacuum from a statistical perspective, the nagging question still remains, "how did we get here." Clearly it is therefore very important to understand both the statistical and dynamical properties of the landscape. Within the domain of dynamics we must include both the quantum mechanical tunneling solutions found in chapter 2 as well as the classical slow-roll scenarios investigated in chapter 4. Furthermore, it is worth emphasizing that the subject of statistics and dynamics are necessarily intertwined. In particular the density of vacua, and thus the distance between them in moduli space, can certainly be argued to impact tunneling rates. Thus, even the work presented in chapter 3 can be taken to impact the question of dynamics.

It is worth noting that even the fundamental problem of the landscape is not clearly insurmountable. In fact, even quantum field theory suffers from a landscape problem which in fact is much worse on the face of it than the corresponding issue in string theory. In defining any quantum field theory one must specify a set of coupling constants and masses. These are real parameters and as such one finds a multidimensional (continuous) landscape of coupling constants. This is to be contrasted with string theory where one must specify a set of *discrete* parameters – the fluxes. As an example, even the simplest supersymmetric extension of the standard model, the MSSM, contains 124 different parameters. The difference of course between string theory and quantum field theory, and the reason why no one is throwing their hands up in despair in response to the landscape of the MSSM, is that there is a well understood formalism that can be utilized in deriving the physical signatures in quantum field theory and furthermore that this formalism is invertible so that any set of physical observations can be directly used to constrain the space of coupling constants. However there is no analogous formalism for string theory. It is conceivable that if such a general method was developed, the landscape of string theory would no longer be an issue. In fact, since the landscape of string theory is fundamentally discrete, it is in principle possible to find the precise vacuum that corresponds to our world whereas for quantum field theory any experimental uncertainty will always manifest itself in a corresponding uncertainty in the values for the coupling constants.

As a concluding remark, it is worth noting that even the existence of the landscape is debatable. It is not clear how a thorough understanding of quantum gravity will alter our understanding of these solutions and so looking to the future it is not clear that the notion of the landscape will survive. However, one thing is clear: if the landscape *does* survive, a thorough understanding of its dynamics, statistics, and cosmology will be essential.

Bibliography

[1] P. Candelas, G.T. Horowitz, A. Strominger, and E. Witten, “Vacuum configurations for superstrings,” Nucl. Phys. B **258**, 46 (1985).

[2] P. Candelas, X. C. de la Ossa, P. S. Green and L. Parkes, “A pair of Calabi-Yau manifolds as an exactly soluble superconformal theory,” Nucl. Phys. B **359**, 21 (1991).

[3] P. Candelas, X. C. de la Ossa, “Moduli Space of Calabi-Yau Manifolds,” Nucl. Phys. B **355** (1991) 455.

[4] P. Candelas, P. S. Green, T. Hubsch, “Rolling Among Calabi-Yau Vacua,” Nucl. Phys. B **330** (1990) 49.

[5] P. Candelas, X. C. de la Ossa, “Comments on Conifolds,” Nucl. Phys. B **342** (1990) 246.

[6] B.R. Greene, D. R. Morrison, A. Strominger, “Black Hole Condensation and the Unification of String Vacua,” Nucl. Phys. B **451** (1995) 109.

[7] B. R. Greene and M. R. Plesser, “Duality in Calabi-Yau moduli space," Nucl. Phys. B **338**, 15 (1990).

[8] A. Strominger, “Special Geometry,” Commun. Math. Phys. **133** (1990) 163.

[9] S. Martin, “A Supersymmetry primer,” [arXiv: 9709356 [hep-ph]].

[10] J. Maldacena and C. Nunez “Supergravity description of field theories on curved manifolds and a no go theorem,” [arXiv: 0007018 [hep-th]].

[11] I. R. Klebanov and M. J. Strassler, “Supergravity and a confining gauge theory: Duality cascades and chiSB-resolution of naked singularities,” JHEP **0008**, 052 (2000) [arXiv:hep-th/0007191].

[12] S. B. Giddings, S. Kachru and J. Polchinski, “Hierarchies from fluxes in string compactifications,” Phys. Rev. D **66** (2002) 106006 [arXiv:hep-th/0105097].

[13] S. Coleman “Fate of the false vacuum: Semiclassical theory,” Phys. Rev. D **15** (1977) 2929.

[14] C. Callan and S. Coleman “Fate of the false vacuum II: First quantum corrections,” Phys. Rev. D **16** (1977) 1762.

[15] S. R. Coleman and F. De Luccia, “Gravitational Effects On And Of Vacuum Decay,” Phys. Rev. D **21**, 3305 (1980).

[16] W. H. Press, S. Teukolsky, W. T. Vetterling, and B. P. Flanery (2007). *Numerical Recipes: The Art of Scientific Computing*. Cambridge University Press.

[17] L. Susskind, “The anthropic landscape of string theory,” arXiv:hep-th/0302219.

[18] R. Bousso and J. Polchinski, “Quantization of four-form fluxes and dynamical neutralization of the cosmological constant,” JHEP **0006**, 006 (2000) [arXiv:hep-th/0004134].

[19] A. D. Linde, V. Vanchurin and S. Winitzki, “Stationary Measure in the Multiverse,” JCAP **0901**, 031 (2009) [arXiv:0812.0005 [hep-th]].].

A. De Simone, A. H. Guth, A. D. Linde, M. Noorbala, M. P. Salem and A. Vilenkin, “Boltzmann brains and the scale-factor cutoff measure of the multiverse,” Phys. Rev. D **82**, 063520 (2010) [arXiv:0808.3778 [hep-th]].

J. Garriga, A. H. Guth and A. Vilenkin, “Eternal inflation, bubble collisions, and the persistence of memory,” Phys. Rev. D **76**, 123512 (2007) [arXiv:hep-th/0612242].

J. Garriga, D. Schwartz-Perlov, A. Vilenkin and S. Winitzki, “Probabilities in the inflationary multiverse,” JCAP **0601**, 017 (2006) [arXiv:hep-th/0509184].

R. Bousso, B. Freivogel and I. S. Yang, “Eternal inflation: The inside story,” Phys. Rev. D **74**, 103516 (2006) [arXiv:hep-th/0606114].

R. Easther, E. A. Lim and M. R. Martin, “Counting pockets with world lines in eternal inflation,” JCAP **0603** (2006) 016 [arXiv:astro-ph/0511233].

[20] A. R. Brown, S. Sarangi, B. Shlaer and A. Weltman, “A Wrinkle in Coleman - De Luccia,” Phys. Rev. Lett. **99**, 161601 (2007) [arXiv:0706.0485 [hep-th]].

[21] J. J. Blanco-Pillado, D. Schwartz-Perlov and A. Vilenkin, “Quantum Tunneling in Flux Compactifications,” JCAP **0912**, 006 (2009) [arXiv:0904.3106 [hep-th]].

[22] H. Davoudiasl, S. Sarangi and G. Shiu, “Vacuum sampling in the landscape during inflation,” Phys. Rev. Lett. **99**, 161302 (2007) [arXiv:hep-th/0611232].

S. Sarangi, G. Shiu and B. Shlaer, “Rapid Tunneling and Percolation in the Landscape,” arXiv:0708.4375 [hep-th].

S. Sarangi, “DBI Global Strings,” JHEP **0807**, 018 (2008) [arXiv:0710.0421 [hep-th]].

S. H. Henry Tye, "A new view of the cosmic landscape," arXiv:hep-th/0611148.

S. H. Tye and D. Wohns, "Resonant Tunneling in Scalar Quantum Field Theory," arXiv:0910.1088 [hep-th].

[23] A. Aguirre, M. C. Johnson and M. Larfors, "Runaway dilatonic domain walls," Phys. Rev. D **81** (2010) 043527 [arXiv:0911.4342 [hep-th]].

[24] I. S. Yang, "Stretched extra dimensions and bubbles of nothing in a toy model landscape," Phys. Rev. D **81**, 125020 (2010) [arXiv:0910.1397 [hep-th]].

[25] A. R. Brown and A. Dahlen, "Small Steps and Giant Leaps in the Landscape," Phys. Rev. D **82** (2010) 083519 [arXiv:1004.3994 [hep-th]].

[26] U. H. Danielsson, N. Johansson and M. Larfors, "The world next door: Results in landscape topography," JHEP **0703**, 080 (2007) [arXiv:hep-th/0612222].

[27] M. C. Johnson and M. Larfors, "Field dynamics and tunneling in a flux landscape," Phys. Rev. D **78**, 083534 (2008) [arXiv:0805.3705 [hep-th]].

[28] B. R. Greene and C. I. Lazaroiu, "Collapsing D-branes in Calabi-Yau moduli space. I," Nucl. Phys. B **604**, 181 (2001). [arXiv:hep-th/0001025].

[29] S. Kachru, R. Kallosh, A. Linde and S. P. Trivedi, "De Sitter vacua in string theory," Phys. Rev. D **68**, 046005 (2003) [arXiv:hep-th/0301240].

[30] V. Balasubramanian, P. Berglund, J. P. Conlon and F. Quevedo, "Systematics of Moduli Stabilisation in Calabi-Yau Flux Compactifications," JHEP **0503**, 007 (2005) [arXiv:hep-th/0502058].

[31] C. F. Doran and J. W. Morgan, "Mirror symmetry and integral variations of Hodge structure underlying one-parameter families of Calabi-Yau threefolds," arXiv:math/0505272.

[32] A. Giryavets, S. Kachru and P. K. Tripathy, "On the taxonomy of flux vacua," JHEP **0408** (2004) 002 [arXiv:hep-th/0404243].

[33] J. P. Conlon and F. Quevedo, "On the explicit construction and statistics of Calabi-Yau flux vacua," JHEP **0410**, 039 (2004) [arXiv:hep-th/0409215].

[34] M. R. Douglas, "The statistics of string / M theory vacua," JHEP **0305**, 046 (2003) [arXiv:hep-th/0303194].

[35] C. I. Lazaroiu, "Collapsing D-branes in one-parameter models and small/large radius duality," Nucl. Phys. B **605**, 159 (2001) [arXiv:hep-th/0002004].

[36] J. T. Giblin, L. Hui, E. A. Lim and I. S. Yang, "How to Run Through Walls: Dynamics of Bubble and Soliton Collisions," Phys. Rev. D **82**, 045019 (2010) [arXiv:1005.3493 [hep-th]].

R. Easther, J. T. . Giblin, L. Hui and E. A. Lim, "A New Mechanism for Bubble Nucleation: Classical Transitions," Phys. Rev. D **80** (2009) 123519 [arXiv:0907.3234 [hep-th]].

[37] G. Torroba, "Finiteness of flux vacua," Nucl. Phys. Proc. Suppl. **171** (2007) 322.

[38] A. Ceresole, G. Dall'Agata, A. Giryavets, R. Kallosh and A. D. Linde, "Domain walls, near-BPS bubbles, and probabilities in the landscape," Phys. Rev. D **74**, 086010 (2006) [arXiv:hep-th/0605266].

[39] D. Arean, D. E. Crooks and A. V. Ramallo, "Supersymmetric probes on the conifold," JHEP **0411** (2004) 035 [arXiv:hep-th/0408210].

[40] A. Giryavets, S. Kachru, P. K. Tripathy and S. P. Trivedi, "Flux compactifications on Calabi-Yau threefolds," JHEP **0404** (2004) 003 [arXiv:hep-th/0312104].

[41] O. DeWolfe, A. Giryavets, S. Kachru and W. Taylor, "Enumerating flux vacua with enhanced symmetries," JHEP **0502**, 037 (2005) [arXiv:hep-th/0411061].

[42] S. B. Giddings and A. Maharana, "Dynamics of warped compactifications and the shape of the warped landscape," Phys. Rev. D **73** (2006) 126003 [arXiv:hep-th/0507158].

[43] G. Shiu, G. Torroba, B. Underwood and M. R. Douglas, "Dynamics of Warped Flux Compactifications," JHEP **0806**, 024 (2008) [arXiv:0803.3068 [hep-th]].

[44] M. R. Douglas and G. Torroba, "Kinetic terms in warped compactifications," JHEP **0905** (2009) 013 [arXiv:0805.3700 [hep-th]].

[45] L. Martucci, "On moduli and effective theory of N=1 warped flux compactifications," JHEP **0905** (2009) 027 [arXiv:0902.4031 [hep-th]]

[46] H. Y. Chen, Y. Nakayama and G. Shiu, "On D3-brane Dynamics at Strong Warping," Int. J. Mod. Phys. A **25** (2010) 2493 [arXiv:0905.4463 [hep-th]].

[47] M. R. Douglas, J. Shelton and G. Torroba, "Warping and supersymmetry breaking," arXiv:0704.4001 [hep-th].

[48] A. R. Frey, G. Torroba, B. Underwood and M. R. Douglas, "The Universal Kaehler Modulus in Warped Compactifications," JHEP **0901** (2009) 036 [arXiv:0810.5768 [hep-th]].

[49] S. W. Hawking and I. G. Moss, "Bubble collisions in the very early universe," Phys. Lett. 110B, 1982, 35.

[50] J. C. Hackworth and E. J. Weinberg, "Oscillating bounce solutions and vacuum tunneling in de Sitter spacetime," Phys. Rev. D **71**, 044014 (2005) [arXiv:hep-th/0410142].

[51] P. Ahlqvist, B. R. Greene, and D. Kagan, "Warped Vacuum Statistics,"' JHEP **1207**, 066 (2012) [arXiv:1202.3172[hep-th]].

[52] P. Ahlqvist, B. R. Greene, D. Kagan, E. A. Lim, S. Sarangi and I-S. Yang, "Conifolds and Tunneling in the String Landscape,"' JHEP **1103**, 119 (2011) [arXiv:1011.6588[hep-th]].

[53] S. Ashok and M. R. Douglas, "Counting flux vacua," JHEP **0401**, 060 (2004) [hep-th/0307049].

[54] F. Denef and M. R. Douglas, "Distributions of flux vacua," JHEP **0405**, 072 (2004) [hep-th/0404116].

[55] P. Koerber, "Lectures on Generalized Complex Geometry for Physicists," Fortsch. Phys. **59**, 169 (2011) [arXiv:1006.1536 [hep-th]].

[56] N. Hitchin, "Generalized Calabi-Yau manifolds," Quart. J. Math. Oxford Ser. **54**, 281 (2003) [math/0209099[math-dg]].

[57] A. Sen, "Orientifold limit of F theory vacua," Phys. Rev. D **55**, 7345 (1997) [hep-th/9702165].

[58] I.-S. Yang, "The Strong Multifield Slowroll Condition and Spiral Inflation," arXiv: 1202.3388 [hep-th]

[59] M.P.Hertzberg, M. Tegmark, S. Kachru, J. Shelton, and O. Ozcan, "Searching for Inflation in Simple String Theory Models: An Astrophysical Perspective," Phys. Rev. D **76** (2007) 103521 [arXiv:0709.0002 [astro-ph]].

[60] V. Balasubramanian, P. Berglund, R. Jimenez, J. Simon, and L. Verde, "Topology from Cosmology," JHEP **0806** (2008) 025 [arXiv:0712.1815 [hep-th]].

[61] M. Sasaki and E.D. Stewart, "A General Analytic Formula for the Spectral Index of the Density Perturbations Produced During Inflation," Prog. Theor. Phys. **95** (1996) 71-78 [arXiv: astro-ph/9507001 [astro-ph]].

[62] S. Gukov, C. Vafa and E. Witten, "CFT's from Calabi-Yau four folds," Nucl. Phys. B **584**, 69 (2000) [hep-th/9906070].